AD 350001

NOTICE: When government or other drawings, specifications or other data are used for any purpose other than in connection with a definitely related government procurement operation, the U. S. Government thereby incurs no responsibility, nor any obligation whatsoever; and the fact that the Government may have formulated, furnished, or in any way supplied the said drawings, specifications, or other data is not to be regarded by implication or otherwise as in any manner licensing the holder or any other person or corporation, or conveying any rights or permission to manufacture, use or sell any patented invention that may in any way be related thereto.

NOTICE:

THIS DOCUMENT CONTAINS INFORMATION AFFECTING THE NATIONAL DEFENSE OF THE UNITED STATES WITHIN THE MEANING OF THE ESPIONAGE LAWS, TITLE 18, U.S.C., SECTIONS 793 and 794. THE TRANSMISSION OR THE REVELATION OF ITS CONTENTS IN ANY MANNER TO AN UNAUTHORIZED PERSON IS PROHIBITED BY LAW.

FINAL REPORT

PROJECT NO. A-628

SETTLEMENT OF CYLINDRICAL MINES
INTO THE SEA BED UNDER GRAVITY WAVES

M. R. CARSTENS and C. S. MARTIN

Navy Mine Defense Laboratory,
Code 700

Contract N600(24)59885 November 1963

Engineering Experiment Station
GEORGIA INSTITUTE OF TECHNOLOGY
Atlanta, Georgia

CONFIDENTIAL

FINAL REPORT

PROJECT NO. A-628

SETTLEMENT OF CYLINDRICAL MINES

INTO THE SEA BED UNDER GRAVITY WAVES

M. R. CARSTENS and C. S. MARTIN

Contract N600(24)59885

Navy Mine Defense Laboratory, Code 700

CONFIDENTIAL

TABLE OF CONTENTS

ACKNOWLEDGMENTS

This study was accomplished under Contract N600(24)59885 which was instigated and supported by the U.S.N. Mine Defense Laboratory at Panama City, Florida. Dr. E. A. Hogge initially explained the problem and has been the technical liaison person between the writers and the U.S.N.M.D.L. since the beginning of the study. The writers wish to express their appreciation for the amicable manner in which this duty was performed. The writers also wish to thank many of the staff of the U.S.N.M.D.L. and, in particular, Messrs. Dowling and Tolbert for openly sharing their experiences concerning mine burial with the writers. This excellent cooperation is exemplified by the furnishing of prototype mine-burial information in exactly the form that the writers needed in order to include a model-prototype comparison.

LIST OF FIGURES

NOMENCLATURE

a	empirical constant
b	empirical constant, sec^{-1}
D	diameter of cylinder
d	mean diameter of bed material
F	sediment Froude number, $U_m / \sqrt{(s-1)gd}$
g	acceleration of gravity
K_b	constant of integration, bed-load movement
K_g	constant of integration, suspended-load movement
L	length of cylinder
m	an exponent in the bed-load transport function
N	ratio of ripple amplitude to cylinder diameter at which ripples affect the scour
n	an exponent in the suspended-load transport function
Q_s	sediment-transport rate, length ^{3}/time
Q_{so}	sediment-transport rate out of the scour hole
s	ratio of the specific weight of the bed material to the specific weight of the fluid medium
t	time
U_m	maximum undisturbed velocity of the fluid near the bottom above the boundary layer
y_s	vertical distance between the bottom of the cylinder and the surrounding bed level
y_{s1}	initial burial

NOMENCLATURE (Continued)

α	angle of orientation measured between the cylinder axis and the wave crest
α_o	initial orientation
η	total amplitude of ripple from crest to trough
λ	ripple wave length
σ_{dg}	geometric standard deviation of particle diameter
ϕ	angle of repose of bed material

ABSTRACT

The settlement of cylindrical mines into the sea bed as the result of gravity waves was experimentally studied in the Georgia Tech Hydraulics Laboratory under general technical supervision of the U.S.N. Mine Defense Laboratory at Panama City, Florida. Three simplications were employed in the model tests as follows: (1) the undisturbed velocity approaching the mine was made to correspond to the bottom velocity under a first-order Stokian gravity wave; (2) the length-to-diameter ratio of the cylinder was four; and (3) the bed materials were limited to being well-rounded and uniformly sized having mean diameters of 0.297 mm and 0.585 mm.

The test program was conducted in the bottom horizontal section of a large U tube. The test section was 1 ft (vertical) by 4 ft (horizontal) in cross section in which the water oscillated over a 4-in thick bed of sand. Cylinder settlement as a function of time was optically measured through the transparent walls of the test section. The effects of initial submergence and initial burial were investigated. Settlement was observed under waves with total amplitude of water motion at the bed of 2.8 ft and 1.0 ft and with a period of 3.6 seconds. Intermediate waves could not be utilized in the model-test program because of the formation of ripples around the model.

Settlement and turning was found to occur spasmodically when the support under the cylinder collapsed as the surrounding scour hole deepened and laterally expanded. In the absence of ripples, sediment

transport out of the scour hole was observed to be bed-load movement with the lower amplitude waves and to be suspended-load movement with the higher amplitude waves. In the presence of ripples, settlement did not occur as the cylinder simply joined the ripple system.

The data were analyzed by evaluating the rate of sediment removal from the scour hole. By consideration of the forces on the particles, by analyzing scour data of others, and by incorporating the model test results, rate of sediment removal functions were formulated for bed-load transport and for suspended-load transport. These transport functions were then incorporated into the equation of continuity resulting in a differential equation of settlement which was then integrated. Initial submergence and initial orientation were analyzed as being initial conditions. In this manner settlement functions were formulated.

Finally the settlement functions were applied to compare with the observed settlement of mines. Data on mine settlement, bottom velocity, and bed material were obtained and furnished by the personnel of the U.S.N. Mine Defense Laboratory. Three cases of mine settlement were studied in detail. The agreement between the predicted settlement and the observed settlement was good in all three cases.

INTRODUCTION

Mines placed upon the sea bottom are known to bury in the bottom sands by settling into the encompassing scour hole. The scour hole results from the increased bed-material transport capacity of the flow adjacent to the mine. Mine burial can be expected to be important in performance, in recovery, and in sweeping. As a result of the interest and encouragement from the Mine Defense Laboratory, a model study of mine burial was conducted in the Hydraulics Laboratory of the Georgia Institute of Technology on Contract NOBs-84327 for the U. S. Navy Bureau of Ships, Code 631.

Model studies involving bed-material transport are characterized by a large number of independent variables involving flow, geometry, fluid, and bed material. The main problem in an experimental study is to eliminate the independent variables of negligible influence and yet to retain all those of major influence. The writers, by considering the lift, drag, fluid inertia, and gravity forces on particles resting on the surface of the bed, concluded that a sediment Froude number is the primary similarity parameter involving sediment properties (Appendix A). The modelling relation for the cylindrical mine on a movable bed is

$$\frac{y_s}{D} = f\left(\frac{U_m}{\sqrt{(s-1)\,gd}},\ \frac{U_m t}{D},\ \frac{L}{D},\ \frac{y_{s1}}{D},\ \alpha_o,\ \sigma_{dg}\right) \qquad (1)$$

in which

U_m = maximum fluid velocity;

t = time;

y_s = depth of burial; y_{s1} = initial depth of burial;

D = cylinder diameter;

L = cylinder length;

α_o = initial orientation of cylinder;

s = ratio of the bed-material density to the fluid density;

d = mean diameter of the bed particles; and

σ_{dg} = geometric standard deviation of particle diameter

The model tests were performed using three simplifications. First the undisturbed velocity approaching the mine was made to be simple harmonic corresponding to the bottom velocity under a first-order gravity wave. Second, the model was a right circular cylinder with a length-to-diameter ratio of four. Third only uniformly-sized bed materials were used thereby eliminating the variable σ_{dg} from the experimental program.

The model tests were performed in the horizontal bottom leg of a large U-tube. The amplitude of oscillation within the U-tube could be controlled but the frequency was constant. The cylindrical model was placed on the bed at various angles of orientation, α_o , and with various initial submergence levels, y_{s1}/D. A record of burial was obtained by means of a cathetometer during the majority of runs and by means of 16-mm motion pictures during two runs. Four of the independent variables of equation (1), namely, $U_m t/D$, y_{s1}/D, and α_o were varied as desired during the experiments.

The sediment Froude number, $Um/\sqrt{(s-1)\ gd}$, could not be varied throughout the desired range even though the velocity, U_m, and the sediment diameter, d, could be varied. With intermediate values of the sediment Froude number, ripples formed on the bed. The appearance of ripples on the bed of the same order of magnitude as the model precluded performing model tests with a rippled bed. Early in the experimental program the discovery was made that ripples would form at conditions less than the incipient-motion condition with the result that the flow disturbance created by the model would initiate ripples which would then spread over the bed. The unexpected appearance of ripples severely limited the range through which the sediment Froude number could be varied. Consequently tests were made at conditions of low wave amplitude and at conditions of high wave amplitude in order to avoid ripples. A detailed analysis of scour was executed (Appendix A) in order to interpolate the test results for the intermediate wave amplitudes.

EXPERIMENTAL PROGRAM

In order to study scour on the sea bed resulting from wave action, the decision was made to model only the mass of the water adjacent to the bed. The water motion at a fixed point close to the bed under a first-order Stokian wave is simple harmonic and is parallel to the bed. A large U-tube with forced oscillation of the water was designed in order to model the water motion under a wave.

U-Tube

Description - The description of this large U-tube is facilitated by referring to Figure 1. The vertical legs of the U-tube are in two rectangular steel tanks (A) at the ends of the horizontal leg which is the test section (B). Forced oscillation of the water mass is achieved by blowing air into the West vertical leg as the water surface is falling and then exhausting this air as the water surface is rising.

The vertical legs of the U-tube are formed within the rectangular steel tanks which are 3 ft by 4 ft in cross section, by streamlined inserts (C). The water passage in each vertical leg is 1 ft by 4 ft in cross section inasmuch as the water surface is never allowed to fall to the curved section of the upper insert (C). In all tests the equilibrium water level was established 48-1/2 in above the top of the test section (B).

The horizontal leg of the U-tube is the test section which is 1 ft (vertical) by 4 ft (horizontal) in cross section and which is 10 ft long. The central portion of the floor is depressed in order to form a container for the erodible bed material. The erodible bed (D) is 6 ft long by 4 ft wide by 4 in deep. The walls of the test section are fabricated of 1/2-in

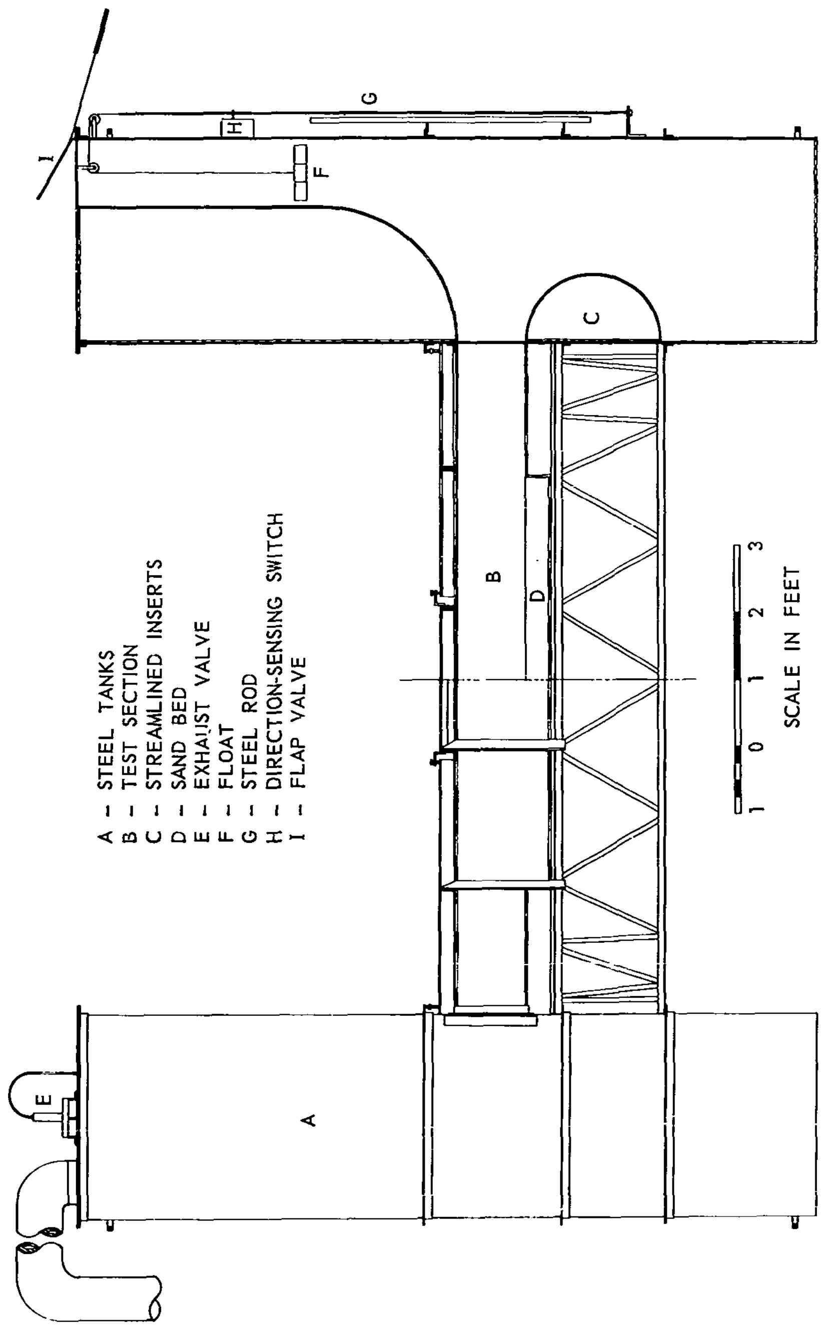

Figure 1. Side Elevation and Cross Section of Tube.

clear plastic and are framed on the exterior with steel angles and channels. The test section rests upon three prefabricated steel trusses which span from steel tank (A) to steel tank. A 3-ft square flush-mounted door is located in the center of the roof in order to be able to place the bed material and models.

The water in the U-tube is made to oscillate at the resonant frequency. The output of a centrifugal blower is discharged continuously into the air space above the water surface of the West vertical leg. Two 7-in diameter, pneumatically powered, exhaust valves (E) in the top of West vertical leg are opened upon receipt of the signal that the minimum water level in this leg is attained.

The feedback mechanism by which the exhaust valve is sequence-operated at the resonant frequency is as follows. The float (F) in the East vertical leg is attached by a light flexible cable to a steel rod (G) which moves vertically past the direction-sensing switch (H). The direction-sensing switch (H) is a lever-operated microswitch. A permanent magnet on the end of the microswitch operating lever is in contact with the steel rod (G) which, in turn, follows the motion of the float (F). Whenever the steel rod (G) is rising the switch (H) is closed and whenever the steel rod (G) is falling the switch (H) is open. When the steel rod (G) changes direction and starts to rise, a circuit is closed which, in turn, actuates a single-cycle timer. This timer makes one revolution in 2 seconds and then stops. A second microswitch is contained within the timer. By means of an adjustable cam this second microswitch can be made to open or close at any time within the two-second interval. Solenoid valves which operate the pneumatic pistons on the exhaust valves are in the circuit with the timer microswitch. The timer microswitch is set such that the exhaust valves open when the timer starts and such that the exhaust valves remain open for a half period. The feedback mechanism described above insures that the water is oscillated at resonant frequency with the result that the frequency of oscillation cannot be controlled.

An electrically operated counter is placed in the circuit containing the direction-sensing switch (H) for the purpose of indicating the number of oscillations or waves from the beginning of each run.

The amplitude of the oscillation can be controlled by positioning the cone valve placed on the inlet to the centrifugal blower. For the determination of amplitude a scale is fixed parallel to the steel rod (G). A pointer on the steel rod passes over the face of the fixed scale.

A blow-down system and a quick-opening flap valve (I) were installed in the East vertical leg in order to eliminate the transients associated with starting the desired oscillation. A solenoid valve in the high-pressure air line leading to the top of the East vertical leg permitted the water surface to be depressed to the lowest elevation of the final oscillatory motion. The flap valve is fitted with a quick-release mechanism in order to be able to begin the oscillation when the water surface was blown down to the desired value. Upon release of the flap valve, the feedback mechanism associated with the direction-sensing switch is activated with the steady cyclic motion being maintained thereafter.

The photograph, Figure 2, shows the South wall of the test section.

Calibration - The operating characteristics of the U-tube and the flow characteristics within the test section have been reported in a separate report (1). The principal conclusions were (1) that the motion

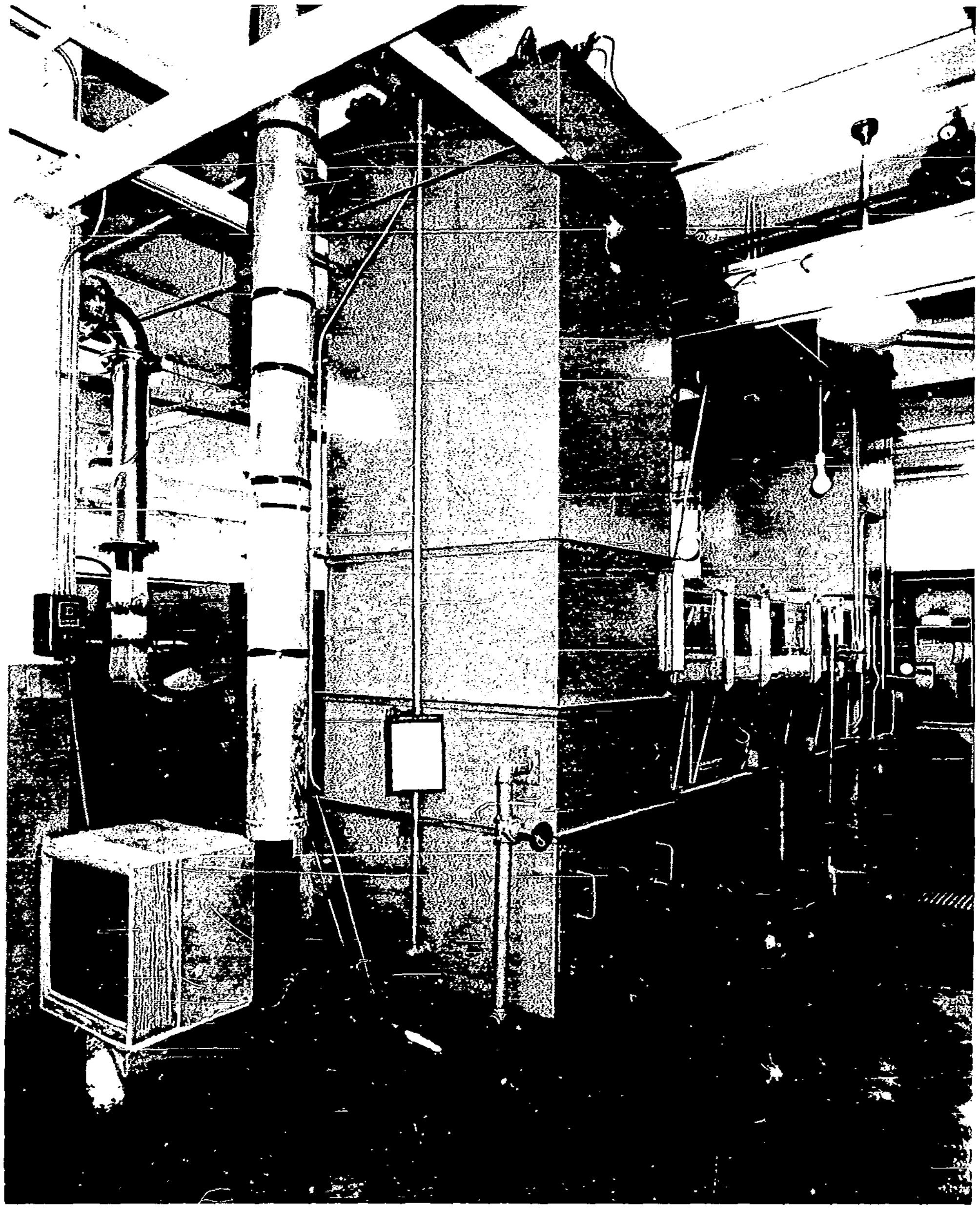

Figure 2. Photograph of U-Tube.

is simple harmonic within the test section, (2) that the fluid-particle amplitude within the test section is equal to the float amplitude, and (3) that the velocity distribution is essentially uniform within the test section.

Models

The right-circular cylinder models are fabricated from aluminum with diameters of 0.501 in, 1.002 in, 1.702 in, and 3.450 in and with a length-to-diameter ratio of four. Perpendicular diameter markings on the ends connected by four axial markings on the curved surface, Figure 3, are aids in visual determination of displacement.

Bed Material

The bed materials are either glass beads, catalog number 090, obtained from the Minnesota Mining and Manufacturing Company or "Flint Shot" Ottawa sand obtained from the Ottawa Silica Company. The principal advantage of these materials is their uniformity in regard to diameter. Size characteristics were determined by sieving. Specific gravity was determined by a standard pycnometer technique. Angle of repose was determined by repeated measurements of the slope of a submerged pile of the sand which was formed by pouring between parallel glass plates. The characteristics are tabulated below

Material	Mean Diameter d (mm)	Geometric Std. Dev. σ_{gd}	Specific Gravity s	Angle of Repose ϕ (deg)
Glass Beads	0.297	1.06	2.47	24
Ottawa Sand	0.585	1.16	2.62	32.5

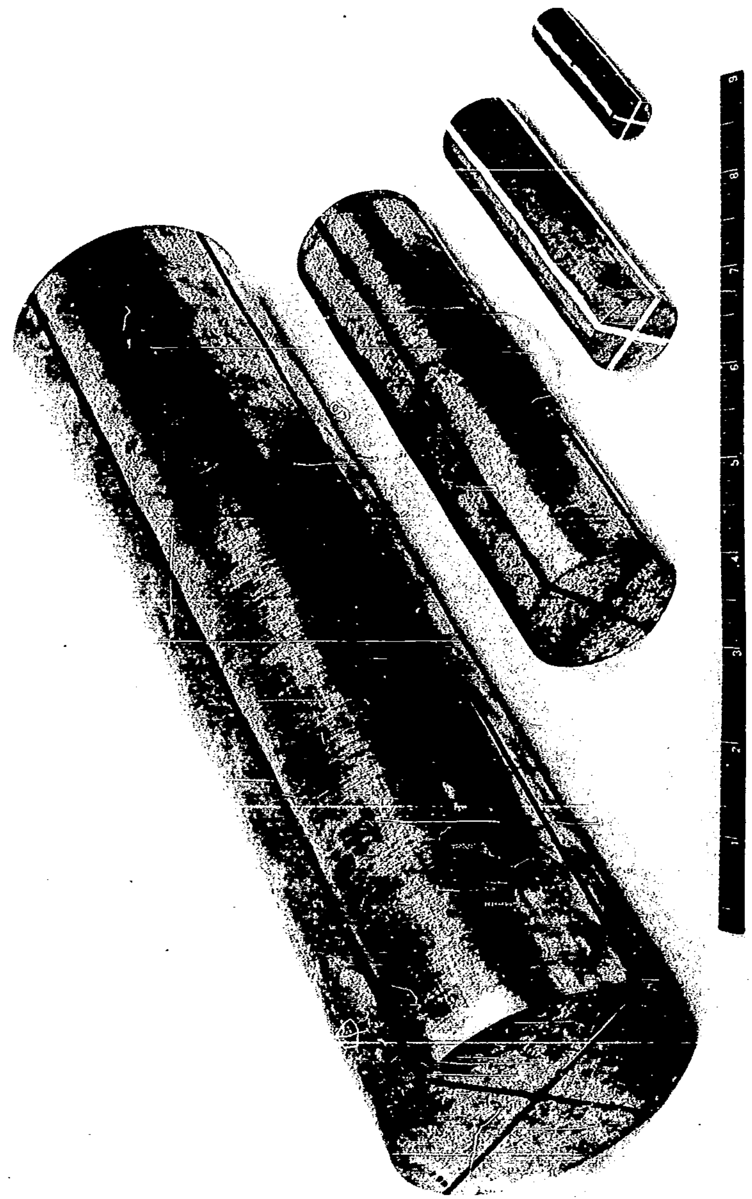

Figure 3. Models.

Experimental Procedure

Prior to making a run the following operations were accomplished. First, the sand bed was leveled with a 2-in by 2-in wooden screed which spanned the six-foot length of the bed. The sand was kept saturated during the leveling. An external vibrator was moved over the exterior of the test section to facilitate compaction of the bed and to facilitate removal of trapped air. When the bed was level, water was admitted until the water surface was approximately 6 in above the bed surface. A string was then stretched across the inside of the tunnel just above the water surface as an aid in aligning the model. A model was then gently lowered to the bed matching the string and the axial marks on the model in order to attain the desired orientation. Then the door in the roof was replaced and rebolted in position. Next the U-tube was filled with water to equilibrium level.

After the model had been positioned in the test section, a cathetometer with a 20X telescope was placed adjacent to the South wall of the test section. Elevations of the top of the sand bed and top of the model were then determined and recorded.

Four observers were required during a run. The functions of the first observer were (1) to blow down the East leg to a predetermined level, (2) to release the flap valve at the top of the East leg, (3) to flash a 300-watt lamp at selected intervals (generally 5 cycle intervals), (4) to read and record amplitude, and (5) to read and record elapsed time for a given number of cycles. The second observer manned the cathetometer telescope maintaining the cross hairs on the top of the model. The third observer read and recorded the cathetometer reading when the first observer flashed the lamp. The fourth observer was stationed on top of the test section with a large protractor. The fourth observer read and recorded the model orientation as the signal lamp was flashed.

Water temperature was read and recorded either just before or just after a run.

The procedure was altered during Model tests 8 and 43 when the model settlement was recorded by a 16-mm motion picture camera. During these two runs a running clock was placed in the field of view of the camera. Burial-time data were determined by scaling from projected images of the 16-mm colored-film strip.

The fourth observer was not required during the runs where the model axis was initially parallel to the wave crest, that is, for runs in which $\alpha_o = 0$.

Results

All model-test data are tabulated and enclosed in the colored sheets, pages 13-48, inclusive.

MODEL TEST 5

BED MATERIAL--GLASS BEADS TEMPERATURE=65.0° F

TOTAL AMPLITUDE=32.60 IN D=1.702 IN α_o=15°

CYCLES	Y/D SOUTH	CYCLES	Y/D SOUTH
0	0.127	19	0.717
4	0.430	24	0.836
9	0.594	29	0.926
14	0.717	34	0.970

MODEL TEST 6

BED MATERIAL--GLASS BEADS TEMPERATURE=64.0° F

TOTAL AMPLITUDE=33.30 IN D=1.702 IN α_o =30°

CYCLES	Y/D SOUTH	CYCLES	Y/D SOUTH
0	0.032	14	0.836
4	0.490	19	0.889
9	0.662	24	0.975

MODEL TEST 7

BED MATERIAL--GLASS BEADS TEMPERATURE=64.0° F

TOTAL AMPLITUDE=33.55 IN D=1.702 IN α_0=60°

CYCLES	Y/D SOUTH	CYCLES	Y/D SOUTH
0	0.058	14	0.773
4	0.548	19	0.850
9	0.620	24	0.940
		29	0.954

MODEL TEST 8

BED MATERIAL--GLASS BEADS TEMPERATURE=67.0° F

TOTAL AMPLITUDE=34.20 IN D=1.702 IN $\alpha_0 = 0°$

CYCLES	Y/D SOUTH	CYCLES	Y/D SOUTH
0.000	0.040	4.070	0.490
0.132	0.049	4.575	0.507
0.258	0.064	5.095	0.507
0.346	0.067	5.660	0.507
0.565	0.131	6.005	0.515
0.658	0.119	7.085	0.558
0.805	0.117	8.060	0.643
1.022	0.303	8.700	0.677
1.217	0.396	10.070	0.694
1.317	0.345	12.050	0.728
1.545	0.363	14.000	0.762
1.816	0.363	16.010	0.813
2.040	0.439	18.530	0.813
2.440	0.465	20.570	0.848
2.560	0.473	23.480	0.915
3.067	0.490	26.732	0.949
3.580	0.490	27.400	0.966
		49.000	1.197

MODEL TEST 9

BED MATERIAL--GLASS BEADS TEMPERATURE=67.2° F

TOTAL AMPLITUDE=34.10 IN D=3.45 IN α_o=14°

CYCLES	Y/D SOUTH	CYCLES	Y/D SOUTH
0	0.062	39	0.713
4	0.142	44	0.760
9	0.171	49	0.800
14	0.251	54	0.819
19	0.411	59	0.848
24	0.483	64	0.872
29	0.621	69	0.904
34	0.643	74	0.910
		80	0.955

MODEL TEST 10

BED MATERIAL--GLASS BEADS TEMPERATURE=69.0° F

TOTAL AMPLITUDE=34.00 IN D=3.45 IN α_o=60°

CYCLES	Y/D SOUTH	CYCLES	Y/D SOUTH
0	0.078	39	0.761
4	0.257	44	0.860
9	0.428	49	0.857
14	0.519	54	0.904
19	0.632	59	0.947
24	0.664	64	0.973
29	0.691	69	1.001
34	0.728	74	1.021
		91	1.120

MODEL TEST 11

BED MATERIAL--GLASS BEADS

TEMPERATURE=70.0° F

TOTAL AMPLITUDE=33.70 IN D=3.45 IN α_o=30°

CYCLES	Y/D SOUTH	CYCLES	Y/D SOUTH
0	0.077	44	0.731
9	0.312	49	0.760
14	0.420	54	0.793
19	0.477	59	0.843
24	0.568	64	0.882
29	0.587	69	0.913
34	0.679	74	0.929
39	0.700	91	0.940

MODEL TEST 12

BED MATERIAL--GLASS BEADS TEMPERATURE=67.0° F

TOTAL AMPLITUDE=33.80 IN D=3.45 IN α_0=15°

CYCLES	Y/D SOUTH	CYCLES	Y/D SOUTH
0	0.082	44	0.816
4	0.312	49	0.824
9	0.387	54	0.830
14	0.477	59	0.855
19	0.571	64	0.886
24	0.607	69	0.924
29	0.663	74	0.961
34	0.730	79	0.981
39	0.798	88	1.000

MODEL TEST 13

BED MATERIAL--GLASS BEADS TEMPERATURE=70.0° F

TOTAL AMPLITUDE=33.60 IN D=3.45 IN α_o =0°

CYCLES	Y/D SOUTH	CYCLES	Y/D SOUTH
0	0.078	40	0.732
5	0.524	45	0.759
10	0.369	50	0.799
15	0.474	55	0.851
20	0.540	60	0.892
25	0.528	65	0.927
30	0.618	70	0.956
35	0.711	75	0.987
		90	1.007

MODEL TEST 14

BED MATERIAL--GLASS BEADS TEMPERATURE=64.2° F

TOTAL AMPLITUDE=33.70 IN D=3.45 IN α_o =90°

CYCLES	Y/D WEST	CYCLES	Y/D WEST
0	0.078	70	0.375
5	0.172	75	0.384
10	0.290	80	0.389
15	0.245	90	0.407
20	0.281	95	0.413
25	0.308	105	0.431
30	0.324	110	0.439
35	0.335	115	0.445
40	0.338	120	0.455
50	0.346	130	0.465
55	0.351	145	0.491
60	0.357	155	0.507
65	0.364	165	0.520

MODEL TEST 15

BED MATERIAL--GLASS BEADS TEMPERATURE=65.2° F

TOTAL AMPLITUDE=34.00 IN D=3.45 IN α_o =75°

CYCLES	Y/D SOUTH	CYCLES	Y/D SOUTH
0	0.089	30	0.663
5	0.166	35	0.729
10	0.291	40	0.774
15	0.397	45	0.831
20	0.493	50	0.893
25	0.610	55	0.962

MODEL TEST 16

BED MATERIAL--GLASS BEADS TEMPERATURE=66.0° F

TOTAL AMPLITUDE=33.80 IN D=3.45 IN $\alpha_o = 80^\circ$

CYCLES	Y/D EAST	CYCLES	Y/D EAST
0	0.065	45	0.712
5	0.226	50	0.747
10	0.334	55	0.772
15	0.397	60	0.777
20	0.436	65	0.782
25	0.479	70	0.800
30	0.573	75	0.794
35	0.616	80	0.800
40	0.658	95	0.917

MODEL TEST 17

BED MATERIAL--GLASS BEADS TEMPERATURE=65.5° F

TOTAL AMPLITUDE=34.40 IN D=1.702 IN α_o =75°

CYCLES	Y/D EAST	CYCLES	Y/D EAST
0	0.145	10	0.747
5	0.633	15	0.931

MODEL TEST 18

BED MATERIAL--GLASS BEADS TEMPERATURE=66.0° F

TOTAL AMPLITUDE=34.05 IN D=1.702 IN α_o =89.5°

CYCLES	Y/D WEST	CYCLES	Y/D WEST
0	0.100	20	0.702
5	0.476	25	0.791
10	0.586	30	0.811
15	0.638	35	0.837

CONFIDENTIAL

MODEL TEST 24

BED MATERIAL--OTTAWA SAND TEMPERATURE=74.3° F

TOTAL AMPLITUDE=12.15 IN D=0.501 IN $\alpha_o = 0^\circ$

CYCLES	Y/D SOUTH	Y/D NORTH
0	0.075	0.075
5	0.378	
10	0.551	
15	0.567	
20	0.575	
25	0.583	
30	0.630	
35	0.618	0.433
40	0.685	
45	0.693	
50	0.709	
55	0.709	
60	0.717	
65	0.748	
70	0.748	

CYCLES	Y/D SOUTH	Y/D NORTH
75		0.551
80	0.764	
85	0.787	
90	0.787	
95	0.803	
100	0.808	
05	0.827	
115	0.843	
130		0.630
140	0.827	
145	0.906	
150	0.921	
160	0.921	
170	0.992	
180		0.606
190	1.000	

MODEL TEST 25

BED MATERIAL--OTTAWA SAND

TEMPERATURE=73.5° F

TOTAL AMPLITUDE=12.09 IN D=0.501 IN α_o =0°

CYCLES	Y/D SOUTH	Y/D NORTH
0	0.032	0.032
5	0.350	
15		0.216
20	0.555	
25		0.087
30	0.587	
35	0.587	
40		0.106
45	0.606	
50	0.854	
55		0.036
60	0.874	
65	0.874	
70	0.874	
75		0.098

CYCLES	Y/D SOUTH	Y/D NORTH
80	0.831	
90		0.240
95		0.240
100		0.272
105	0.854	
110		0.299
120		0.331
125	0.913	
130		0.370
135		0.386
140	0.890	
145		0.380
150		0.417
155		0.417
160		0.417
170	0.894	0.417

MODEL TEST 26

BED MATERIAL--OTTAWA SAND TEMPERATURE=77.0° F

TOTAL AMPLITUDE=11.90 IN D=0.501 IN $\alpha_o = 0°$

CYCLES	Y/D SOUTH	Y/D NORTH
0	0.004	
5	0.402	
10		0.295
15	0.406	
20		0.248
25	0.630	
30		0.197
35	0.697	
40		0.197
45	0.760	
50		0.197
55	0.764	
60	0.764	
65	0.764	
70		0.331
75	0.705	

CYCLES	Y/D SOUTH	Y/D NORTH
85	0.894	
90		0.264
95	0.886	
100	0.886	
110	0.886	
115		0.327
120	0.870	
125	0.870	
130		0.402
135	0.941	
140		0.413
145		0.413
150		0.413
160	0.953	
165		0.429
170	0.953	0.429

MODEL TEST 27

BED MATERIAL--OTTAWA SAND TEMPERATURE=78.4° F

TOTAL AMPLITUDE=12.14 IN D=0.501 IN α_o =0°

CYCLES	Y/D SOUTH	Y/D NORTH	CYCLES	Y/D SOUTH	Y/D NORTH
0	0.077	0.077	180		0.416
5	0.272	0.272	185		0.406
10	0.272		190		0.406
15	0.350		195		0.406
20		0.280	200		0.406
25	0.496		205		0.429
30	0.515		210		0.429
35		0.260	215		0.437
40	0.606		220		0.437
45	0.622		225		0.437
50	0.681		230		0.437
55		0.295	235		0.437
60	0.705		240		0.437
65		0.343	245		0.437
70	0.689		250		0.437
75		0.382	255		0.437
80	0.669		260		0.437
85		0.382	265		0.437
90	0.823		270		0.437
95		0.315	275		0.437
100	0.906		280		0.390
105		0.299	285		0.390
110	0.827		290		0.390
115		0.311	297		0.453
120	0.835		305		0.539
125		0.327	310		0.575
130	0.980		315		0.594
135		0.350	320		0.594
140	0.988		325		0.594
145		0.354	330		0.657
150	0.996		335		0.669
155		0.386	340		0.693
160	0.980		345		0.748
165		0.406	350		0.823
170	0.969		355		0.823
175		0.437	358	1.449	0.776

MODEL TEST 28

BED MATERIAL--OTTAWA SAND TEMPERATURE=79.5° F

TOTAL AMPLITUDE=12.23 IN D=0.501 IN α_o =0°

CYCLES	Y/D SOUTH	Y/D NORTH
0	0.274	0.274
2	0.378	
5	0.465	
10	0.603	
15	0.701	
20	0.717	
25	0.736	
30		0.213
35	0.791	
40		0.272
45	0.776	
50		0.280
55	0.791	
65	1.012	
70		0.228
75	0.998	
80		0.287
85	0.996	
90		0.413
95	1.087	
100		0.413
105	1.094	
110		0.492
115	1.047	
120		0.543
125	1.122	
130		0.531
135	1.138	
140		0.567
145	1.106	

CYCLES	Y/D SOUTH	Y/D NORTH
150		0.634
155	1.067	
160		0.665
165	1.028	
170		0.720
175	1.020	
180		0.728
185	1.035	
190		0.736
195	1.051	
200		0.756
205	1.051	
210		0.748
220		0.756
225	1.079	
230		0.748
235	1.079	
245		0.756
250	1.067	
255		0.736
265		0.736
270	1.150	
275		0.720
280	1.173	
285		0.882
290		0.831
295		0.839
300		0.839
330		0.839
355	1.590	0.839

MODEL TEST 29

BED MATERIAL--OTTAWA SAND   TEMPERATURE=78.5° F

TOTAL AMPLITUDE=12.16 IN   D=0.501 IN $\alpha_o = 0°$

CYCLES	Y/D SOUTH	Y/D NORTH
0	0.360	0.360
2	0.472	0.472
5	0.472	
10	0.474	0.474
15	0.492	
20	0.480	
25		0.528
30	0.543	
35		0.559
40	0.555	0.555
45	0.559	0.559
50	0.598	
55		0.587
60	0.665	
65		0.587
70	0.701	
75		0.559
80	0.756	
85		0.555
95	0.788	
100		0.508
105	0.906	
110		0.472
115	0.976	
120		0.472
125	0.969	
130		0.465
135	0.967	
140		0.474
150	1.118	

CYCLES	Y/D SOUTH	Y/D NORTH
155		0.500
160	1.122	
165		0.504
170	1.051	
175		0.543
180	1.102	
185		0.583
190	1.071	
195		0.591
200	1.185	
205		0.610
210		0.610
215		0.610
225		0.646
230		0.646
235		0.646
240		0.689
245		0.689
250		0.689
255		0.713
275		0.713
300		0.713
305		0.724
310		0.724
315		0.724
320		0.748
330		0.748
355		0.748
370		0.748
375	1.201	0.748

MODEL TEST 30

BED MATERIAL--OTTAWA SAND TEMPERATURE=78.0° F

TOTAL AMPLITUDE=12.00 IN D=0.501 IN α_o =0°

CYCLES	Y/D SOUTH	Y/D NORTH
0	0.551	0.551
2	0.555	0.555
5	0.555	0.555
10	0.559	0.559
15	0.559	0.559
20	0.559	0.559
25	0.559	0.559
30	0.559	0.559
35	0.559	0.559
40	0.559	0.559
45	0.543	
50		0.614
55	0.575	
60	0.618	0.618
65	0.661	
70	0.689	0.689
75	0.717	0.717
80	0.764	
85		0.701
90	0.764	
95	0.764	
100	0.772	
105		0.697
110	0.779	
115	0.811	
120		0.689
125	0.874	
130	0.890	
135		0.677
140	0.898	
145		0.638
150	0.902	
155		0.634
160	0.902	
165	0.902	
170	0.902	
175		0.630
180	0.906	
185	0.906	
190	0.906	
195	0.906	
200	0.906	
205	0.906	
210		0.630
220	1.067	
225		0.559
230	1.079	
235		0.579
240		0.579
245		0.504
250		0.504
255		0.504
260		0.520
265		0.520
270		0.520
275		0.520
280		0.534
285		0.540
290		0.574
295		0.614
300		0.618
305		0.624
310		0.701
315		0.760
320		0.764
325		0.784
330		0.795
335		0.811
340		0.819
345		0.827
350		0.854
355		0.890
360		0.937
365	1.405	0.961

MODEL TEST 31

BED MATERIAL--OTTAWA SAND   TEMPERATURE=77.5° F

TOTAL AMPLITUDE=11.93 IN   D=1.00 IN α_o =0°

CYCLES	Y/D SOUTH	Y/D NORTH
0	0.060	0.060
2	0.123	0.123
5	0.210	0.210
10	0.273	0.273

CYCLES	Y/D SOUTH	Y/D NORTH
15	0.279	0.279
20		0.264
25	0.278	
30	0.284	

RIPPLES STARTED FORMING, TEST DISCONTINUED

MODEL TEST 32

BED MATERIAL--OTTAWA SAND TEMPERATURE=76.5° F

TOTAL AMPLITUDE=12.25 IN D=0.501 IN α_o =0°

L/D = 8

CYCLES	Y/D SOUTH	Y/D NORTH
0	0.063	
2	0.150	
5	0.417	
10		0.343
15	0.417	
20	0.394	
25	0.402	
30	0.402	
35	0.500	
40		0.390
45	0.587	
50	0.515	
55		0.327
60	0.701	
65		0.322
70	0.715	
75	0.815	
80		0.325
85	0.803	
90	0.842	
95		0.394
100	0.852	
105	0.852	
110		0.363
115	0.890	
120	0.881	
125		0.386
130	0.922	
135	0.922	
140	0.905	
145		0.386
150	0.933	
160	0.972	
165		0.410
170	0.997	
175	0.968	
180		0.441
185	0.961	
190	0.961	
195	0.977	
200	0.980	
205	0.968	
210		0.512
215	1.000	
220		0.499
225		0.563
230		0.563
235		0.563
240		0.563
245		0.510
255	1.016	
260		0.504
265		0.504
270	1.016	
275	1.016	
280		0.512
285		0.512
290		0.512
295		0.512
300		0.512
305		0.543
310		0.543
315		0.543
340		0.543

MODEL TEST 33

BED MATERIAL--OTTAWA SAND TEMPERATURE=76.5° F

L/D = 12

TOTAL AMPLITUDE=12.23 IN D=0.501 IN $\alpha_0 = 0°$

CYCLES	Y/D SOUTH	Y/D NORTH
0	0.145	
2	0.241	
5	0.421	
10	0.437	
15	0.437	
20	0.437	
25	0.437	
30	0.437	
35	0.437	
40	0.437	
45	0.437	
50	0.437	
55	0.437	
60	0.437	
65	0.437	
70	0.437	
75	0.437	
80	0.437	
85	0.495	
90	0.520	
95	0.559	
100		0.500
110	0.481	
120	0.602	
125		0.402
130	0.527	
135	0.591	
140	0.527	
145		0.504
150	0.650	
160	0.516	
165		0.552
170	0.652	
175		0.612
180	0.665	
185		0.520
190	0.634	
195	0.662	
200	0.697	
205		0.527
210	0.752	

CYCLES	Y/D SOUTH	Y/D NORTH
235	0.732	
240	0.673	
255	0.685	
260	0.733	
265		0.606
270	0.764	
275	0.764	
280	0.740	
285		0.669
290	/)717	
295	733	
300	0.799	
305		0.606
310	0.748	
315	0.748	
320	0.748	
325	0.748	
330	0.819	
335		0.658
340	0.827	
345	0.827	
350	0.795	
355	0.795	
360	0.850	
365		0.674
370	0.847	
375	0.847	
380	0.772	
385	0.772	
395	0.906	
400		0.726
405	0.906	
410	0.906	
420	0.906	
440	0.906	
460	0.906	
480	0.906	
500	0.906	
515		0.787
520		0.787
565	0.894	

MODEL TEST 34

BED MATERIAL--OTTAWA SAND TEMPERATURE=76.0° F

TOTAL AMPLITUDE=12.12 IN D=0.501 IN $\alpha_o = 0°$

L/D = 16

CYCLES	Y/D SOUTH	Y/D NORTH
0	0.063	
2	0.227	
5	0.245	
10	0.110	
15		0.263
20	0.331	
25	0.331	
30		0.276
35	0.346	
40	0.346	
45	0.346	
50	0.346	
55	0.346	
60	0.346	
65		0.292
70		0.292
75	0.339	
80	0.339	
85	0.339	
90	0.339	
95	0.339	
100	0.339	
105		0.292
110	0.339	
115	0.339	
120	0.339	
125	0.339	
130	0.339	
135	0.339	

CYCLES	Y/D SOUTH	Y/D NORTH
140	0.339	
145	0.339	
150	0.345	
155		0.292
160	0.346	
165	0.346	
170	0.346	
175	0.346	
180	0.346	
185		0.292
190	0.354	
195	0.354	
200	0.354	
205	0.354	
210	0.354	
215	0.354	
220	0.366	
225	0.366	
230	0.366	
235	0.366	
240	0.366	
245	0.385	
250	0.385	
255	0.385	
260	0.385	
265	0.385	
270	0.385	
275	0.385	
310	0.385	
315	0.385	

MODEL TEST 37

BED MATERIAL--OTTAWA SAND TEMPERATURE=75.0° F

TOTAL AMPLITUDE=11.99 IN D=0.501 IN α_o =0°

CYCLES	Y/D SOUTH	Y/D NORTH
0	0.022	0.022
2	0.335	0.335
5	0.367	
10	0.374	
15	0.382	
20	0.524	
25		0.303
30	0.610	
35		0.287
40	0.618	
45	0.602	
50		0.397
55	0.653	

CYCLES	Y/D SOUTH	Y/D NORTH
60		0.378
65	0.658	
70		0.429
75	0.607	
80		0.462
85	0.618	
90		0.488
95	0.626	
100		0.528
105	0.650	
110		0.517
115	0.682	
120		0.532
125	0.768	

MODEL TEST 38

BED MATERIAL--OTTAWA SAND TEMPERATURE=73.5° F

TOTAL AMPLITUDE=12.26 IN D=0.501 IN α_o =0°

L/D = 8(ROUNDED ENDS)

CYCLES	Y/D SOUTH	Y/D NORTH	CYCLES	Y/D SOUTH	Y/D NORTH
0	0.064		170	0.905	
2	0.205		180	0.913	
5	0.386		195		0.635
10	0.414		200	0.937	
15	0.414		205	0.953	
20	0.414		210	0.965	
25	0.414		215	0.976	
30	0.474		220		0.630
35	0.552		230		0.630
40		0.442	235	0.976	
45	0.591		260		0.607
50	0.604		290	0.976	
55		0.488	295		0.607
60	0.630		300	0.984	
65		0.481	305		0.662
70	0.685		315	0.999	
75		0.544	330	1.000	
80	0.682		335		0.662
85	0.701		355	0.992	
90		0.583	360		0.653
95	0.717		365		0.653
100	0.717		370		0.677
105		0.613	375	0.945	
110	0.787		380		0.705
115	0.803		395		0.705
120		0.606	400	0.945	
125	0.831		415	0.913	
130	0.843		420		0.756
135	0.843		425	0.910	
140	0.863		435	0.910	
145		0.614	440		0.764
150	0.874		455	0.897	
155		0.635	465	0.913	
160	0.997		470		0.788
160	0.897		470		0.788

MODEL TEST 39

BED MATERIAL--OTTAWA SAND TEMPERATURE=74.5° F

TOTAL AMPLITUDE=12.16 IN D=0.501 IN $\alpha_0=0°$

CYCLES	Y/D SOUTH	Y/D NORTH
0	0.245	0.145
2	0.250	0.250
5	0.286	0.286
10	0.354	
15	0.321	0.321
20	0.335	0.335
25	0.370	
30	0.402	0.402
35	0.468	
40		0.419
45	0.488	
50		0.433
55	0.535	
60		0.449
65	0.578	
70		0.457
75	0.591	
80		0.508
85	0.559	0.559
90	0.559	0.559
95	0.622	
100		0.528
105	0.646	
110		0.551
115	0.661	
120		0.571
125	0.646	
130	0.667	
135		0.587
140	0.701	
145		0.615
150	0.693	
155	0.693	

CYCLES	Y/D SOUTH	Y/D NORTH
160	0.725	0.725
165		0.674
170	0.740	
175	0.748	0.748
180	0.748	0.748
185	0.772	0.772
190	0.858	
195		0.736
200	0.882	
205		0.811
210	0.835	0.835
215	0.835	0.835
220	0.851	0.851
225	0.886	
230		0.792
235	0.886	
240		0.891
245	0.882	
250		0.827
255	0.966	
260		0.795
265	0.976	
270		0.799
275	0.968	
280		0.795
285	0.968	
290		0.811
295	0.976	
300		0.811
305	0.976	
310		0.811
315	1.000	
320		0.732

MODEL TEST 41

BED MATERIAL--GLASS BEADS TEMPERATURE=75.0° F

TOTAL AMPLITUDE=33.80 IN D=3.45 IN α_o=0°

CYCLES	Y/D SOUTH	Y/D NORTH	CYCLES	Y/D SOUTH	Y/D NORTH
0	0.068	0.032	60	0.792	
5	0.243		65	0.801	
10	0.318		70	0.811	
15	0.464		75	0.844	
20	0.540		85	0.905	
25	0.626		90	0.932	
30	0.649		95	0.959	
35	0.611		100	0.989	
40	0.796		105	1.012	
45	0.768		110	1.023	
50	0.776		115	1.041	
55	0.782		120	1.064	
			126	1.072	1.103

MODEL TEST 42

BED MATERIAL--GLASS BEADS TEMPERATURE=76.2° F

TOTAL AMPLITUDE=33.90 IN D=3.45 IN α_o =0°

CYCLES	Y/D SOUTH	Y/D NORTH	CYCLES	Y/D SOUTH	Y/D NORTH
0	0.030	0.044	55	0.791	
2	0.182		60	0.792	
5	0.264		65	0.826	
9.5	0.372		70	0.861	
15	0.447		75	0.886	
20	0.546		80	0.903	
25	0.550		85	0.921	
30	0.667		90	0.942	
35	0.676		95	0.963	
40	0.692		100	0.992	
45	0.784		105	1.018	
50	0.788		110	1.079	1.107

MODEL TEST 43

BED MATERIAL--GLASS BEADS TEMPERATURE=74.5° F

TOTAL AMPLITUDE=33.80 IN D=3.45 IN $\alpha_o = 0°$

CYCLES	Y/D SOUTH	CYCLES	Y/D SOUTH
1.92	0.206	24.65	0.582
3.15	0.247	27.40	0.587
4.11	0.284	30.15	0.638
5.03	0.308	32.85	0.639
6.04	0.321	35.60	0.653
7.21	0.326	38.35	0.710
8.04	0.326	41.15	0.762
9.28	0.352	44.10	0.762
11.77	0.420	46.60	0.765
11.95	0.441	49.35	0.768
13.21	0.452	52.20	0.771
14.25	0.456	55.20	0.778
15.21	0.459	59.30	0.793
16.30	0.465	64.30	0.799
17.62	0.512	68.90	0.820
19.00	0.560	74.80	0.862
19.78	0.562	79.60	0.888
20.82	0.564	86.50	0.927
22.60	0.572	93.40	0.950
		95.80	0.963

MODEL TEST 44

BED MATERIAL--GLASS BEADS TEMPERATURE=75.0° F

TOTAL AMPLITUDE=33.50 IN D=3.45 IN $\alpha_o = 0°$

CYCLES	Y/D SOUTH	Y/D NORTH
0	0.195	0.204
2	0.195	
5	0.240	
10	0.380	
15	0.447	
20	0.525	
25	0.560	
30	0.615	
35	0.664	
40	0.695	
45	0.733	
50	0.775	
55	0.813	
60	0.884	
65	0.876	
70	0.905	
75	0.923	
80	0.942	
85	0.959	
90	0.979	
95	0.993	

MODEL TEST 45

BED MATERIAL--GLASS BEADS TEMPERATURE=75.8° F

TOTAL AMPLITUDE=33.60 IN D=3.45 IN $\alpha_o = 0°$

CYCLES	Y/D SOUTH	Y/D NORTH
0	0.287	0.250
6	0.303	
11	0.446	
16	0.492	
21	0.536	
26	0.618	
31	0.653	
36	0.679	
41	0.707	
46	0.748	

CYCLES	Y/D SOUTH	Y/D NORTH
51	0.788	
56	0.810	
61	0.856	
66	0.893	
71	0.914	
76	0.926	
81	0.943	
86	0.956	
92	0.999	
96	1.011	
101	1.023	

MODEL TEST 46

BED MATERIAL--GLASS BEADS TEMPERATURE=75.5° F

TOTAL AMPLITUDE=33.40 IN D=3.45 IN α_0 =0°

CYCLES	Y/D SOUTH	Y/D NORTH	CYCLES	Y/D SOUTH	Y/D NORTH
0	0.526	0.482	55	0.792	
2	0.554		60	0.805	
5	0.554		65	0.829	
10	0.554		70	0.850	
15	0.554		75	0.866	
20	0.554		80	0.886	
25	0.554		85	0.904	
30	0.662		90	0.914	
35	0.676		95	0.925	
40	0.708		100	0.936	
45	0.742		105	0.951	
50	0.776		110		

MODEL TEST 47

BED MATERIAL--GLASS BEADS TEMPERATURE=76.8° F

TOTAL AMPLITUDE=33.60 IN D=1.702 IN α_o =0°

CYCLES	Y/D SOUTH	Y/D NORTH	CYCLES	Y/D SOUTH	Y/D NORTH
0	0.217	0.205	16	0.739	
4	0.371		20	0.787	
8	0.554		24	0.905	
12	0.625		28	0.954	
			32	0.984	

MODEL TEST 50

BED MATERIAL--GLASS BEADS TEMPERATURE=76.6° F

TOTAL AMPLITUDE=34.10 IN D=1.702 IN $\alpha_s = 0^\circ$

CYCLES	Y/D SOUTH	CYCLES	Y/D SOUTH
0	0.058	12	0.743
4	0.460	16	0.801
8	0.616	20	0.861
		24	0.977

DISCUSSION OF RESULTS

The model-test program was executed at two values of the sediment Froude number, $U_m/\sqrt{(s-1)\,gd}$; namely, 2.8 for Tests 25-39, inclusive and 11.2 for Tests 5-18, 41-47, and 50. Model tests were impossible to perform at intermediate values of the sediment Froude number, F, because of the formation of ripples on the bed. These bed ripples are of the same order of size as the models and, in fact, the cylindrical models become part of the ripple system with the axis of the cylinder coinciding with a ripple crest. This condition is illustrated in Figure 4 for which the value of F was 5.9. When the model is part of the ripple system no scour occurs. In contrast, when the bed ripples are nonexistent or insignificant in height a scour hole develops around the model as shown in Figure 5 for which the value of F was 11.2.

The lower value of F, that is 2.8, was selected as the maximum value at which model tests could be made without the formation of ripples on the bed. This value was selected by considering the critical scour parameter (Appendix A)

$$C = \frac{U_m}{\sqrt{(s-1)gd(\tan\phi\ \cos\alpha\ +\ \sin\alpha\ )}} \tag{2}$$

in which α is the angle of inclination of the bed with the horizontal. The value of C for incipient motion of bed-particles in oscillatory flow is about 3.5 (Table 3, Appendix A). The angle of repose of the Ottawa sand used in Tests 25-39, inclusive, is 32.5 degrees. For an originally level bed α is zero. Substituting these values into equation (2) the value of F of 2.8 is obtained.

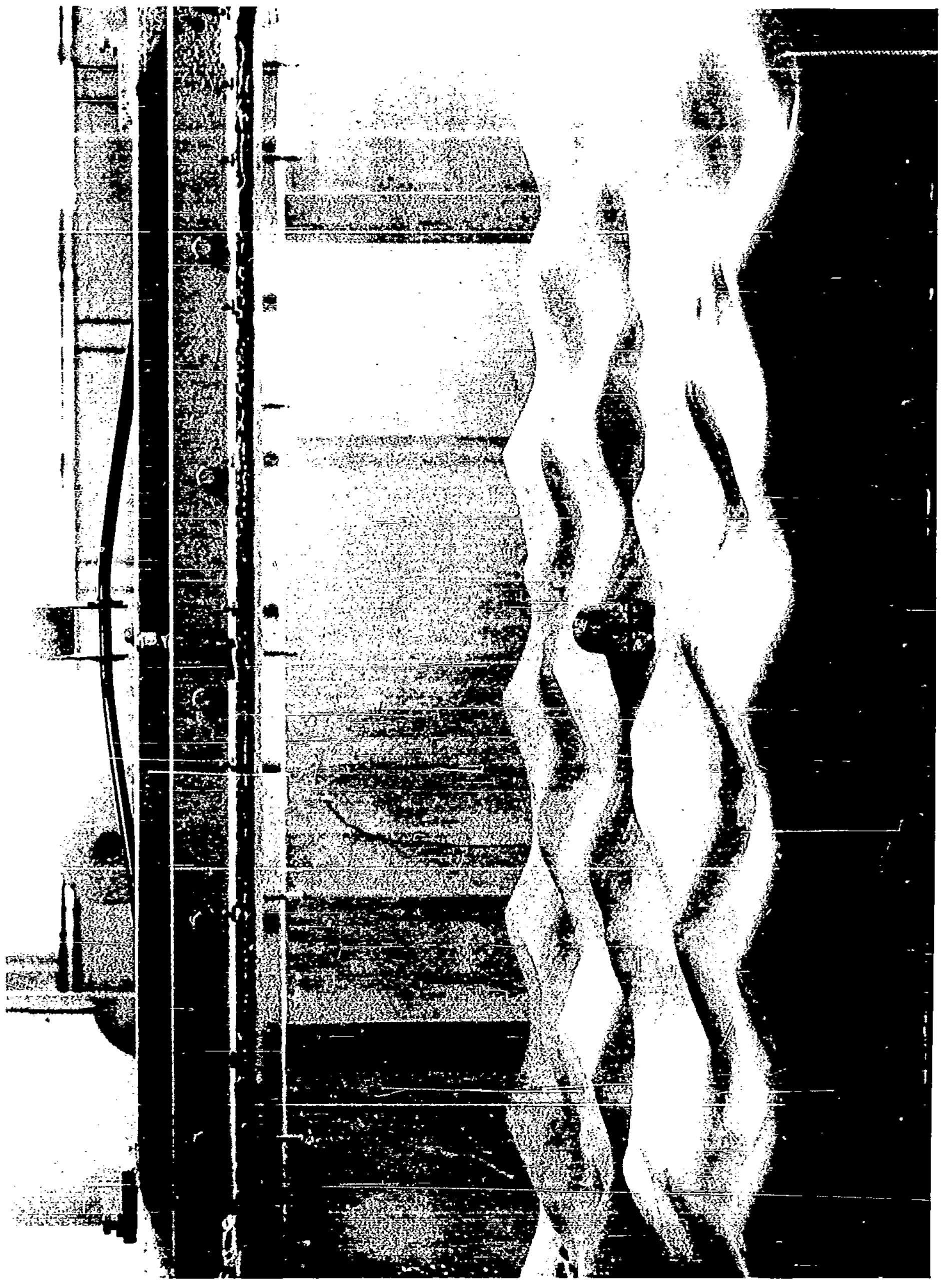

Figure 4. Model Incorporated into Ripple System (F = 5.9).

Figure 5. Scour Hole.

The criterion that F be equal to or less than 2.8 was found to be inadequate. In the following table are listed the model tests and the pertinent characteristics which were performed for the purpose of determining the conditions of ripple formation.

Test No.	D(in)	d(mm)	D/d	$\frac{U_m}{\sqrt{(s-1)gd}}$	Bed Condition Around Model
1	1.002	0.297	85.8	1.39	scoured
2	1.002	0.297	85.8	2.85	rippled from beginning
3	1.702	0.297	145.6	2.12	rippled @ 1340 cycles
20	1.002	0.585	43.6	2.16	rippled @ 300 cycles
21	1.002	0.585	43.6	2.72	rippled @ 150 cycles
22	1.002	0.585	43.6	3.21	rippled @ 120 cycles
23	1.702	0.585	74.0	3.15	rippled from beginning
24	0.501	0.585	21.8	2.78	scoured
48	0.501	0.297	42.9	3.25	rippled @ 35 cycles

The tests results shown above indicate that the bed is quasi-stable in that bed ripples will form at values of F less than for the incipient-motion condition; for example, in Test 20. Ripple inception is definitely a function of F as shown by Tests 20, 21, and 22 in which the time for ripple inception to occur decreased as the value of F was increased. In addition, the magnitude of the disturbance is quite significant as evidenced by Tests 2 and 24 for which the values of F were nearly equal. Ripples existed from the beginning of Test 2 but did not exist in Test 24. The principal difference between these two runs is in the magnitude of the disturbance as evidenced by the cylinder diameter-to-particle diameter ratio. No further investigation of the role of disturbance magnitude in ripple inception was made. The decision was made to conduct some of the model tests with the 0.501-in diameter model on the Ottawa-sand bed at a value of F of 2.8.

The higher value of F, that is 11.2, was selected as the minimum value at which the bed ripples are sheared off. In this range the uppermost particles of the bed are in motion over the entire bed and ripples disappear. Inman (2) presents results from the studies of Manohar (3) and Menard (4) showing that the velocity at which ripples disappear increased with increasing grain size. This observation was verified in the present experiments in that ripples would disappear or be insignificant at a maximum velocity, U_m, of 2.4 fps with the 0.297-mm diameter bed material but the ripples would not disappear at a value of U_m of 2.7 fps with the 0.585 mm diameter bed material. Since U_m of 2.7 fps was the maximum attainable in the U-tube, the tests in which the ripples disappeared were limited to the smaller bed material with a value of F of 11.2.

Phenomenological Discussion of Tests with F of 2.8

The following discussion is presented chronologically. In all tests, the starting transients were eliminated by utilizing an initial blowdown in the East vertical leg of the U-tube.

Immediately upon the start of a run scour holes begin to form at the ends of the cylinder. These scour holes deepen and expand with much of the scoured material being carried toward the middle of the cylinder forming a central ridge which decreases in height away from the model.

When the scour-hole bottom is below the bottom of the model, material slides out from under the model forming a flow passage under the cylinder. Once the flow passage under the model is started, material is carried under the cylinder and these flow passages increase in size by lateral movement toward the center. The central support upon which the cylinder rests diminishes in size until the support is inadequate at which time the cylinder rocks on the support and settles rapidly. Upon settling the supporting base is broadened only to be narrowed again by scour under the cylinder. The burial proceeds in this manner settling spasmodically with ever increasing time intervals between settlement increments. The model settles in an essentially level manner upon collapse of the central support. The largest observed deviation from the horizontal was 26 degrees.

The material which is removed from under the cylinder must obviously be disposed of in some manner. The large eddies formed at the ends of the cylinder appear to be the main mechanism for excavating and removing material scoured from under the cylinder. In the tests with F of 2.8, the material was moved by rolling along the bed. This type of movement is called bed-load movement. The fully developed scour hole resembles an inverted frustum with the peripheral surface being inclined at the angle of repose of the bed material.

In summary, the settlement can be described as a destruction of the cylinder support by scour under the cylinder. Simultaneously the eddy pattern created as a result of flow separation is the mechanism for the enlargement of the surrounding scour hole. Both scour in the vicinity of the model and under the model are necessary for settlement to occur. In fact the rate at which material can be scoured from under the cylinder is limited by the rate at which material can be carried out of the surrounding scour hole.

Phenomenological Discussion of Tests with F of 11.2

As before the discussion is chronological.

Upon starting, the model rolls to and fro in the first cycle and settles rapidly. No rolling occurs after the first cycle. Visual observation of the progress of scour is difficult since the removed material leaves the scour hole in suspension as shown in Figure 6. There is no reason to believe that the basic process of settlement is any different in the tests in which F is 11.2 than those in which F is 2.8. The difference is solely in the mechanism of removal; that is, as suspended load in the former and as bed load in the latter. No difference could be detected in the scour-hole geometry between the two sets of tests.

The cylinder rests on a fulcrum at the instant of settling which permits the cylinder not only to rock but also to turn. When the initial orientation α_o is different from zero the cylinder also pivots during settlement. The cylinder continues to pivot in increments until the axis is parallel to the wave crest.

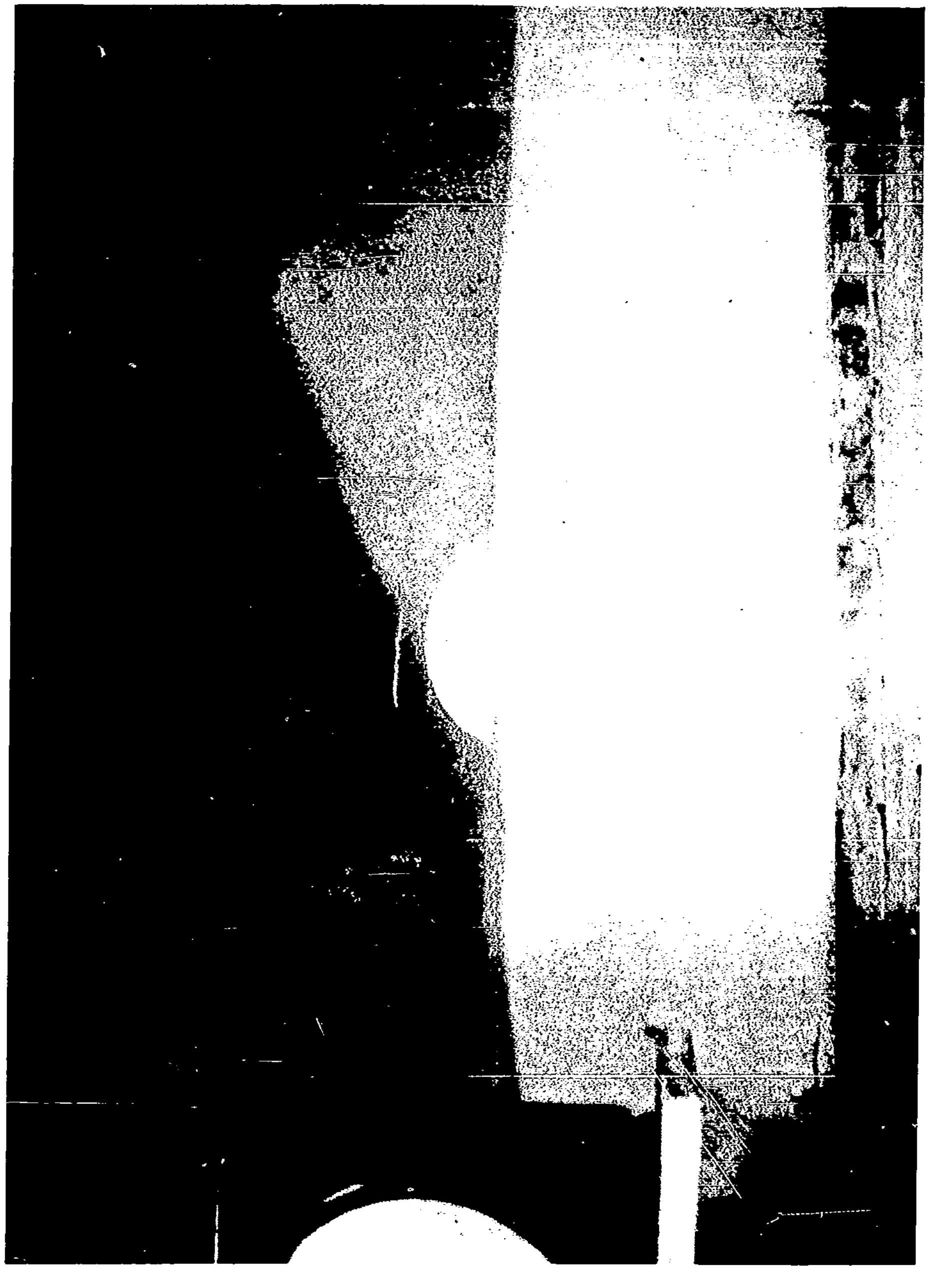

Figure 6. Removal by Suspended Transport (F = 11.2).

ANALYSIS OF RESULTS

The model study was severely limited by the existence of ripples of the same order in size as the model. Only two values of the sediment Froude number, F, could be obtained. The higher value, F = 11.2, corresponds to a gravity wave system generated by a severe storm; whereas, the lower value, F = 2.8, corresponds to a wave system generated in a moderate sea. Since the experimental method could not be employed for the intermediate range of F, the writers were forced to make a detailed analysis of the results of other scour studies. The results of two excellent studies, Laursen (5) and Rouse (6), of jet scour were analyzed (Appendix A). In neither of these studies was ripple formation a factor. Consequently both Laursen and Rouse were able to vary systematically the sediment Froude number. The sediment-transport functions (Appendix A, equations 11 and 16) form the basis for interpolating and extrapolating these model test results throughout the entire region of interest.

Scour-Hole Geometry

The scour hole formed around the cylinder is three-dimensional in form as shown in Figure 5. After Test 47, the scour hole was mapped by using a vertical point gage to determine the elevation. The point gage was located in various positions in the horizontal plane. From these measurements a contour map of the scour hole was prepared as shown in Figure 7. The scour-hole can be represented as an inverted frustum with the side slope equal to the angle of repose, ϕ , of the bed material. Using the volume computed from Figure 7, the diameter of the bottom surface (bottom of the scour hole) of the frustum is L + 0.24 D in which

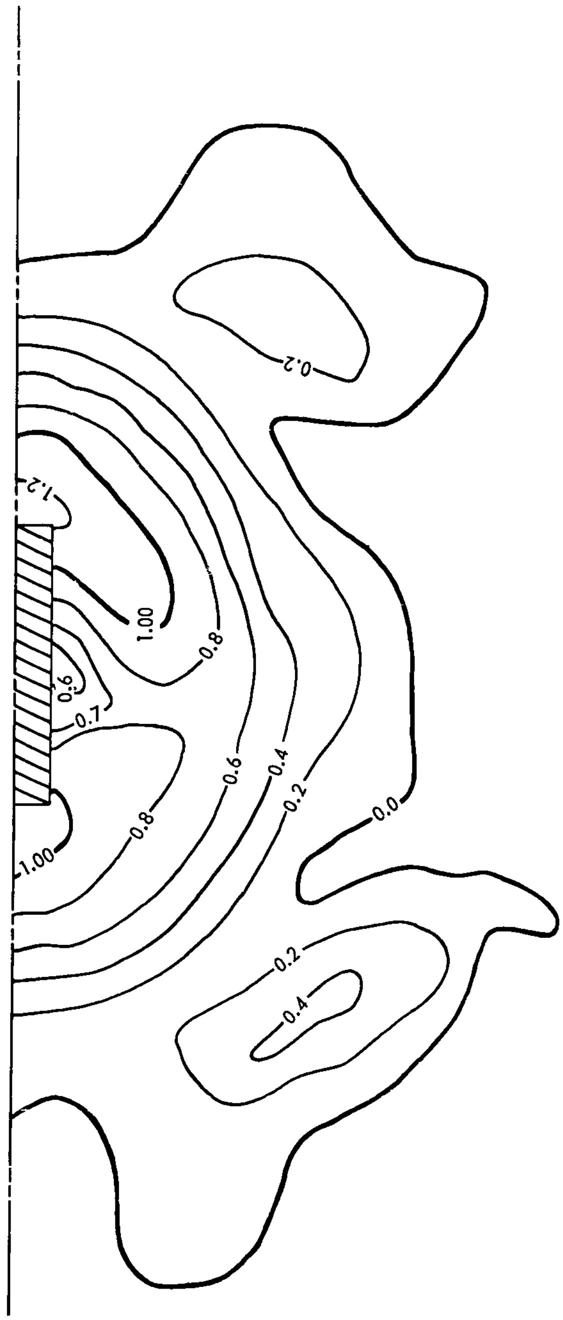

Figure 7. Contour Map of Scour Hole (Elevations given in D units).

L and D are the cylinder length and diameter, respectively. Using this representation the volume of the scour hole $\forall$, is related to the depth as follows,

$$\forall = \frac{\pi}{3} D^2 L \left(\frac{1}{(L/D)\tan^2\phi}\left(\frac{y_s}{D}\right)^3 + \frac{1.59}{\tan\phi}\left(\frac{y_s}{D}\right)^2 + (0.843)\left(\frac{L}{D}\right)\left(\frac{y_s}{D}\right) \right) \quad (3)$$

Since L/D is constant at a value of 4, equation (3) can be simplified to

$$\forall = D^2 L \left(\frac{0.262}{\tan^2\phi}\left(\frac{y_s}{D}\right)^3 + \frac{1.67}{\tan\phi}\left(\frac{y_s}{D}\right)^2 + 3.53\left(\frac{y_s}{D}\right) \right) \quad (4)$$

<u>Transport Functions</u>

The rate that bed material is removed from the scour hole is simply the time rate of change of $\forall$ with respect to time, t, that is

$$Q_{so} = \frac{d\forall}{dt} \quad (5)$$

in which Q_{so} is the sediment discharge out of the scour hole. Performing the operation indicated in equation (5) on equation (4).

$$Q_{so} = D^2 L \left(\frac{0.786}{\tan^2\phi}\left(\frac{y_s}{D}\right)^2 + \frac{3.34}{\tan\phi}\left(\frac{y_s}{D}\right) + 3.53 \right) \frac{d(y_s/D)}{dt} \quad (6)$$

Making equation (6) dimensionless,

$$\frac{Q_{so}}{U_m {y_s}^2} = \left(\frac{3.144}{\tan^2\phi} + \frac{13.4}{(y_s/D)\tan\phi} + \frac{14.14}{(y_s/D)^2} \right) \frac{d(y_s/D)}{d(U_m t/D)} \quad (7)$$

All of the quantities on the RHS of equation (7) can be evaluated from experimental results. As an aid in determining the slope, $d(y_s/D)/d(U_m t/D)$, the data were plotted on logarithmic paper. Only data for which the scour hole was well-formed, that is $y_s/D > 0.5$, were used in computing the transport function, $Q_s/U_m\ y_s^2$.

As explained previously the model tests were severely limited in regard to the variation of the sediment Froude number, $U_m/\sqrt{(s-1)\ gd}$. This limitation was overcome by analyzing the scour experiments of Laursen (5), Rouse (6), and Ahmad (7) (Appendix A). From these analyses, the writers concluded that the sediment transport functions of scour are of the following form

$$\frac{Q_{so}}{U_m\ y_o^2} = F\left(\frac{y_s}{D}\right)^n$$

for suspended transport and

$$\frac{Q_{so}}{U_m\ y_s^2} = F^8\left(\frac{y_s}{D}\right)^m$$

for bed-load transport. The exponents of the F terms were determined from the experiments of others. The exponents of y_s/D were determined using equation (7) and model-test data.

The resulting transport functions for a cylinder lying on the sea bed under an oscillatory wave are shown graphically in Figure 8 for suspended transport and in Figure 9 for bed-load transport. These functions are

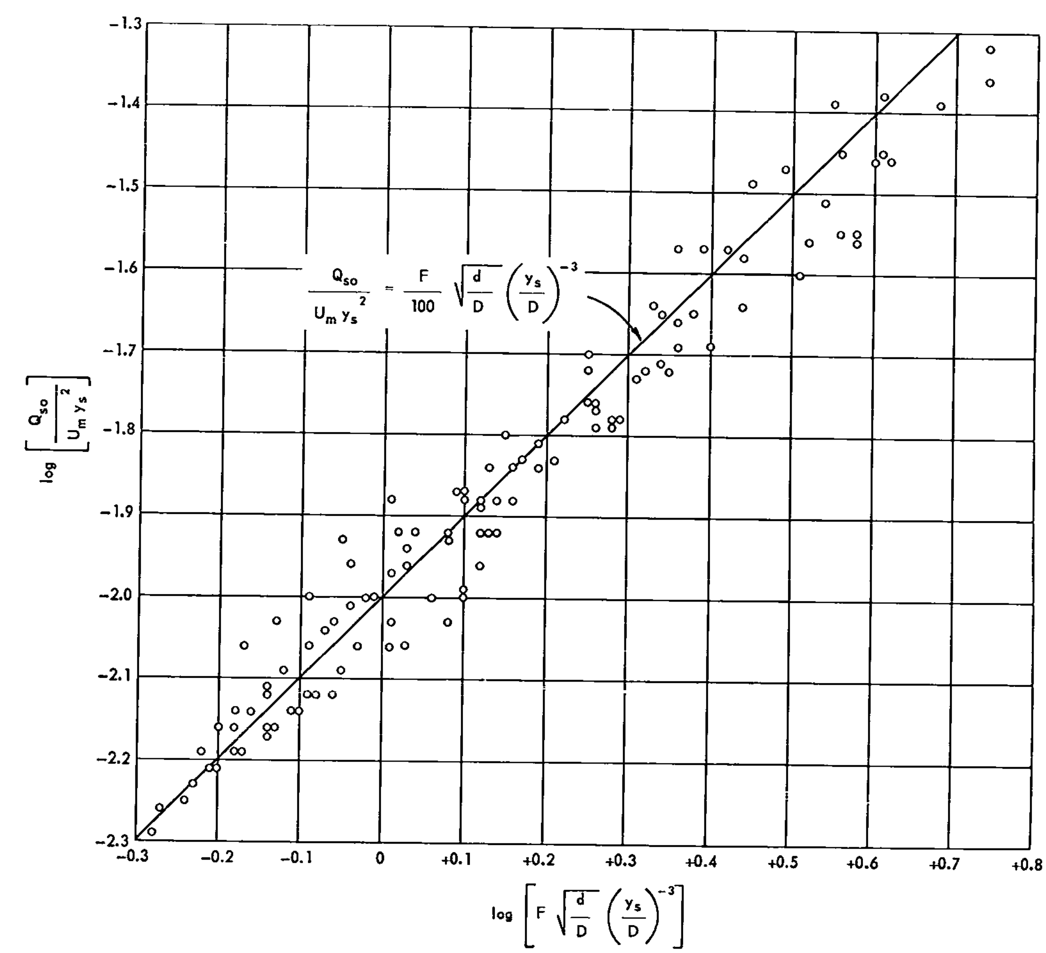

Figure 8. Suspended-Load Transport Function for a Horizontal Cylinder (L/D = 4).

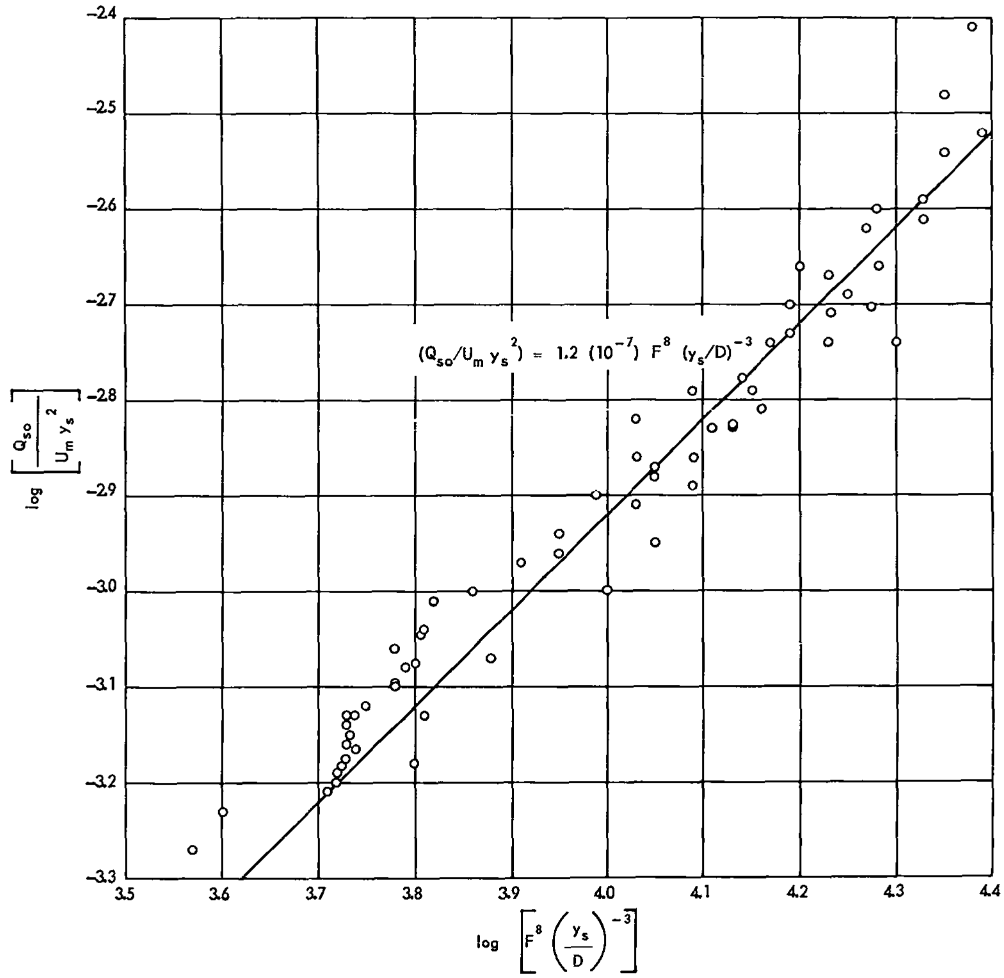

Figure 9. Bed-Load Transport Function for a Horizontal Cylinder (L/D = 4).

$$\frac{Q_{so}}{U_m \; y_s^2} = 0.01 \; F\left(\frac{d}{D}\right)^{1/2}\left(\frac{y_s}{D}\right)^{-3} \tag{8}$$

for suspended transport and

$$\frac{Q_{so}}{U_m \; y_s^2} = 1.2 \; (10^{-7}) \; F^8\left(\frac{y_s}{D}\right)^{-3} \tag{9}$$

for bed-load transport. Classification as to the mode of transport is required since the transport was by bed-load movement during model tests with F = 2.8 (Tests 25-39, inclusive) and the transport was by suspended load movement with F = 11.2 (Tests 5-13, inclusive, 41-47, inclusive, and 50).

Settlement Functions

Having obtained the sediment-transport functions, equations (8) and (9), equation (6) can be integrated to obtain the settlement functions. The reason for analyzing the problem in this apparently roundabout manner is that prior history is removed by evaluating a rate function. Thus the constant of integration obtained from the settlement-differential equation, equation (6), will be a function of the initial conditions. Substituting equation (8) into equation (6) and integrating

$$(10^{-2})F\sqrt{\frac{d}{D}}\left(\frac{U_m t}{D}\right) + K_s = \frac{0.786}{\tan^2\phi}\left(\frac{y_s}{D}\right)^4 + \frac{4.45}{\tan\phi}\left(\frac{y_s}{D}\right)^3 + 7.07\left(\frac{y_s}{D}\right)^2 \tag{10}$$

in which K_s is the constant of integration to be obtained using model-test data. A similar expression is obtained upon substitution of equation (9) into equation (6) and integrating, that is,

$$1.2\,(10^{-7})F^8\left(\frac{U_m t}{D}\right) + K_b = \frac{0.786}{\tan^2\phi}\left(\frac{y_s}{D}\right)^4 + \frac{4.45}{\tan\phi}\left(\frac{y_s}{D}\right)^3 + 7.07\left(\frac{y_s}{D}\right)^2 \qquad (11)$$

Again the constant of integration, K_b, can be obtained by using the model-test data.

Initial Conditions

The value of the constant of integration, K_s in equation (10) and K_b in equation (11), is dependent upon initial conditions. The obvious initial conditions are the initial burial, y_{s1}/D, and the initial orientation, α_o. Two other conditions, initial development of scour hole and initial scour under the cylinder, are not initial conditions but can be treated as initial conditions. The constants of integration were computed by substituting values of the experimental parameters, F, ϕ, and d/D and of the experimentally determined parameters, $U_m t/D$ and y_s/D, into equations (10) and (11) for each test. Only data for which the scour hole was fully developed, that is $y_s/D > 0.5$, were used in the determination of K. An arithmetic mean of the values of the K's for each datum point was used as the correct value of K for that test.

Initial Burial - The constant, K_b, of equation (11) was determined using the method described above using the data Tests 25, 27, 28, 29, 30, and 39 for which α_o was zero. The value of K_b was found to vary systematically with initial burial, y_{s1}/D. The values of K_b obtained from these six tests are shown in Figure 10. The constant of integration,

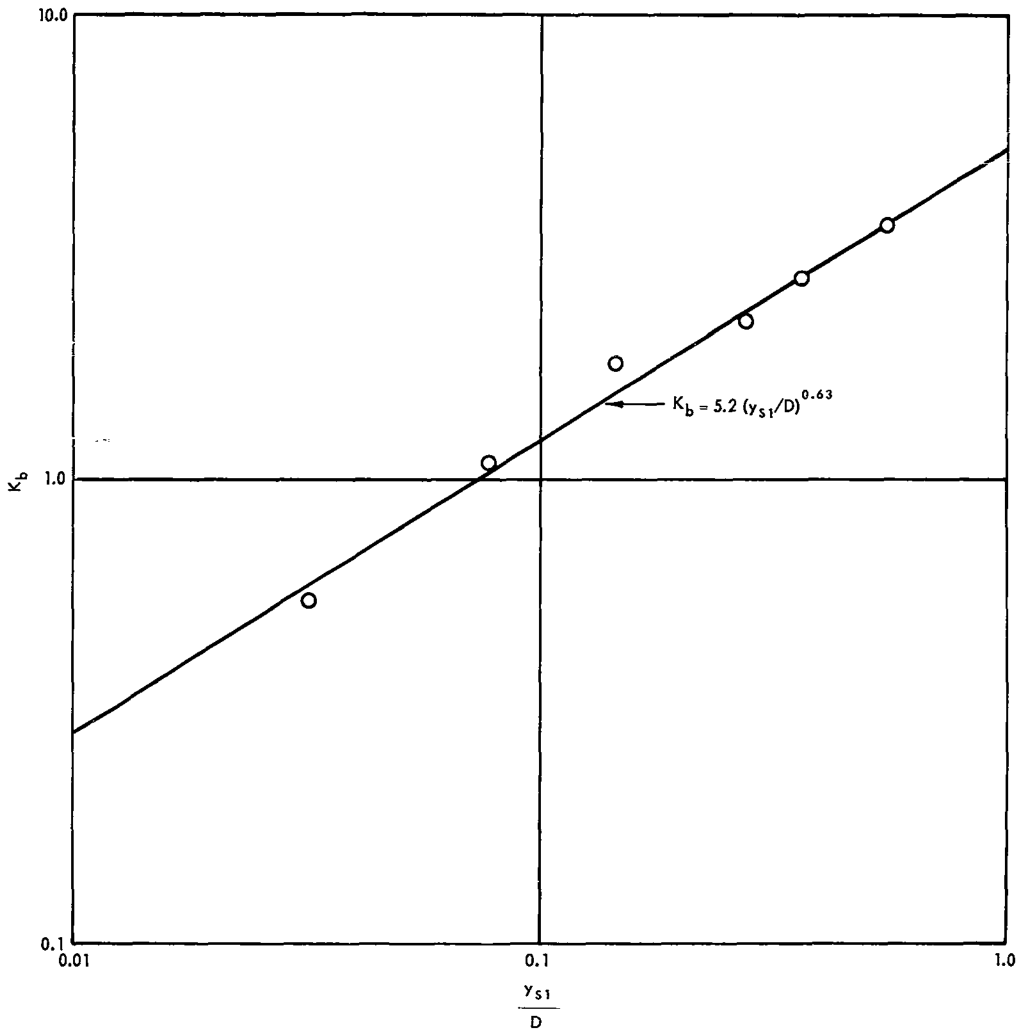

Figure 10. Constant of Integration for Bed-Load Transport.

K_b, in the settlement equation, equation (11), can be approximated by

$$K_b = 5.2 \left(\frac{y_{s1}}{D}\right)^{0.63} \tag{12}$$

A similar procedure was applied to the data of Tests 8, 13, 41-45, 47, and 50 in order to determine the constant of integration, K_s, in the settlement equation, equation (10), when the material was removed as suspended load. No variation in K_s could be detected with values of initial burial, y_{s1}/D, which ranged from 0.037 for Test 41 to 0.269 for Test 45. In fact for this series of tests the value of K_s was negligible. Hence the value of K_s in equation (10) was taken as zero for $\alpha_o = 0$ irrespective of initial burial.

Initial Orientation - Whenever the angle α between the cylinder axis is different from 0 or 90 degrees, the flow exerts a torque on the cylinder tending to decrease the angle. A cylinder placed at an initial orientation of α_o pivots in increments until α is zero. The settlement of the cylinder occurs in increments as the central support under the cylinder is scoured away. The central support under the cylinder also serves as a pivot for turning. The history of turning is shown in Figure 11 in which data from Tests 5-7, 10-12, and 14-18 are included. If α_o were less than 60 degrees, (a) the cylinder turned rapidly; (b) an ordinary scour hole developed; and (c) settlement occurred at essentially the same rate as a cylinder placed with $\alpha_o = 0$. Therefore, for values of α_o less than 60 degrees, the constants of integration required no adjustment for initial orientation.

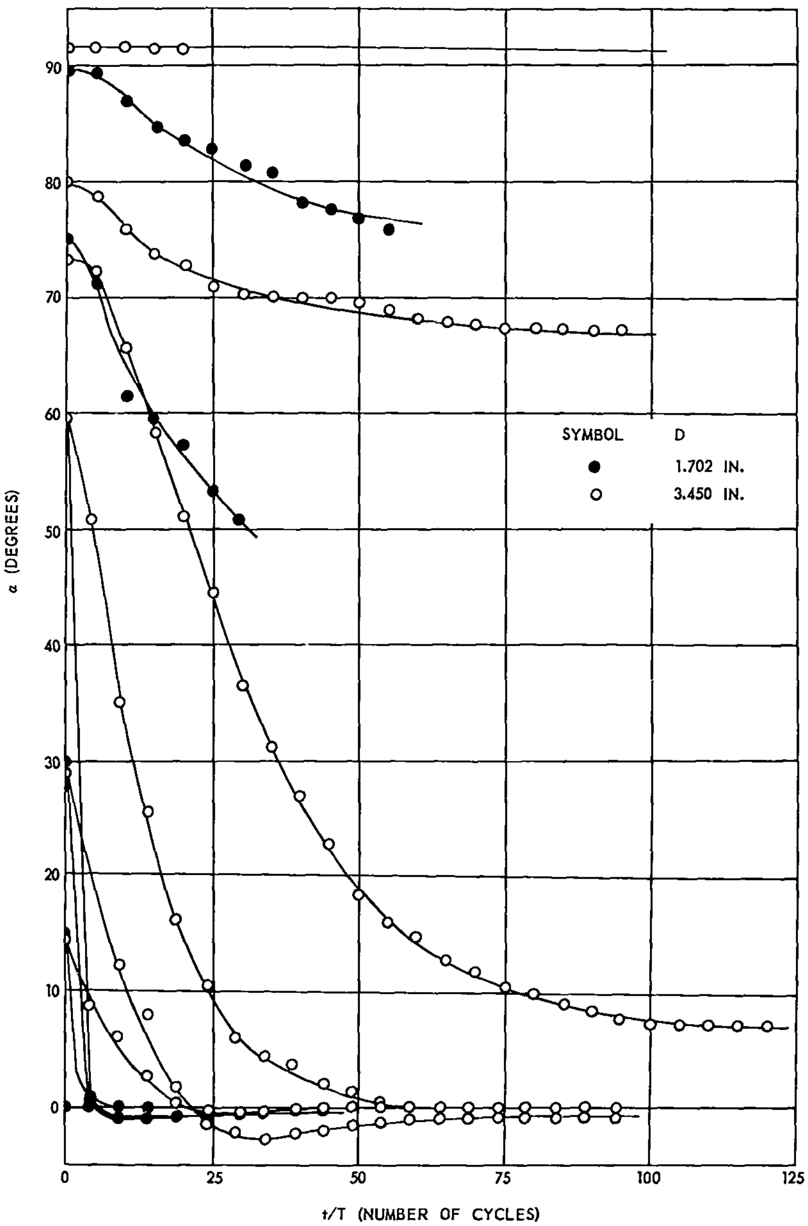

Figure 11. History of Turning.

With values of α_o greater than 60 degrees an abnormal scour hole developed for which the analysis based upon geometrically similar scour patterns would not apply. As a consequence, the analysis and the results presented in this report apply only if α_o is less than 60 degrees. This limitation is not serious because 2/3 of the cases of random placement can be analyzed and because the settlement rate is not drastically different for the remaining 1/3 of the cases.

Initial Development of the Scour Hole - The scour hole begins as two isolated scour holes at the ends of the cylinder. The scour hole continues to change in geometric configuration until the cylinder has settled about one-half a diameter, that is, until $y_s/D = 0.5$. The scour hole is geometrically similar with further settlement having the geometric features shown in Figures 5 and 7. The constant of integration, K_s in equation (10) and K_b in equation (11) is computed from experimental measurements taken after the scour hole is well-developed. Thus the value of the constant of integration determined in this manner reflects the effect of the development stage.

Initial Scour Under the Cylinder - Settlement of the cylinder occurs in steps. Scour occurs under the cylinder decreasing the width of the central support until the central support collapses. Then the process is repeated. Since scour under the cylinder is the direct cause of settlement, an exploratory study was conducted of flow under a partially imbedded cylinder. The results are presented in Appendix B. At a later date, the conclusion was reached that the settlement rate was limited to the rate at which material could be removed from the scour hole rather than from under the cylinder. Consequently, the final analysis presented in this report is based entirely upon the scour-hole geometry and rate of removal of material from the scour hole.

Summary - Two initial conditions have been analyzed in respect to the effect of these conditions upon the value of the constant of integration in the settlement equation. The initial burial, y_{s1}/D, was found to influence the constant of integration when the bed material was removed by bed-load transport. On the other hand no effect of initial burial could be discerned when the bed material was removed by suspended-load transport. The constant of integration was not influenced by the initial orientation, α_o, if α_o was less than 60 degrees. Even for values of α_o greater than 60 degrees following settlement functions are tolerable.

Inserting the constant of integration into equation (10),

$$\frac{F}{100}\sqrt{\frac{d}{D}}\;\frac{U_m t}{D} = \frac{0.786}{\tan^2\phi}\left(\frac{y_s}{D}\right)^4 + \frac{4.45}{\tan\phi}\left(\frac{y_s}{D}\right)^3 + 7.07\left(\frac{y_s}{D}\right)^2 \qquad (10a)$$

Equation (10a) is the settlement function for a horizontal cylinder of L/D = 4 when the removal of bed material is by suspended-load transport. All of the experimentally determined data from Tests 5-18, 41-47, and 50 are shown in Figure 12. Equation (10a) is also shown in Figure 12 in which a value of ϕ of 24 degrees was used. On account of the difficulty of solving equation (10a) for a value of y_s/D, Figure 13 has been prepared as a graphical aid for problem solving.

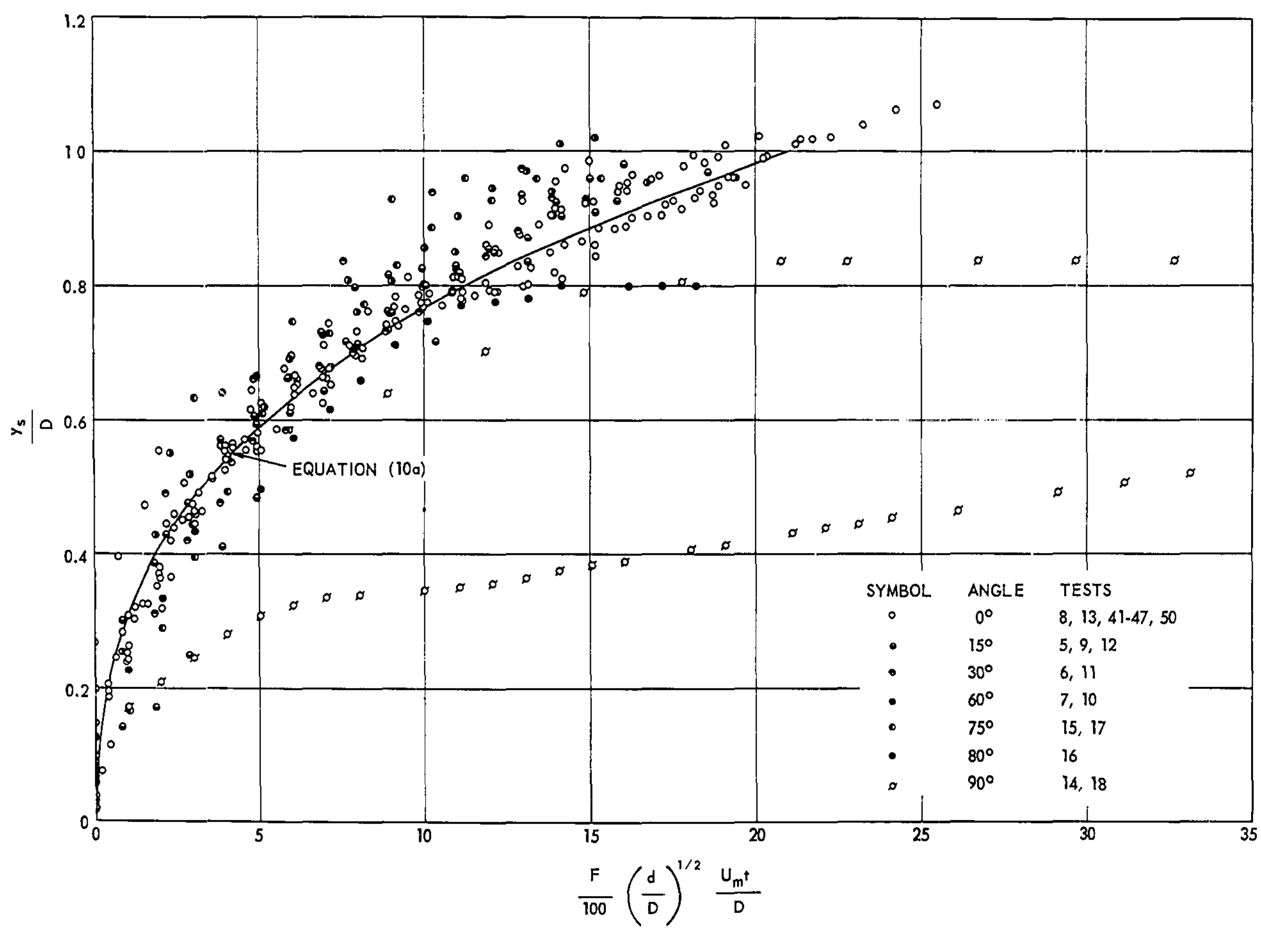

Figure 12. Experimental Results for Suspended-Load Transport Tests.

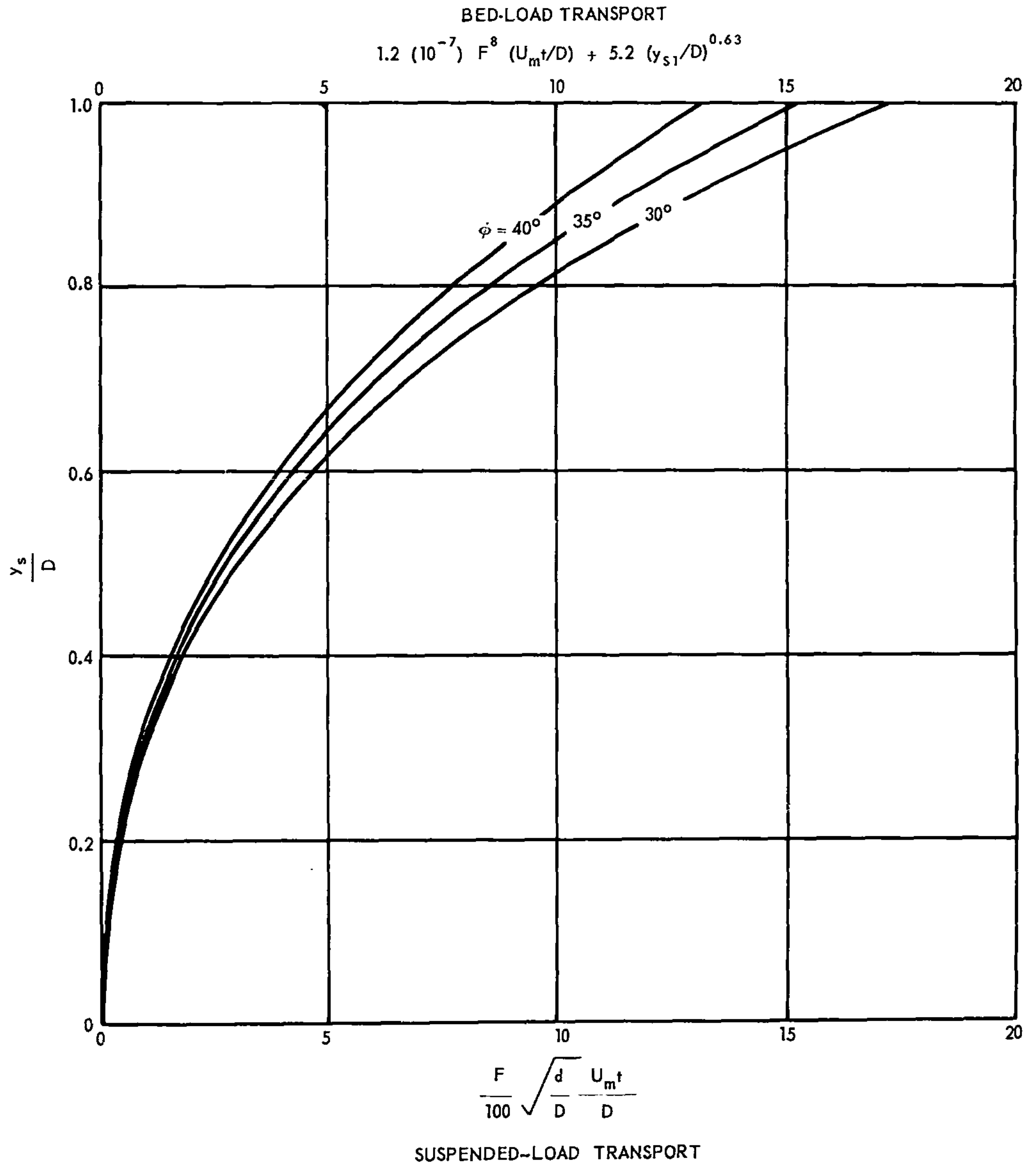

Figure 13. Settlement Function.

Inserting the constant of integration, equation (12) into equation (11),

$$1.2\,(10^{-7})F^8\left(\frac{U_m t}{D}\right) + 5.2\left(\frac{y_{s1}}{D}\right)^{0.63} = \frac{0.786}{\tan^2\phi}\left(\frac{y_s}{D}\right)^4 + \frac{4.45}{\tan\phi}\left(\frac{y_s}{D}\right)^3 + 7.07\left(\frac{y_s}{D}\right)^2 \qquad \text{(11a)}$$

Equation (11a) is the settlement function for a horizontal cylinder of L/D = 4 when the removal of bed material is by bed-load transport. All of the experimentally determined data from Tests 25-30, 37, and 39 are shown in Figure 14. Equation (11a) is also shown in Figure 14 in which a value of ϕ of 32.5 degrees was used. On account of the difficulty of solving equation (11a) for a value of y_s/D, Figure 13 has been prepared as a graphical aid for problem solving.

Range of Applicability

The question arises as to which of the settlement functions, equation (11a), is applicable in a given situation. The limit between bed load transport is found by equating the RHS of equation (8) to the RHS of equation (9) and then solving for the limiting value of F. Performing these operations

$$F(\text{limit}) = 5.04\ (d/D)^{1/14} \qquad (13)$$

The limiting value of F, $U_m \big/ \sqrt{(s-1)gd}$, is weakly dependent upon the sediment diameter, d, and the model diameter, D, as shown in the following table.

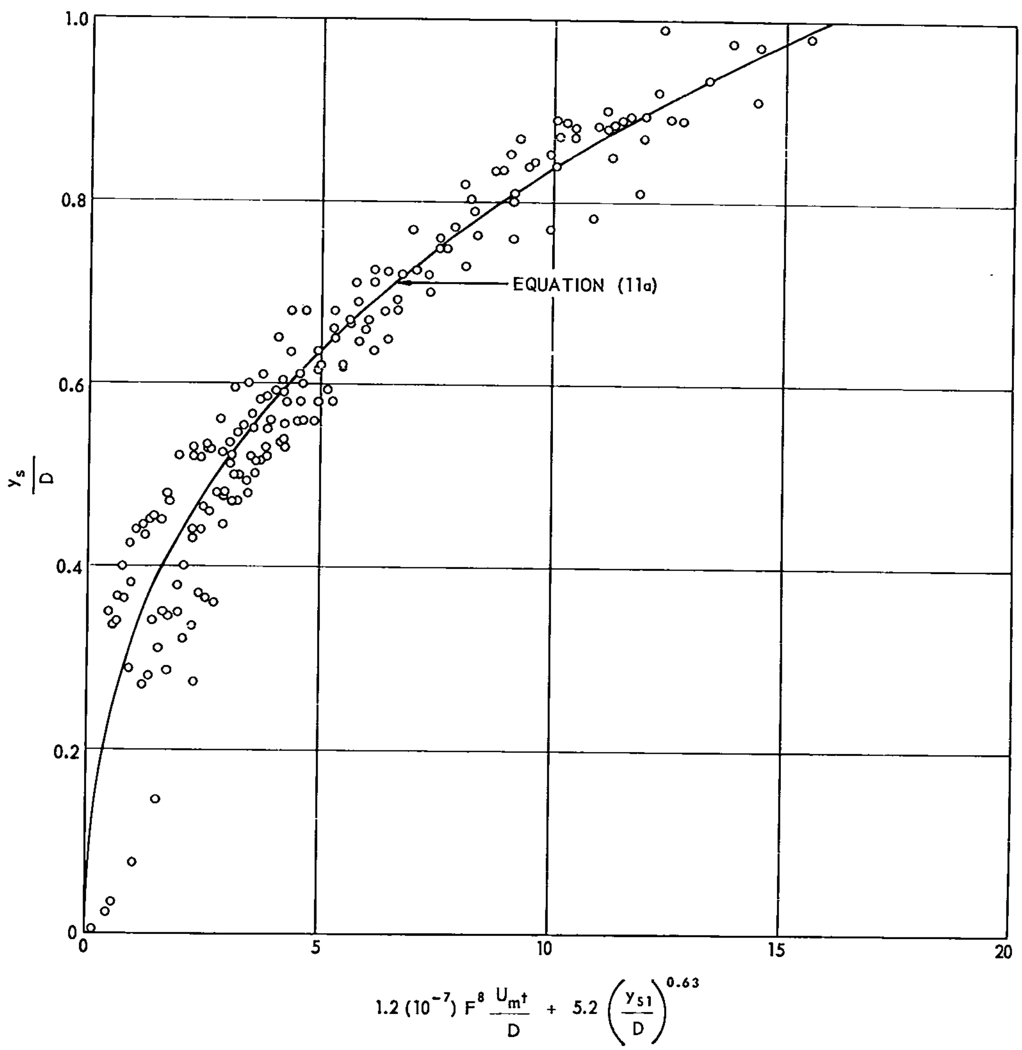

Figure 14. Experimental Results for Bed-Load Transport.

d(mm)	D(in)	F(limit)
0.2	18	2.9
0.4	18	3.0
0.6	18	3.1

If the value of F is greater than the value in the third column, suspended-load transport predominates and the settlement equation, equation (11a), applies. Conversely if the value of F is less than the value in the third column of the table, bed-load transport predominated and the settlement equation, equation (10a), applies.

As discussed previously, neither settlement equation, equation (10a) nor equation (11a), applies when the cylinder becomes part of the ripple system. In fact settlement ceases when the cylinder becomes part of the ripple system. The question then arises as to whether and under what conditions would a prototype mine become part of the ripple system. A rational criterion can be formulated based upon the concept that if the ratio of the ripple amplitude, η , to the cylinder diameter, D, exceeds a certain value, N, then the cylinder will be a part of the ripple system, that is if $\eta/D \geq N$. From Inman (2)

$$\lambda/\eta \approx 6 \tag{14}$$

In which λ is the wave length of the ripples. Also from Inman's results the following empirical equation can be derived

$$\lambda \approx 1200\ d \tag{15}$$

Combining equations (14) and (15) with the definition of N

$$N = \frac{\eta}{D} = 200 \left(\frac{d}{D} \right) \tag{16}$$

A reasonable estimate is that if $N \leq 1/4$ bed ripples will not influence the settlement. Using this criterion in equation (16) for an 18-in diameter cylinder, no influence of bed ripples is anticipated if the sediment diameter is less than 0.57 mm and if there is no initial burial.

If the mine has been subjected to a prior storm in which settlement occurred and after which the scour hole filled, the protusion above the bed would be less than D as assumed in the above example. If the mine had previously buried to $y_s/D = 0.5$, the protusion would be 9 in rather than 18 in. Again one might anticipate that, if the ripple height were one fourth of the protruded height, the mine would become part of the ripple system. Since equations (14), (15), and (16) are all linear relations bed-material diameter would simply be one half of 0.57 mm or 0.28 mm. In other words, if a mine had buried halfway as the result of a previous storm, if the scour hole were filled, if the bed-material diameter were greater than 0.28 mm, and if F were in the range of 2 to 10, the mine could be expected to become part of the ripple system with no settlement during the second storm. The implications are that if a mine does not become completely buried during the first storm after placement the mine is more likely to become a part of the ripple system in succeeding storms.

The range through which the settlement functions, equations (10a) and (11a) apply are summarized in Figure 15. The boundaries of the "no settlement" region were not established in this model study. The upper boundary was established from Manohar's (3) experimental results for the disappearance of ripples. The vertical boundary at $d = 0.57$ mm or 0.28 mm was established as explained above. The lower boundary is very approximately located on the basis of the incomplete tests mentioned in DISCUSSION OF RESULTS. The "no settlement" zone as shown in Figure 15 is qualitatively verified by the observations reported by Salsman and Talbert (8). They report a case in which two mines were located in proximity. The bed material surrounding one mine had a median diameter of 0.550 mm and the bed material surrounding the other had a mean diameter of 0.112 mm. Both mines were subjected to the same wave action. The mine resting on the coarser bed material became part of the ripple system whereas a normal scour pattern developed around the mine placed on the finer material.

Comparison with Prototype

The field tests conducted by the Navy Mine Defense Laboratory (USNMDL) during the winter of 1962-63 will be analyzed in order to compare observed field results with predictions based upon the model tests. The mines were dropped onto the sea bed and their settlement measured at various intervals. Some mines were repositioned by divers to the prone position ($y_s/D = 0$) after the measurements were recorded whereas other mines were left in their scour holes. Hence the effect of initial burial on settlement could be determined. The pressure signature on the sea bottom was recorded in order

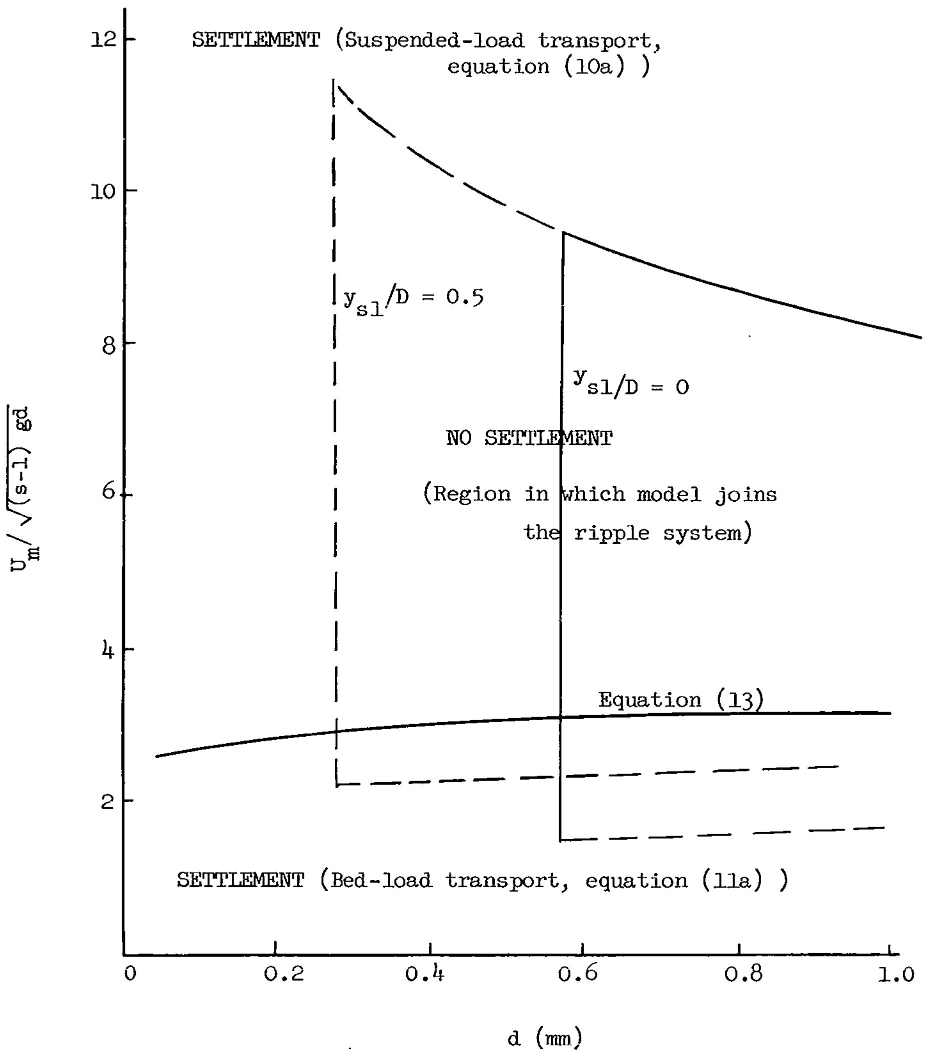

Figure 15. Range of Applicability of Settlement Functions for D = 18 in.

that the wave amplitude and bottom velocity could be determined. A total of three mines were placed on the sea bed at two sites, having water depths of 40 ft and 60 ft.

Bed Materials - The USNMDL took core samples of the bed materials at the two sites and ran size distribution analyses. The average size of the sediment at the bed is 0.221 mm for the 40-ft depth and 0.360 mm for the 60-ft depth. The sand will be assumed to have a density corresponding to that of quartz, i.e., in sea water, $s = 2.60$. The angle of repose will be assumed to be 35° for the larger sand and 30° for the smaller.

Mines - A MK-39 mine ($L = 88$ in, $D = 22.5$ in) was dropped at the 40-ft depth site on 21 December 1962, and removed on 27 March 1963. During this period the settlement of the mine was measured at intervals. Two MK-36 mines ($L = 71$ in, $D = 18.5$ in), referred to as A and B by USNMDL, were dropped at the 60-ft depth site on 12 October 1962. Mine B was repositioned during some of the visits made for settlement measurements while mine A was allowed to settle continually from 21 December. The mine at the 40-ft depth will be referred to as mine C for convenience. The dimensions of the mines and sediment characteristics at the mine sites are tabulated below:

Mine	Mine Length (L)	Mine Diameter (D)	Water Depth	Mean Sediment Diameter, d	Angle of Repose, ϕ (Assumed)
A	71 in	18.5 in	60 ft	0.360 mm	35 degrees
B	71 in	18.5 in	60 ft	0.360 mm	35 degrees
C	88 in	22.5 in	40 ft	0.221 mm	30 degrees

Sea Conditions - Personnel of the USNMDL have resolved a pressure spectrum and a bottom velocity spectrum from recorded bottom pressures at the 60-ft depth mine site. The velocity spectrum data were further analyzed and the workable results along with a letter of description were communicated by the USNMDL. In the letter of description:

> "..... the velocity estimates represent the amplitude A in $A\cos \omega t$ (where ω is the frequency of the peak in the spectrum). This amounts to replacing the original random spectral process by a single frequency constant amplitude process which has the same energy in the root mean square sense."

The bottom velocity amplitude A will be equated to U_m in the analysis of the field test results. The bottom velocity amplitude, U_m, and the peak frequency, ω , are tabulated below for the period between 2400 hours 18 February and 0300 hours 21 February. This period corresponds to the duration of a mild storm and constitutes the total active scouring time between 13 February and 28 February.

Date	Time	Bottom Velocity Amplitude U_m (in/sec)		Peak Frequency ω (cps)	
		Depth of Water		Depth of Water	
		40 ft d = 0.221 mm	60 ft d = 0.360 mm	40 ft	60 ft
18 Feb.	2400	3.934	2.161	0.1750	0.1667
19 Feb.	0300	5.169	3.165	0.1538	0.1500
	0600	5.566	3.878	0.1250	0.1250
	0900	9.584	6.720	0.1250	0.1250
	1200	9.604	7.204	0.1167	0.1167
	1530	8.304	5.934	0.1167	0.1083
	1800	6.744	5.098	0.1167	0.1167
	2100	5.546	4.206	0.1167	0.1167
	2400	5.565	4.231	0.1167	0.1167
20 Feb.	0300	5.011	3.820	0.1167	0.1167
	0600	4.583	3.420	0.1250	0.1167
	0900	4.002	3.004	0.1167	0.1167
	1200	3.241	2.424	0.1167	0.1167
	1500	3.011	2.237	0.1167	0.1167
	1800	2.437	1.741	0.1250	0.1250
	2100	2.147	1.516	0.1250	0.1250
	2400	1.957	1.293	0.1333	0.1250
21 Feb.	0300	1.943	1.220	0.1417	0.1333

Recorded Settlement - The position of each mine on both 13 February and 28 February are as listed below:

Mine	y_s/D	
	13 February	28 February
A	0.460	0.460
B	0.000	0.405
C	0.205	0.955

Predicted Settlement - Since the bottom velocity, U_m, varies with time the settlement functions will have to be evaluated by

$$(0.01)\sqrt{\frac{d}{D}}\int_0^t F\,\frac{U_m}{D}\,dt = \frac{0.786}{\tan^2\phi}\left(\frac{y_s}{D}\right)^4 + \frac{4.45}{\tan\phi}\left(\frac{y_s}{D}\right)^3 + 7.07\left(\frac{y_s}{D}\right)^2 \qquad (19a)$$

for suspended-load transport, and

$$1.2(10^{-7})\int_0^t F^8\,\frac{U_m}{D}\,dt + 5.2\left(\frac{y_{s.l}}{D}\right)^{0.63} = \frac{0.786}{\tan^2\phi}\left(\frac{y_s}{D}\right)^4 + \frac{4.45}{\tan\phi}\left(\frac{y_s}{D}\right)^3 + 7.07\left(\frac{y_s}{D}\right)^2 \qquad (19b)$$

for bed-load transport. The RHS of equations (19a) and (19b) is equal to the RHS of equation (10a) or (11a) which is graphically presented as the abscissa on Figure 13. Hence, upon evaluating the LHS of equations (19a) or (19b) the settlement, $\frac{y_s}{D}$, can be determined from Figure 13 for a given angle of repose, ϕ.

The variation in the bottom velocity, U_m, during the period of the storm is shown graphically in Figure 16 for the 40-ft water depth and in Figure 17 for the 60-ft water depth. Linear variation of U_m with time, t, is a reasonable representation of the experimental points as shown in Figures 16 and 17. The bottom velocity, U_m, and F will be represented mathematically by these straight lines in order that the LHS of equations (19a) and (19b) can be evaluated. Since the sediment Froude number, $F = U_m/\sqrt{(s-1)\,gd}$, the integrand of the LHS of equations (19a) and (19b) can be written as F^2 and F^9, respectively. For each interval on Figures 16 and 17, the sediment Froude number

$$F = a + bt$$

in which a is a dimensionless constant and b is a constant having the dimensions of sec^{-1}. The values of a and b for their various time intervals are tabulated below.

From		To		a	b (sec^{-1})	Time Interval, t (sec)
40-ft Depth:						
2400 hrs.	18 Feb.	0600 hrs.	19 Feb.	1.69	$3.29(10^{-5})$	$2.16(10^4)$
0600	19 Feb.	0900	19 Feb.	2.40	$1.60(10^{-4})$	$1.08(10^4)$
0900	19 Feb.	1200	19 Feb.	4.14	0	$1.08(10^4)$
1200	19 Feb.	2118	19 Feb.	4.14	$-5.20(10^{-5})$	$3.35(10^4)$
2118	19 Feb.	2400	19 Feb.	2.40	0	$9.72(10^3)$
2400	19 Feb.	2100	20 Feb.	2.40	$-2.08(10^{-5})$	$7.56(10^4)$

From		To		a	b (sec^{-1})	Time Interval, t (sec)
60-ft Depth:						
2400 hrs.	18 Feb.	0600 hrs.	19 Feb.	0.75	$2.58(10^{-5})$	$2.16(10^{4})$
0600	19 Feb.	0900	19 Feb.	1.31	$8.84(10^{-5})$	$1.08(10^{4})$
0900	19 Feb.	1200	19 Feb.	2.27	$1.50(10^{-5})$	$1.08(10^{4})$
1200	19 Feb.	2040	19 Feb.	2.44	$-3.25(10^{-5})$	$3.12(10^{4})$
2040	19 Feb.	2400	19 Feb.	1.42	0	$1.20(10^{4})$
2400	19 Feb.	2100	20 Feb.	1.42	$-1.26(10^{-5})$	$7.56(10^{4})$

The LHS of equations (19a) and (19b) can be readily integrated once the decision is made as to the mode of transport. The criterion for the mode of transport is equation (13), for which

$$F = 5.04 \left(\frac{d}{D} \right)^{1/14}$$

at transition. For values of F below $5.04 \left(\frac{d}{D} \right)^{1/14}$, the mode of transport is bed load; whereas for values of F greater than $5.04 \left(\frac{d}{D} \right)^{1/14}$, the mode of transport is suspended load. For mines A and B, which were placed in the 60-ft depth the mode of transport throughout the storm was bed load as $F \leq 2.44$. For mine A, which was placed in the 40-ft depth, the mode of transport was bed load up until 0654 hours on 19 February, suspended load from 0654 hours to 1836 hours 19 February, and bed load from 1836 hours 19 February throughout the remainder of the storm. The settlement of mines A, B, and C can now be predicted upon integration of the appropriate equations.

Mine A had an initial burial on 13 February of $\frac{y_{s1}}{D} = 0.460$. Upon considering the range of applicability of the settlement functions (Figure 15), mine A falls into the "no settlement" zone for the highest values of F. Since mine A would have been part of a ripple system during the period of highest velocities and, since the velocities during the remainder of the storm were quite low, no scour would be expected. On 18 February the settlement of mine A was $\frac{y_s}{D} = 0.460$, or no change. Mine A was evidently part of a ripple system during the time between 13 February and 28 February.

Mine B, however, did experience scour during the storm. It was repositioned to its prone position ($\frac{y_{s1}}{D} = 0$) on 13 February and on 28 February had settled to $\frac{y_s}{D} = 0.405$. Upon referring to Figure 15 for d = 0.360 mm, $\frac{y_{s1}}{D} = 0$, and the maximum value of F = 2.44, mine B is seen to be in the settlement region for bed-load transport. The cumulative value of equation (19b) is obtained by integrating the LHS between the limits of applicability of each straight-line segment for F and then summing the values of the integrals from the beginning of the storm. The cumulative value of equation (19b) and the corresponding values of $\frac{y_s}{D}$ are tabulated below. The predicted and observed settlement for mines A and B are also shown in Figure 17.

Mine C, which was placed in 40-ft of water, also underwent scour as $\frac{y_s}{D}$ was 0.205 on 13 February and 0.955 on 28 February. Mine C lies in the settlement region of Figure 15 as $\frac{y_{s1}}{D} = 0.205$, and d = 0.221 mm. The maximum value of F is 4.14, meaning that the mode of transport was suspended load during the most severe wave action of the storm. Suspended-load transport prevails for $F > 2.88$, corresponding to the period between

0654 hours and 1836 hours 19 February. This period is indicated on Figure 16. Inasmuch as mine C was initially buried on 13 February, and the mode of transport initially was bed load, the constant of integration, $5.2\left(\frac{y_{s1}}{D}\right)^{0.63}$, must be included in the LHS of equation (19b). The value of the constant of integration is 1.89. Between 2400 hours 18 February and 0654 hours 19 February, equation (19b) is utilized. From 0654 hours to 1836 hours 19 February the suspended-load equation (19a) is integrated and the values of the integrals cumulatively added to the value of equation (19b), obtained previously. From 1836 hours 19 February throughout the remainder of the storm equation (19b) is utilized as bed-load transport prevails. The cumulative values of the LHS of equation (19a) or (19b) and the associated values of $\frac{y_s}{D}$ are tabulated below. The predicted and observed settlement of mine C are shown in Figure 16.

Time		Cumulative Value of LHS of Equation (19a) or (19b)	Predicted Settlement $\frac{y_s}{D}$	Recorded Settlement $\frac{y_s}{D}$
Mine A:				
1200 hrs.	13 Feb.		Mine A is predicted to have been part of a ripple system	0.460
1200	28 Feb.			0.460
Mine B:				
1200 hrs.	13 Feb.	0	0	0
2400	18 Feb.	0	0	-
0600	19 Feb.	0.001	0.040	-
0900	19 Feb.	0.079	0.120	-
1200	19 Feb.	0.587	0.240	-
2040	19 Feb.	1.032	0.325	-
2400	19 Feb.	1.033	0.325	-
2100	20 Feb.	1.039	0.330	-
1200	28 Feb.	1.039	0.330	0.405

Time		Cumulative Value of LHS of Equation (19a) or (19b)	Predicted Settlement $\frac{y_s}{D}$	Recorded Settlement $\frac{y_s}{D}$
Mine C:				
1200 hrs.	13 Feb.	-	0.205(given)	0.205
2400	18 Feb.	-	0.205(given)	-
0600	19 Feb.	2.13	0.435	-
0654	19 Feb.	2.42	0.470	-
0900	19 Feb.	4.36	0.595	-
1200	19 Feb.	8.14	0.755	-
1836	19 Feb.	14.24	0.935	-
2118	19 Feb.	15.04	0.950	-
2400	19 Feb.	15.36	0.955	-
2100	20 Feb.	15.74	0.965	-
1200	28 Feb.	15.74	0.965	0.955

The agreement between predicted and observed settlement for mines A, B, and C is quite satisfactory. The settlement functions derived from the model tests appear to be suitable for prediction of prototype mine settlement.

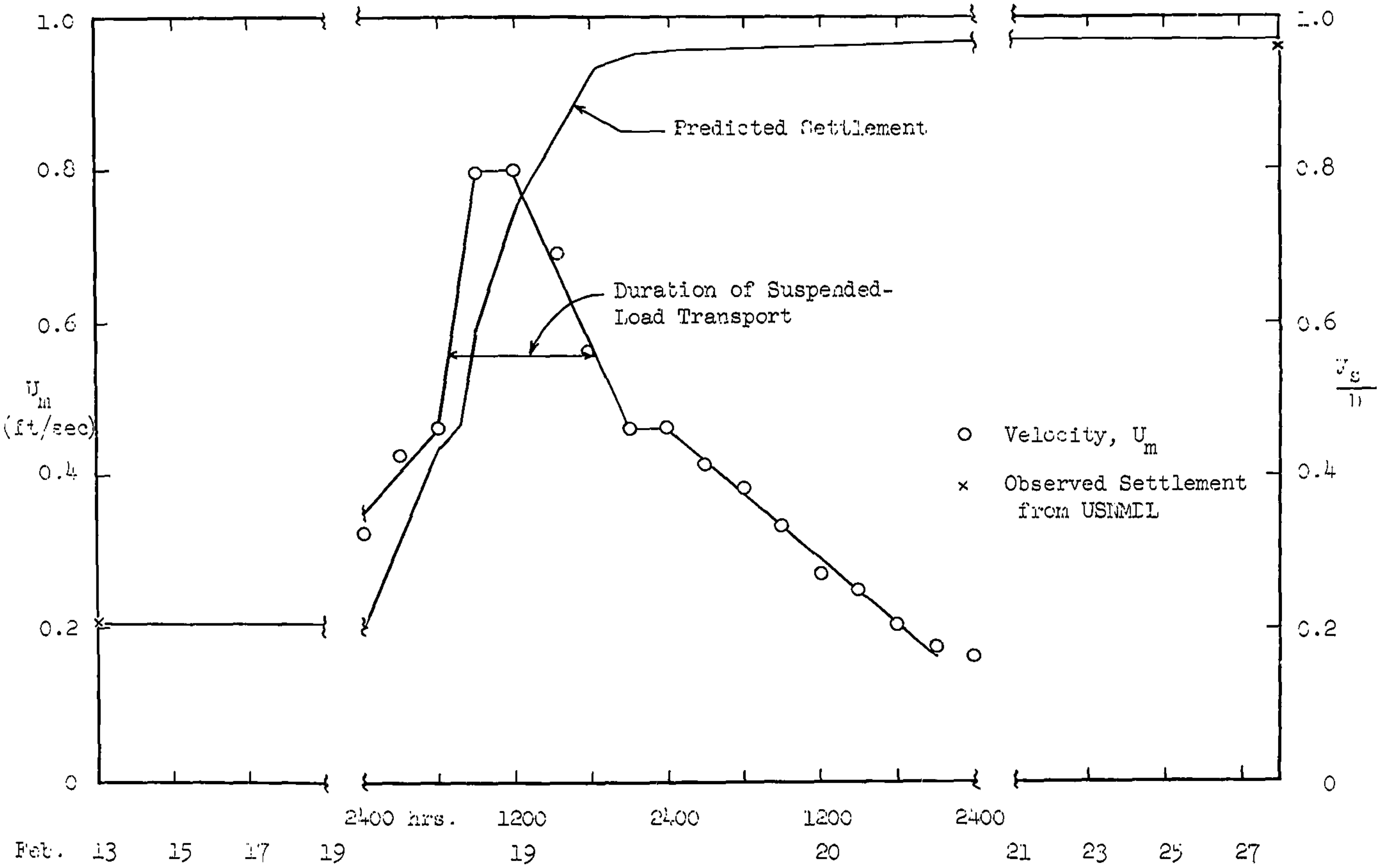

Figure 16. Comparison of Predicted and Observed Settlement of a Mark-39 Mine in 40-ft of Water.

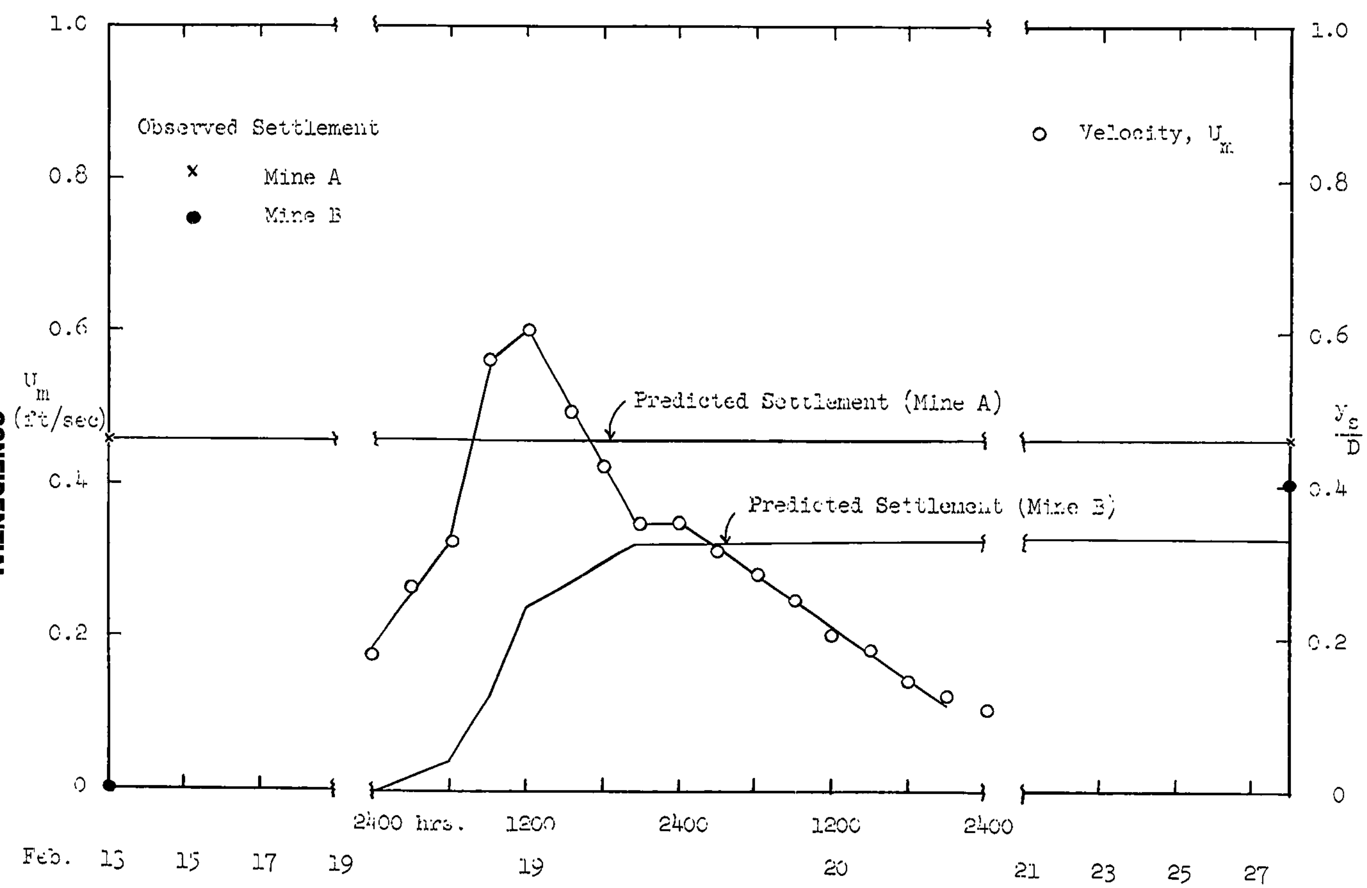

Figure 17. Comparison of Predicted and Observed Settlement of Two Mark-36 Mines in 60-ft of Water.

CONCLUSIONS

The following conclusions were reached from the model study and the associated analyses.

(1) Mine burial occurs as the result of (a) scour around the mine, (b) settlement of the mine into the scour hole, and (c) subsequent refilling of the scour hole between storms.

(2) Scour around the mine occurs either by the material being removed as bed load or as suspended load. The settlement functions have been formulated as equation (10a) for removal as suspended load and as equation (11a) for removal as bed load. The limit between these functions is given by equation (13).

(3) As settlement occurs, turning also occurs such that the mine axis coincides with the direction of the wave crest. The initial orientation has a minor effect upon settlement for initial angles of 60 degrees or less.

(4) Initial burial was found to have no effect upon settlement if the material is removed in suspension. Initial burial was found to have an effect upon settlement if the material is removed as bed load. The initial burial constitutes an initial condition which has been incorporated into the settlement function, equation (11a).

(5) Under certain flow conditions the mine becomes part of the ripple system on the bed. No settlement occurs when the mine is a pseudo ripple. The region of "no settlement" is poorly defined. An attempt to bound this region is shown in Figure 15 for an 18-in. diameter mine. Additional experimental studies will be required in order to more precisely establish the bounds.

REFERENCES

1. Carstens, M. R. and Martin, C. S., "Description and Calibration of Equipment," Technical Report No. 2, Project A-628, Engineering Experiment Station, Georgia Institute of Technology, January 1963.

2. Inman, D. L., "Wave Generated Ripples in Nearshore Sands," Technical Memorandum No. 100, Beach Erosion Board, U. S. Corps of Engineers, October 1957.

3. Manohar, M., "Mechanics of Bottom Sediment Motion due to Wave Action," Technical Memorandum No. 75, Beach Erosion Board, U. S. Corps of Engineers, June 1955.

4. Menard, H. W., "Sediment Movement in Relation to Current Velocity," Jour. Sed. Petrol., Vol. 20, 1950, pp. 148-160.

5. Laursen, E. M., "Observations on the Nature of Scour," Proceedings, 5th Hydraulics Conference, State University of Iowa, Bulletin 34, pp. 179-197.

6. Rouse, H., "Criteria for Similarity in the Transportation of Sediment," Proceedings, 1st Hydraulics Conference, State University of Iowa, Bulletin 20, 1940, pp. 33-49.

7. Ahmad, M., "Experiments on Design and Behavior of Spur Dikes," Proceedings, Minnesota International Hydraulics Convention, 1953, pp. 145-159.

8. Salsman, G. G., and Tolbert, W. H., "The Effects of Oscillatory Wave Motion and Tidal Currents on Cylindrical Ground Mines (U)," U. S. Navy Mine Defense Laboratory, Report No. S-8, July 1961, CONFIDENTIAL.

9. Lamb, H., Hydrodynamics, Dover Publications, 6th Ed., New York, 1932, p. 369.

APPENDIX A

SCOUR

M. R. Carstens and C. S. Martin

Scour is the excavation and removal of bed material by water in motion. A general mathematical expression can be formulated from the principle of conservation of mass which encompasses all scouring situations

$$Q_{so} - Q_{si} = \frac{d\forall}{dt} \tag{1}$$

In equation (1), Q_{so} is the rate that sediment is being removed from the scour hole, Q_{si} is the rate that sediment is being transported into the scour hole, $\forall$ is volume of the scour hole, and $d\forall/dt$ is the rate of change of $\forall$. A uniform stream such as a canal section is stable when the LHS of equation (1) is zero. A canal is scouring when the capacity of the stream to excavate and remove sediment is greater than the rate of sediment inflow. In such a case $Q_{so} > Q_{si}$ for which $d\forall/dt > 0$. The increase in volume $\forall$ of a reach is accomplished by a degradation of the bed and/or an increase in the canal width.

Localized scour occurs in the vicinity of obstructions placed in the flow. The increase in velocity adjacent to an obstruction is accompanied by an increased capacity to carry sediment as compared with unobstructed areas of the bed. In many situations a scour hole adjacent to the obstruction will occur as a result of this localized increase of capacity to excavate and remove bed material.

The analysis of localized scour can be simplified by considering only the case in which sediment transport into the scour hole is negligible. In this case the sediment-transport rate out, Q_{so}, is equal to the rate of change of scour-hole volume. It follows from equation (1) that

$$\forall = \int_{o}^{t} Q_{so} \; dt \qquad (2)$$

The analysis of scour can be systematized by considering separately (a) the beginning, (b) the active phase, and (c) the termination. Both the beginning and termination of scour are dependent upon the condition of incipient motion of the bed particles. The active phase of scour is concerned with the scour-hole geometry and the sediment-transport function.

Scour-Hole Geometry

The mathematical description of scour-hole geometry in unconsolidated materials is greatly simplified because the angle between the sides of the hole and the horizontal is the angle of repose, Φ, of the bed material. Hence the scour-hole volume is proportional to the depth squared, y_s^2, in a two-dimensional case and to the depth cubed, y_s^3, in a three-dimensional case. From equation (1) with no sediment inflow

$$q_{so} \propto y_s \; \frac{dy_s}{dt} \qquad (3)$$

for a two-dimensional hole and

$$Q_{so} \propto y_s^2 \frac{dy_s}{dt} \tag{4}$$

for a three-dimensional hole.

An excellent example which illustrates the comparative ease of formulating a scour-hole geometry function has been reported by Rouse (1). In Rouse's experiment a submerged two-dimensional jet was directed down a vertical wall into an originally level sand bed. As would be expected the measured scour holes were geometrically similar at successive times. The scour hole at any time had essentially the configuration shown in Figure 1.

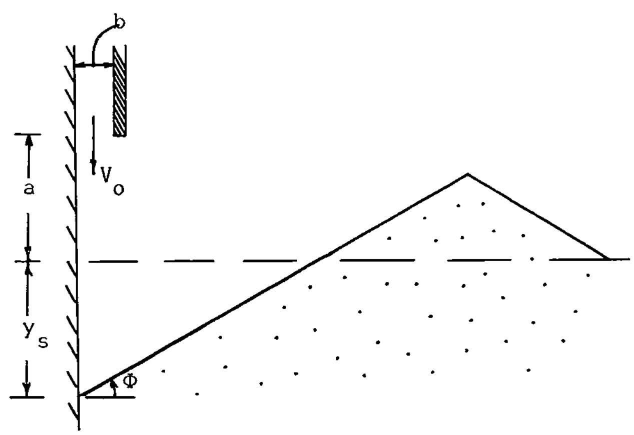

Figure 1. Scour Hole of Rouse's Experiment

From Figure 1 and equation (3)

$$q_{so} = \frac{d\maltese}{dt} = \left(1 + \frac{1}{\sqrt{2}}\right)\left(\frac{1}{\tan \Phi}\right) y_s \frac{dy_s}{dt} \tag{5}$$

in which the scour hole extends to the crest of the dune.

A second example of two-dimensional scour is reported by Laursen (2). Laursen's experiments were very similar to Rouse's except that the two-dimensional jet was directed over the top of an originally level bed. The scour hole at any time had essentially the configuration shown in Figure 2.

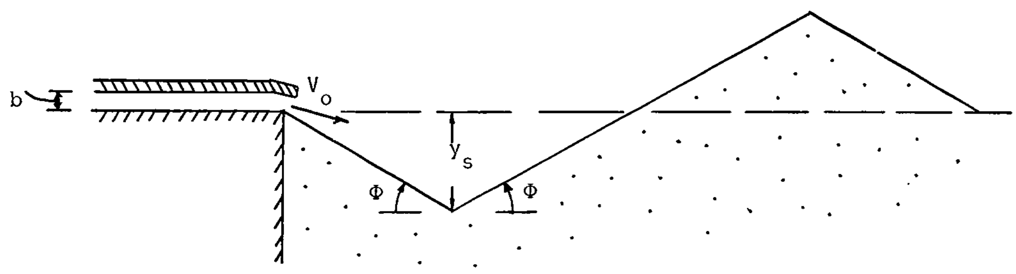

Figure 2. Scour Hole of Laursen's Experiment

From Figure 2 and equation (3)

$$q_{so} = \frac{d\forall}{dt} = \frac{4}{\tan \Phi} \; y_s \; \frac{dy_s}{dt} \qquad (6)$$

in which the scour hole extends to the crest of the dune.

An example of three-dimensional scour is reported by Ahmad (3). In one experiment, Ahmad placed a vertical plane wall in otherwise uniform open-channel flow. The scour hole in the movable bed can be closely approximated by an inverted cone with the apex of the cone at the end of the wall as in Figure 3.

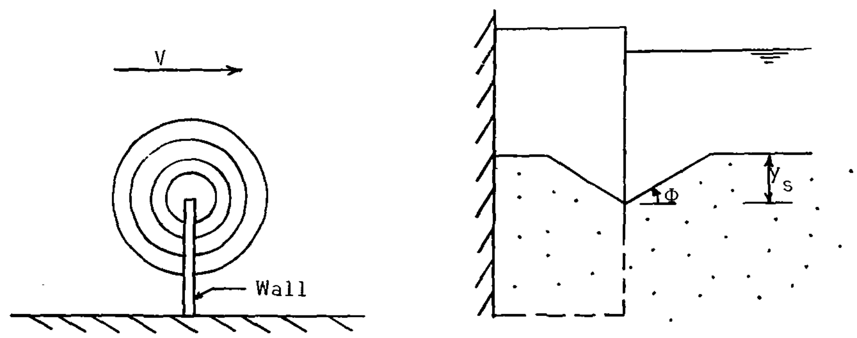

a. Top View

b. Side View in Plane of Wall

Figure 3. Scour-Hole of Ahmad's Experiment

From Figure 3 and equation (4)

$$Q_{so} = \frac{d\forall}{dt} = \frac{\pi}{\tan^2\Phi} y_s^2 \frac{dy_s}{dt} \tag{7}$$

Sediment-Transport Functions

General

In order to apply equation (2) for prediction of scour-hole development with time, the sediment-transport rate Q_{so} must be formulated as a function of fluid properties, flow characteristics, sediment properties, and scour-hole development. The sediment-transport functions which have been formulated for uniform streams are not suitable as transport functions for localized scour for two reasons. First, the uniform-stream transport functions are based upon the average shearing stress between the bed and the fluid. Inasmuch as localized scour occurs in non-uniform flow regions, the spatially-varying shear stress at the surface of the bed is difficult to predict. Second, localized scour will occur where the fluid has been accelerated and the boundary-layer thickness is negligible in contrast to uniform stream flows.

With a negligible boundary layer, the transport function can be formulated qualitatively without reference to the fluid viscosity.

The drag force, $\vec{F}_D$, of the fluid on the particle

$$\vec{F}_D \propto d^2 \rho V^2 \tag{8}$$

in which ρ is the fluid density, and V is the fluid velocity at the top of the particle.

The resistance of particles to motion can readily be determined by observation of the angle of repose Φ of a submerged pile of the bed material in quiescent water. The force of gravity on a particle down the face of the pile is resisted by the particle-to-particle reactions of adjacent particles. Thus for particles of diameter, d,

$$\vec{F}_r \propto (\gamma_s - \gamma) d^3 \sin \Phi \tag{9}$$

in which $\vec{F}_r$ is the resisting force, γ_s is the specific weight of the particles and γ is the specific weight of the water.

The local sediment transport rate ΔQ_s will be a function of the ratio of the motivating force, $\vec{F}_D$, to the resisting force, $\vec{F}_r$. Since the motivating force $\vec{F}_D$ is proportional to the fluid inertial force, equation (8), and the resisting force is proportional to the gravity force on the particle, equation (9), the ratio of the two forces is a sediment Froude number

$$F = V / \sqrt{(s-1)gd}$$

Thus

$$\Delta Q_s = f (F) \quad (10)$$

The sediment Froude number, F, and local sediment transport rate, ΔQ_s, will vary over the surface of the scour hole. The greatest rate of transport will occur where the fluid velocity is greatest which consequently will be the position of greatest scour depth. Since the transport capacity will decrease away from the position of greatest depth, y_s, much of the material scoured at the bottom will deposit on the sides of the scour hole and slide down toward the bottom. Hence the net transport rate Q_{so} out of the hole is the transport out of the periphery of the hole. As the scour hole deepens, the lateral limit of the hole moves further from the flow disturbance. As a result the transport capacity at the edge of the hole decreases as y_s increases.

Thus

$$Q_{so} = f (F , y_s, \text{geometry}) \quad (11)$$

in which the variable, geometry, pertains to the geometry causing the flow disturbance.

A different process of removal might be anticipated either when F is very large or at the beginning of scour when the hole is small. As the water flows over the bed material, some material may be transported vertically as suspended material. If this material leaves the scour hole without being in contact with the bed at the rim of the hole, the functional relation, equation (11), would still be applicable but the function, *per se*, would be different. In other words, different sediment-transport functions are anticipated for removal by suspended load through the top than for removal by bed load over the rim of the scour hole.

Analysis of Scour Experiments

Sediment-transport functions can be formulated from the jet-scour experiments of Laursen (2). The scour-hole geometry is shown schematically in Figure 2. The results are presented such that the depth of scour, y_s, as a function of time, t, can be readily determined for each of the 17 runs. The jet velocity was varied from run to run. The side-elevation view of the scour hole was obtained photographically at successive times during a run. A set of runs was repeated for each of three sand sizes. Using Laursen's results and equation (6), the sediment-transport rate was calculated by the writers. The calculated results are presented in Figures 4 and 5.

In analyzing Laursen's results, different modes of transport were found. During the earlier portions of 15 runs and during the entire run with the finest sand and the highest velocity, the sediment-transport rate was found to be independent of scour-hole depth, y_s; whereas during the later portions of the 15 runs and during the entire run with the coarsest sand and lowest velocity, the sediment-transport rate was found to be dependent upon the value of y_s.

The writers' interpretation of this finding is as follows. In the vicinity where the jet impinges on the bed, the bed material is excavated and thrown into suspension. This suspended material is trans-

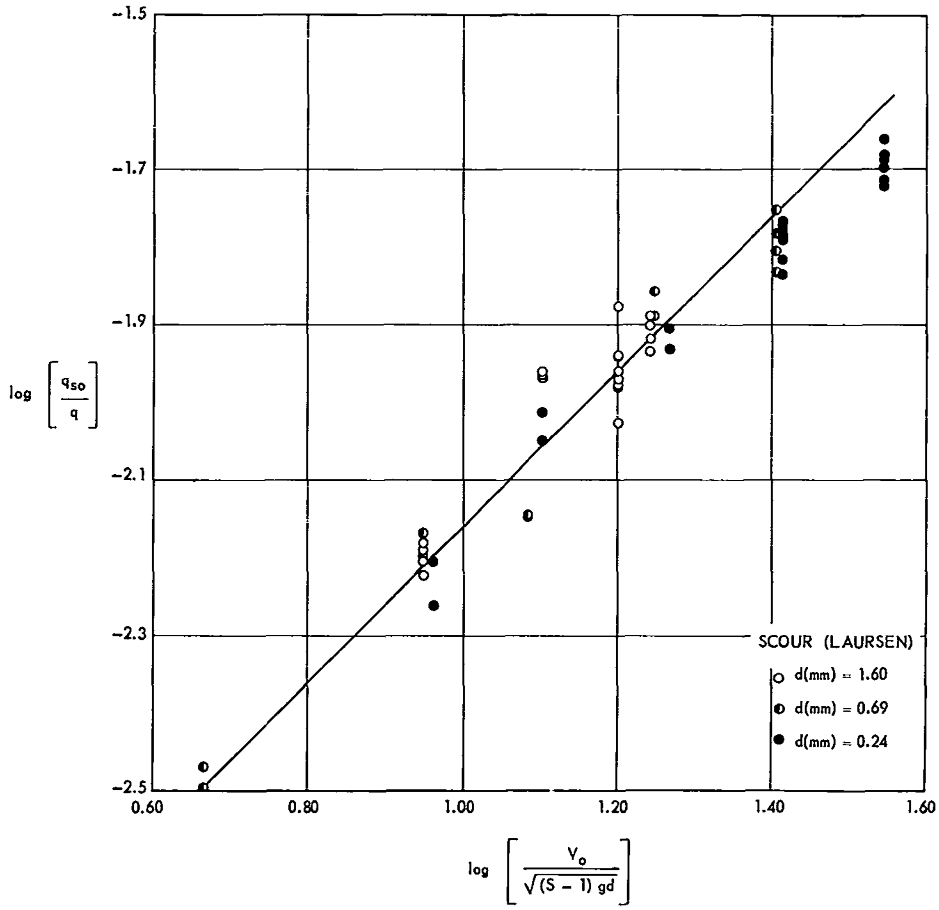

Figure 4. Sediment-Transport Function for Laursen's Suspended-Load Mode of Transport.

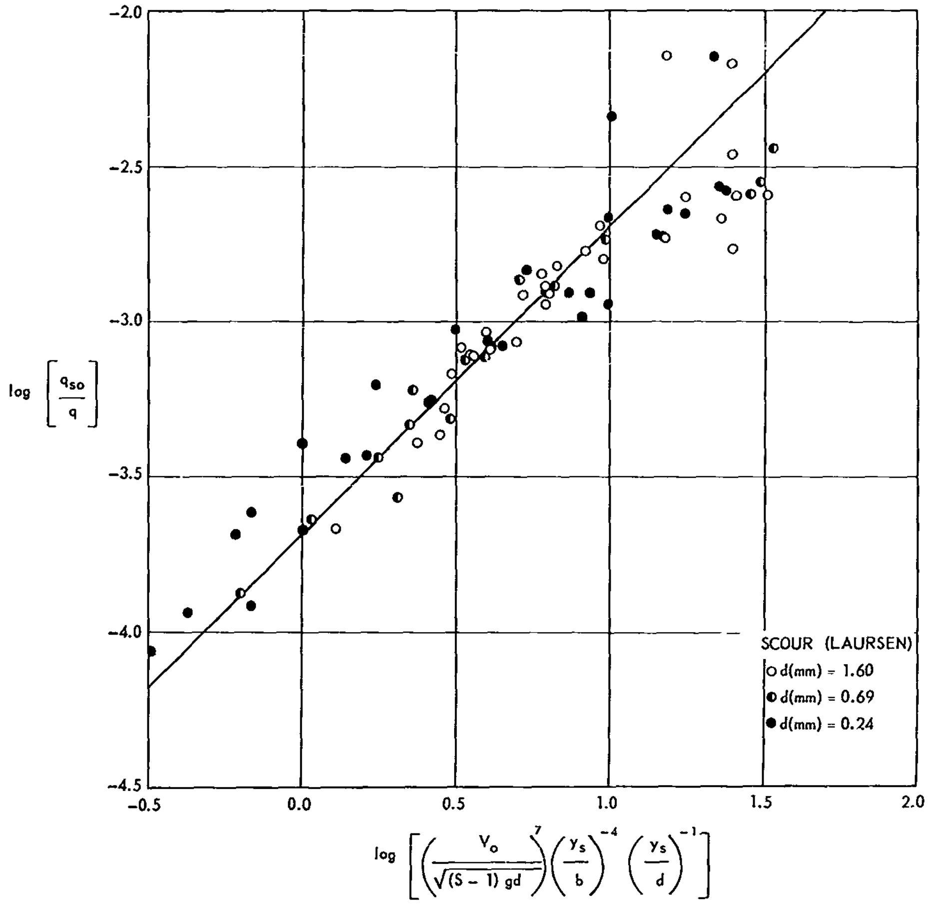

Figure 5. Sediment-Transport Function for Laursen's Bed-Load Mode of Transport.

ported away from the area of jet impingement while settling back to the bed. During the earlier portion of the runs, the scour hole is small enough for the material to be carried out of the hole without contacting the bed. In this situation the transport rate, q_{so}, is directly proportional to the rate at which the jet can excavate material and is independent of y_s. The excavation function can be approximated from Figure 4 as

$$\frac{q_{so}}{q} = 7\ (10^{-4})\ F_o \tag{12}$$

in which F_o is the sediment Froude number based upon the jet velocity, V_o.

As the scour hole deepens and the dune crest moves further from the jet-impingement area, the suspended material settles to the bed before being transported over the crest. In this case the transport out of the hole is bed-load transport over the crest. Since the jet diffuses in traveling over the scour-hole wall the bed-load transport capacity decreases as the dune crest moves further from the jet-impingement area. The bed-load transport function can be approximated from Figure 5 as

$$\frac{q_{so}}{q} = 2\ (10^{-4})\ F_o^{7}\left(\frac{y_s}{b}\right)^{-4}\left(\frac{y_s}{d}\right)^{-1} \tag{13}$$

in which d is the mean diameter of the bed particles.

A transition region exists between the suspended-load transport and bed-load transport conditions. In the transition region, part of the excavated material is transported out of the hole as suspended load and part as bed load. The transition region is surprisingly narrow.

Ignoring the transition region completely, the limits of equation (12) are

$$0 < y_s/b < 0.78\ (d/b)^{1/5}\ F_o^{\ 6/5}$$

and the limit of equation (13) is

$$y_s/b > 0.78\ (d/b)^{1/5}\ F_o^{\ 6/5}$$

Utilizing equations (12) and (13), equation (6) can be integrated to obtain the scour-hole depth as a function of time. Assuming y_s is zero when t is zero, the suspended load scour function is of the form

$$y_s = k_1 t^{1/2} \tag{14}$$

If y_s exceeds the limits stated above then both the suspended-load transport and the bed-load transport functions must be employed in the integration from which a scour function of the form

$$y_s = \left[k_2 t - k_3\right]^{1/7} \tag{15}$$

is obtained. The point to be emphasized here is that the scour depth at any time is dependent upon the history. In Laursen's experiments the change from a suspended-load mode of removal to a bed-load mode of removal results in a complicated scour-time function, equation (15).

Sediment-transport functions can also be formulated from the jet scour experiments of Rouse (1). The scour-hole geometry is shown schematically in Figure 1. Rouse's experiments differ from Laursen's in the following respects: (a) the two-dimensional jet was directed vertically downward onto the bed, (b) the progress of scour was recorded by wax-pencil marking on the glass wall of the flume, and (c) one-half scale tests were performed in which all pertinent geometric dimensions were halved except for the sand size. Rouse observed two distinct flow patterns which he called minimum jet deflection and maximum jet deflection. With minimum jet deflection the main stream followed up the scour-hole slope. With maximum jet deflection, the main stream separated from the scour hole forming a large eddy with return flow down the wall parallel to the jet.

Using Rouse's results and equation (5) the sediment-transport rate was calculated by the writers. The calculated results are presented in Figure 6 for minimum jet deflection and in Figure 7 for maximum jet deflection. The sediment-transport function for minimum jet deflection can be approximated, Figure 6, as follows

$$\frac{q_{so}}{q} = 2.5\ (10^{-6})\ F_o^{\ 8} \left(\frac{y_s}{b} \right)^{-5} \tag{16}$$

Similarly the sediment-transport function for maximum jet deflection can be approximated, Figure 7, as follows

$$\frac{q_{so}}{q} = (10^{-2})\ F_o^{\ 8} \left(\frac{y_s}{b} \right)^{-10} \tag{17}$$

The condition of maximum jet deflection occurred initially and then switched to the condition of minimum jet deflection when

$$\frac{y_s}{b} = 0.064\ \ F_o^{\ 3} \left(\frac{d}{b} \right) \tag{18}$$

Both the initial sediment-transport function, equation (17), and the later sediment-transport function, equation (16), appear to be bed-load functions. This conclusion is reached by comparison with the

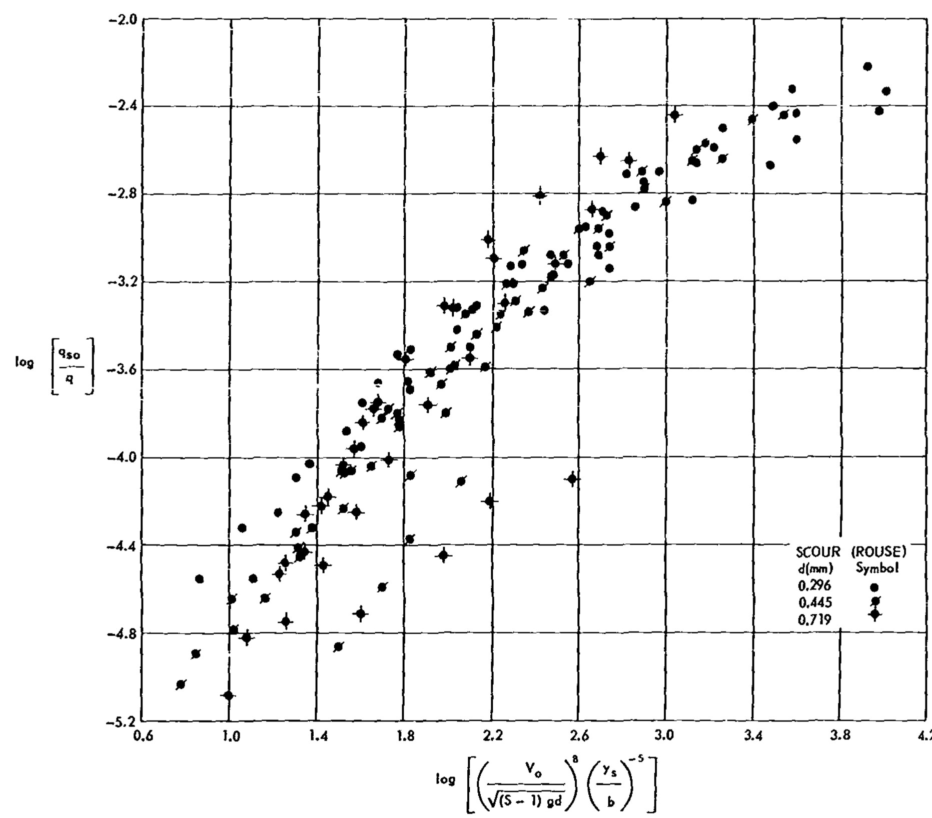

Figure 6. Sediment-Transport Function for Rouse's Minimum Jet Deflection.

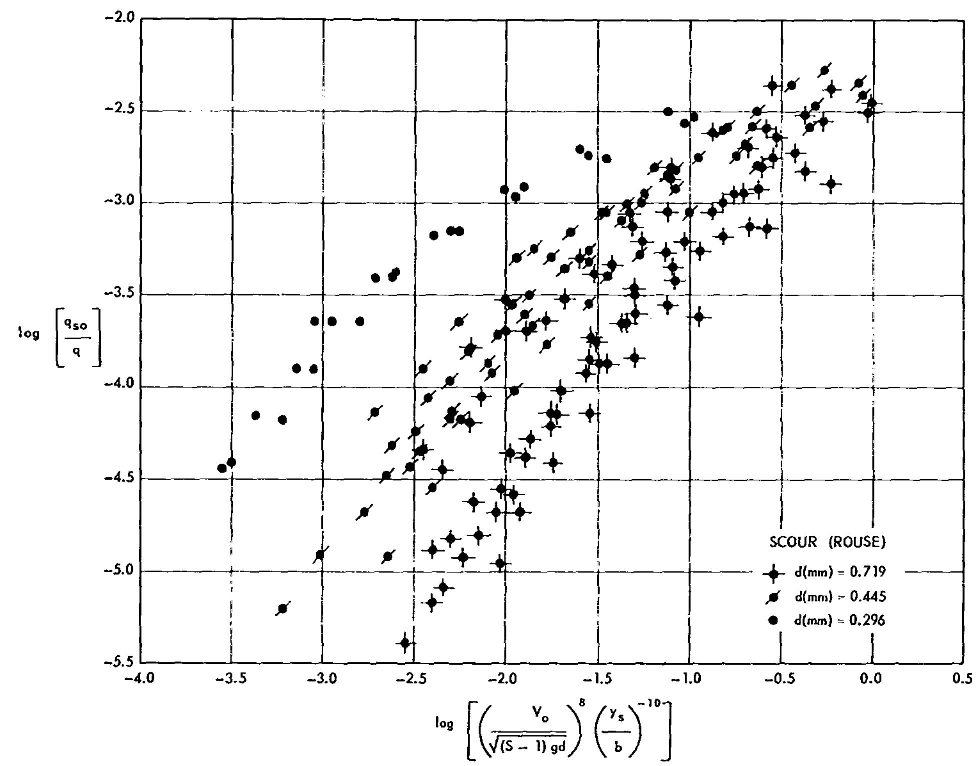

Figure 7. Sediment-Transport Function for Rouse's Maximum Jet Deflection.

sediment-transport function obtained from Laursen's experiments. In other words, equations (16) and (17) closely resemble equation (13) but are quite dissimilar to the suspended-load function, equation (12). The reason is that during the early stages of a run the material excavated by the vertically plunging jet was carried into the recirculating eddy adjacent to the wall. This suspended material either recirculated or settled back into the scour hole rather than being carried out of the hole as suspended load. In contrast to Rouse's experiment, Laursen prevented the separation of the jet stream from the scour hole by placing a lip on the upper edge of the slot through which the jet issued.

Utilizing equations (16) and (17), equation (5) can be integrated to obtain the scour-hole depth as a function of time. Assuming y_s is zero when t is zero,

$$y_s = k_4 \ t^{1/12} \tag{19}$$

if y_s is less than the limit obtained from equation (18). If y_s is greater than this limit,

$$y_s = \left[k_5 \ t - k_6\right]^{1/7} \tag{20}$$

in which the k's are functions of F_o and d/b.

Results of Ahmad's experiments (3) can be analyzed in a similar manner to the analysis performed on Laursen's and Rouse's data. Ahmad's experiments were conducted with bed material of 0.250 mm diameter. The vertical wall extended to one-half the channel width in all five runs. The variation from run to run consisted of varying the channel width from

1.0 ft to 3.0 ft in 0.5 ft increments. The sediment Froude number, $V / \sqrt{(s-1)gd}$, has been calculated using a velocity obtained by dividing the discharge by the cross-sectional area at the constricted section. Details of the experimental procedure are not given in reference (3). The results are graphically presented from which depth of scour, y_s, as a function of time can be obtained. Using these results the transport parameter, Q_s/Vy_s^2, was computed. The variation of the transport parameter is shown in Figure 8. The sediment transport function can be approximated as

$$\frac{Q_s}{Vy_s^2} = 3.5\,(10^{-11})\;F^8\;y_s^{-3} \tag{21}$$

The coefficient of equation (21) has the dimensions of ft^3. The only suitable length with which to make the coefficient dimensionless is the sediment diameter, d. In dimensionless form, equation (21) is

$$\frac{Q_s}{Vy_s^2} = 0.063\;F^8\left(\frac{y_s}{d}\right)^{-3} \tag{22}$$

Utilizing equation (22), equation (7) can be integrated to obtain the scour-hole depth as a function of time. Assuming $y_s = 0$ when $t = 0$

$$y_s = k_7\,t^{1/4} \tag{23}$$

In a recent paper by Laursen (4) the history of scour is presented for a situation similar to that of Ahmad's experiments. The history was determined experimentally at Colorado State University. The chronological

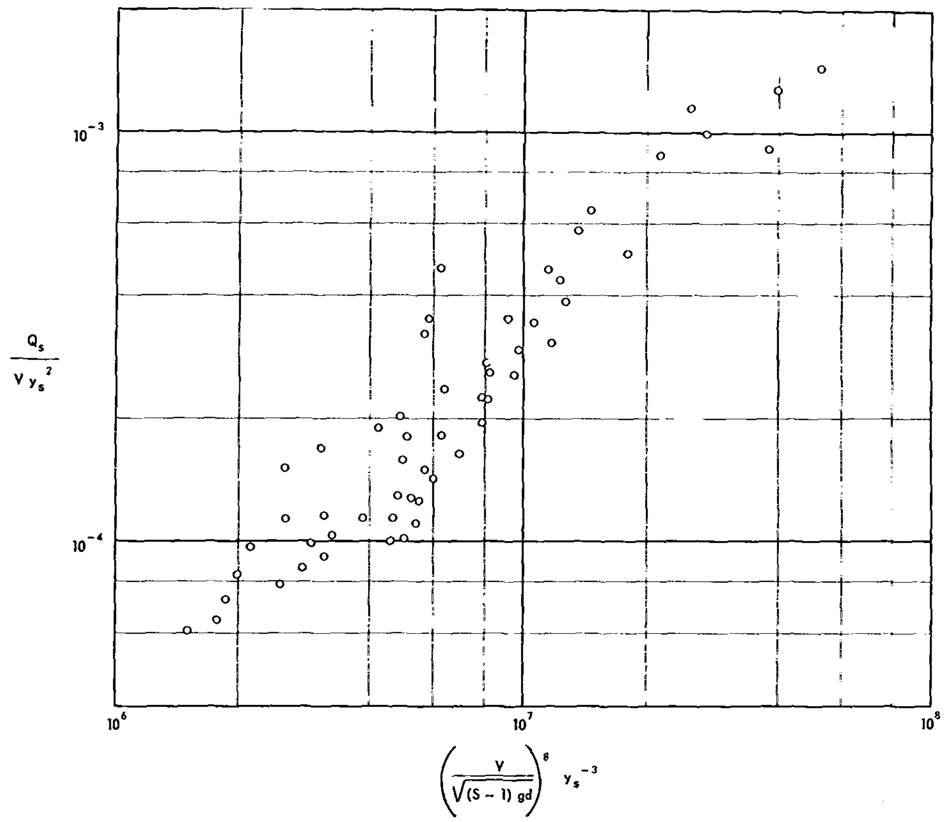

Figure 8. Sediment-Transport Function Derived from Ahmad's Experimental Results.

development of the scour hole is such that y_s is proportional to the fifth root of t rather than the fourth root as indicated in equation (23). Obviously more experimental studies are needed for the precise definition of the sediment transport functions of scour.

Conclusions

Two very carefully executed experiments involving scour by jets were analyzed in order to determine the nature of sediment-transport functions for scouring situations in which the boundary-layer thickness is negligible. The conclusions from this analysis are as follows:

1. The sediment Froude number is a satisfactory similarity parameter for model studies of scour. The pertinent properties of the sediment are correctly incorporated in F as evidenced by the minimum-deflection transport function obtained from Rouse's experiment, that is, equation (16). On the other hand, the inclusion of F did not completely include the sediment properties in the bed-load function, equation (13), obtained from Laursen's experiments. Even here the large exponent of F in comparison to the low exponent on the term containing sediment diameter, d, is reassuring. The sediment Froude number is also a logical parameter for suspended-load movement inasmuch as the major forces on a particle in suspension in a turbulent fluid are the gravity force and the fluid-inertia force. Equation (12) and Figure 4 support this observation.

2. The bed-load transport functions, equations (13) and (16), appear to be typical of most scouring situations in that the transport is by bed load over the rim of the scour hole. The bed-load transport function, equation (22), for a three-dimensional scour situation has the same functional relationship as that for a two-dimensional scour situation,

confirming the inclusion of the sediment Froude number to a large exponent.

3. The fact that scour-hole dimensions at any time are dependent upon history can lead to difficulties in analysis of experimental results. Since scour-hole dimensions are proportional to the integral of transport rate with time, equation (2), interpretation of the integral can be difficult. For example, in Laursen's experiments the removal was initially as suspended load, equation (12), and later as bed-load, equation (13). The writers avoided this difficulty by analyzing the rate of removal which is dependent upon prevailing flow, fluid, and geometric conditions.

Incipient Motion

The sediment Froude number, F, is a similarity parameter for sediment transport in which the boundary layer thickness above the bed is negligible. There is some lower limit of this Froude number at which the bed particles remain in position. This condition is known as incipient motion. From the definition of the angle of repose, Φ, the following relation holds for incipient motion of bed particles lying at an angle α with the horizontal

$$\tan \Phi = \frac{\Sigma F_{\parallel}}{\Sigma F_{\perp}} \tag{24}$$

in which $\Sigma F_{\parallel}$ is the summation of the forces parallel to the bed and $\Sigma F_{\perp}$ is summation of the forces perpendicular to the bed. The parallel forces are the drag force on the particle and the component of the gravity force down the plane. The perpendicular force is the component of gravity force. Thus

$$\tan \Phi \propto \frac{d^2 \rho V^2/2 - (\gamma_s - \gamma) d^3 \sin \alpha}{(\gamma_s - \gamma) d^3 \cos \alpha} \tag{25}$$

in which a positive value of α is associated with flow up the slope. Upon rewriting this relationship a parameter similar to the sediment Froude number appears

$$F \propto \frac{V}{\sqrt{(s-1) gd \left[\tan \Phi \cos \alpha + \sin \alpha\right]}} = C \tag{26}$$

This parameter should have a constant value, C, for incipient scour for which there is a negligible boundary layer. The critical scour parameter, C, will be computed from results of several experiments in order to delineate its value for incipient scour.

White (5) determined the conditions for incipient motion of bed materials in a converging flow of both air and water. With a converging flow and low viscosity fluids, the boundary layer is quite thin. A direct measure of the relative size of a sand grain to the thickness of a turbulent boundary layer is the shearing-velocity Reynolds number

$$R_* = \frac{\sqrt{\tau_c/\rho}\; d}{\nu} = \frac{V_* d}{\nu}$$

in which τ_c is the critical boundary shear stress, ρ is the density of the fluid, and V_* is the defined shearing velocity. As R_* increases the boundary-layer thickness becomes smaller in comparison with the sand grain diameter, d. With the comparatively thin boundary layer and hence no measurable velocity variation over the bed particle, the critical scour parameter, C, should attain a constant value. White's experimental results and computed values of the critical scour parameter, C, are listed in Table 1. The critical scour parameter, C, is essentially constant for R_* of 80 and greater. The highest values of R_* correspond to flows of a localized-scour nature. The minimum value of C of 2.5 appears to be suitable for design against incipient scour.

Ippen and Verma (6) determined the conditions for incipient motion of isolated spherical particles resting on a horizontal sand bed. A steady stream of water passed over the particles. Although Ippen and Verma do not list any values of the natural angle of repose, Φ, the critical scour parameter, C, can still be computed upon using results given by Eagleson and Dean (7). Eagleson and Dean determined the angle of repose for a similar bed configuration. Experimental results from Ippen and Verma and computed values of C are listed in Table 2. The critical scour parameter essentially decreases as the shearing-velocity Reynolds number increases, as with the results of White. The lowest value of C of 1.5 is, of course, less than the corresponding lowest value of 2.5 for White. This difference is due mainly to the fact that the projected flow area of the isolated spheres of Ippen and Verma is considerably larger than that of the imbedded sand particles of White. Nevertheless, the value of C of 1.5 for the isolated spherical particles should represent an absolute minimum for localized scour.

Incipient motion tests for isolated spherical particles of high density were conducted at Georgia Tech. The spherical particles were steel and the fluid was water. The experiment was conducted in a glass-walled, enclosed, rectangular-shaped conduit which has 1/16-in diameter piezometer holes drilled through a smooth floor. The steel particles (5/16-in diameter) were placed such that they rested on the piezometer holes. From the known geometry the natural angle of repose can be computed. Incipient motion was determined by setting the flume at an angle

α with the horizontal and then increasing the velocity in the enclosed section until the ball jumped out of the hole. Experimental values for incipient motion and computed values of C are presented in Table 2. The results here agree quite well with those of Ippen and Verma.

To further illustrate the significance of the critical scour parameter, experimental results for incipient motion of bed particles in oscillatory flow will be analyzed. Manohar (8) determined conditions for incipient motion by oscillating a bed of particles simple harmonically under an otherwise still tank of water. The boundary layer was turbulent for the results to be analyzed here. Manohar conducted many tests for each bed material by varying the amplitude and the frequency of oscillation of the bed. He found that, for each bed material, incipient motion occurred at a constant value of the maximum velocity of the bed, U_m. Since Manohar did not experimentally determine the angle of repose, Φ, of his bed materials, the critical scour parameter cannot be easily determined. However, the writers feel that, after surveying experimental results presented in the literature, the angle of repose of Manohar's bed materials is most probably between 30° and 40°. Values of the critical scour parameter based on the maximum velocity are computed with the angle of repose assumed to be 30° and 40°. The critical scour parameter and Manohar's experimental results for incipient motion are presented in Table 3. The maximum velocity, U_m, for each sand is the average of many runs.

As with the results of White, the critical scour parameter decreases as the bed particle diameter increases indicating that the larger particles are not influenced by the boundary layer nearly as much as are the smaller ones. For the two largest particles the critical scour parameter is essentially constant and should represent the condition for incipient scour. An average value of 2.8 for C would seem suitable for design. This value is only slightly higher than the 2.5 resolved from White's data. The value of C would be somewhat higher from Manohar's data because the maximum velocity U_m was used in calculating C. Manohar defined incipient motion as being when a few particles moved a short distance. Obviously the velocity would have to be greater than a threshold velocity in order for the particles to move a short distance. If this threshold velocity is 0.9 U_m the C values obtained from Manohar's and White's experiment coincide. This analysis for incipient motion in oscillatory flow again demonstrates the significance of the critical scour parameter for flows with negligible boundary layers.

Beginning and Termination of Scour

Scour occurs whenever and wherever the critical scour parameter is exceeded. Once exceeded a scour hole is formed. Scour terminates when the bed particles can no longer be carried over the crest of the dune by the fluid. Thus the critical scour parameter is the governing criterion for both the beginning and the end of scour. The critical scour parameter for beginning of scour is computed with $\alpha = 0$ since the bed is not yet deformed by scour. The critical scour parameter for terminal scour is computed with $\alpha = \Phi$ since the scour hole slope is that of the natural angle of repose of the bed material. In either case the local velocity rather than a mean must be employed in the evaluation of the critical scour parameter, C, by means of equation (26).

Laursen performed some additional experiments from which the value of C can be approximately determined when scour ceases. Laursen determined the minimum jet velocity, V_o, which would transport particles up the slope of the scour hole depicted in Figure 2, but not over the crest. From one of his graphs the critical scour parameter can be resolved. The velocity at the crest, V, which is considerably less than V_o, can be approximated from a relationship given by Albertson, et al.(9) for the diffusion of a two-dimensional jet from a slot. In terms of Laursen's variables

$$\frac{V}{V_o} = 2.28 \sqrt{\frac{b \cos \Phi}{X_L}} \qquad (27)$$

in which X_L is the horizontal distance from the slot to the crest of the dune. The distance $X_L/\cos \Phi$ is the total assumed distance traveled by the water along the bed of the scour hole. This distance corresponds to the centerline distance from slot to the point in question for the study of Albertson, et al. With the angle of repose of 32.6°, with b of 0.025 ft, and with the specific gravity of 2.65, the critical scour parameter, C, was computed by using equation (27) to obtain V and by using $\alpha = \Phi$ in equation (26). The computed values are presented in Table 4. The critical scour parameter is essentially a constant from Laursen's tests for the largest values of X_L, but considerably less than that resolved from White's results. The lower value of C for Laursen's tests is believed to be due to the difference in flow patterns of Albertson's and Laursen's tests. In other words, equation (27) is only qualitatively correct for application to Laursen's scour-hole geometry. In any event the critical scour parameter is a constant for the termination of scour.

An exceptionally neat experiment which demonstrates the usefulness of the critical scour parameter, C, is reported by Chabert and Engeldinger (10). In these experiments water flowed around a single vertical cylinder and over a movable bed of 3-mm diameter gravel. Three different cylinders were used with diameters of 5, 10, and 15 cm. The water depth in the approach channel was systematically varied being either 10 cm, 20 cm, or 35 cm. The remaining variable was velocity, V_1, approaching the cylinder. For each depth of flow a number of runs were made with the velocity at a selected value, ranging from 0.3 to 1.2 m per sec. The terminal depth of scour, y_{st}, was observed for each of the 75 runs. The results are plotted in dimensionless form in Figure 9.

The beginning of scour is shown at a sediment Froude number of 1.25 in Figure 9. For 3-mm gravel a reasonable value of Φ is 45 degrees. At the beginning of scour, the bed is undeformed, that is α is zero. In these circumstances, the critical scour parameter, equation (26), is simply

$$C = \frac{V}{\sqrt{(s-1)gd}} \tag{28}$$

With 3-mm gravel and in an accelerated flow zone, the boundary layer would be insignificant. In this situation a value of C of 2.5 is to be expected. Scour will begin at the point of highest velocity which would occur at about the side tangent points on the cylinder. The velocity at these points can be taken as

$$V = 2V_1 \tag{29}$$

from potential theory. Upon substitution of C = 2.5 and equation (29) into equation (28), the value of $V_1 / \sqrt{(s-1)gd}$ at which scour can be expected to begin is 1.25. The experimental results shown in Figure 9 are in excellent agreement with the prediction of the beginning of scour.

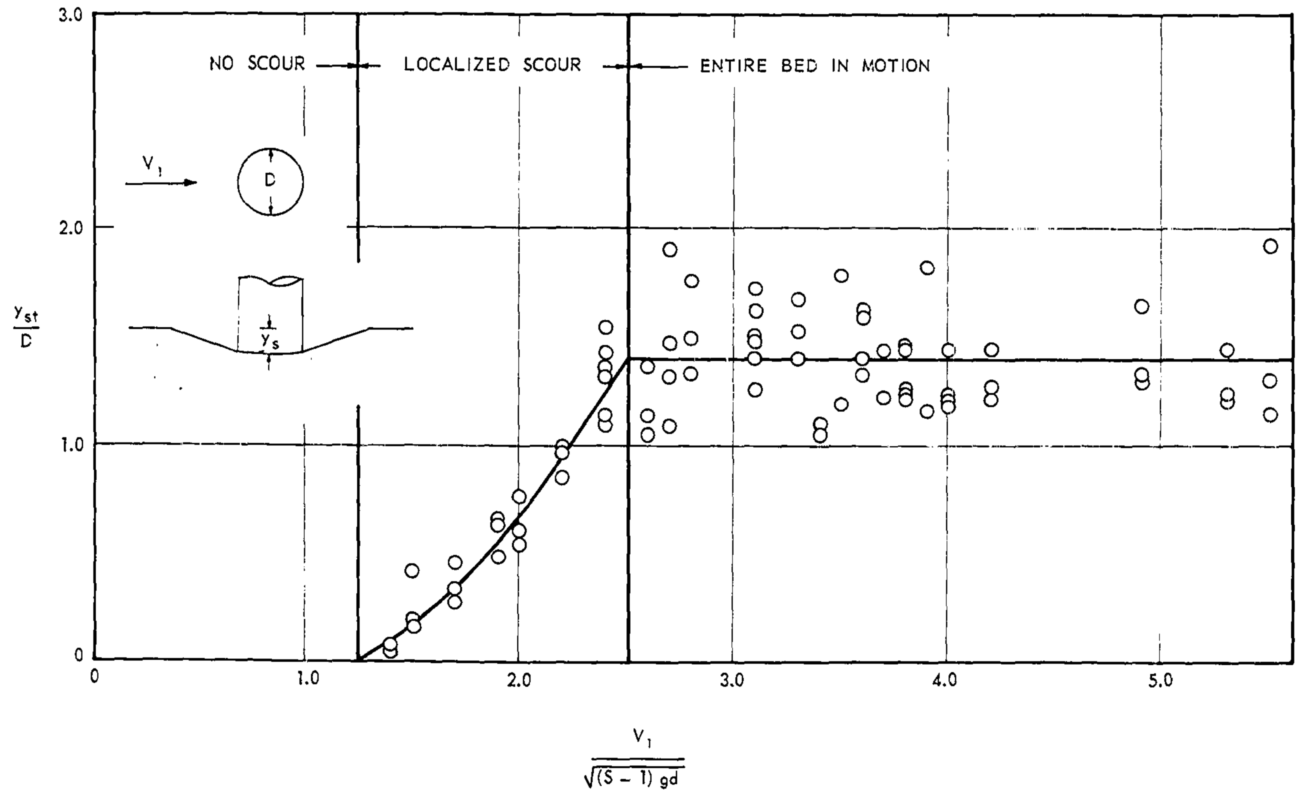

Figure 9. Terminal Scour Depth for Flow Around a Vertical Cylinder.

When the entire bed goes into motion, sediment is carried into the scour hole at the same rate as sediment is removed. Thus after the entire bed is in motion no further increase is expected in the terminal scour depth, y_{st}. Again the experimental results are in excellent agreement with the predicted value of $V_1 / \sqrt{(s-1)gd}$ being 2.5. The value of y_{st}/D is essentially constant for values of $V_1 / \sqrt{(s-1)gd}$ greater than 2.5.

When the value of $V_1 / \sqrt{(s-1)gd}$ is in the range from 1.25 to 2.5 localized scour occurs around the cylinder with the bed being motionless away from the cylinder.

Summary

The critical scour parameter is the governing parameter for incipient and terminal scour since boundary layer effects are negligible where localized scour occurs. The angle of repose is a variable for incipient motion criteria. For the prevention of scour the critical scour parameter should not exceed 2.5 in unidirectional flow.

An engineering example of the use of the critical scour parameter C is the determination of the size of bed material to be placed around a cylindrical pile which is subject to wave-induced flow. The waves will be assumed to be simple harmonic in shape. The still-water depth is h, the wave amplitude from trough to crest is H and the wave length is L. From Lamb (11) the maximum velocity of the water at the bed,

$$U_o = \frac{gH}{2\ c\ \cosh 2\pi h/L} \qquad (30)$$

in which c is the phase velocity of the wave. If the flow in the accelerated flow region adjacent to the pile is assumed to be irrotational, the maximum velocity at the bed, $U_m = 2U_o$. If the value of the critical scour parameter of 2.8 from Manohar's results is used

$$\frac{gH/c \cosh 2\pi h/L}{\sqrt{(s-1)gd \tan \Phi}} = 2.8 \tag{31}$$

for incipient scour. For shallow-water waves, for which h/L is small, $c \approx \sqrt{gh}$ and $\cosh 2\pi h/L \rightarrow 1$. Thus

$$\frac{H}{\sqrt{(s-1)hd \tan \Phi}} = 2.8 \tag{32}$$

for shallow-water waves. Equation (32) is a simple formulation for the prevention of scour at a cylindrical pile. This example shows the ease with which the critical scour parameter criterion may be applied to a particular situation for which the maximum local velocity is known. This example also shows the large diameter of the particles required in order to prevent scour around the pile. If H = 8 ft, h = 40 ft, $\Phi = 45°$, and s = 2.6, the minimum diameter of placed material would be 3.9 cm.

TABLES

Table 1. Incipient-Motion for Unidirectional Flow over a Homogeneous Bed (White's Data)

Bed Material	d (mm)	Fluid	γ_s/γ	α	Φ	V (ft/sec)	$\frac{V_* d}{\nu}$	C
Sand	0.90	Water	2.6	0°	45°	1.25	33	3.2
Steel Shot	0.71	Water	7.9	0°	34.4°	2.03	35	3.4
Sand	0.90	Air	2100	0°	45°	37.5	80	2.7
Sand	5.6	Water	2.6	-24.2°	45°	1.84	360	2.7
Sand	5.6	Water	2.6	0°	45°	2.46	480	2.5
Sand	5.6	Water	2.6	26.2°	45°	2.98	590	2.6
Sand	5.6	Air	2100	0°	45°	88.4	1280	2.5

Table 2. Incipient-Motion Results for Isolated Spherical Particles

Investigator	Material	d(mm)	γ_s/γ	α	Φ	V	$\frac{V_* d}{\nu}$	C
Ippen and Verma	Plastic	2.00	1.28	0°	33.6°	0.35	18	1.8
	Plastic	2.00	1.28	0°	33.6°	0.36	21	1.8
	Plastic	3.17	1.28	0°	23.2°	0.33	27	1.7
	Plastic	3.17	1.28	0°	23.2°	0.35	28	1.7
	Plastic	2.00	1.28	0°	49.7°	0.51	30	1.9
	Plastic	2.00	1.28	0°	49.7°	0.52	33	2.0
	Plastic	2.00	1.28	0°	49.7°	0.53	34	2.0
	Glass	3.17	2.38	0°	23.2°	0.55	42	1.3
	Plastic	3.17	1.28	0°	42.7°	0.46	50	1.6
	Plastic	3.17	1.28	0°	42.7°	0.50	52	1.7
	Glass	3.17	2.38	0°	23.2°	0.69	53	1.6
	Plastic	3.17	1.28	0°	42.7°	0.51	54	1.7
	Glass	4.00	2.38	0°	18.0°	0.52	55	1.3
	Glass	4.00	2.38	0°	18.0°	0.69	67	1.6
	Glass	3.17	2.38	0°	42.7°	1.01	80	1.6
	Glass	3.17	2.38	0°	42.7°	0.97	80	1.5
	Glass	3.17	2.38	0°	42.7°	1.04	83	1.6
	Glass	4.00	2.38	0°	38.3°	0.99	100	1.5
	Glass	4.00	2.38	0°	38.3°	1.02	103	1.5
	Glass	4.00	2.38	0°	38.3°	1.04	106	1.5
Georgia Tech Tests	Steel	7.93	7.63	-6°	11.3°	0.97	-	1.8
	Steel	7.93	7.63	-2°	11.3°	1.25	-	1.7
	Steel	7.93	7.63	0°	11.3°	1.29	-	1.5
	Steel	7.93	7.63	2°	11.3°	1.40	-	1.5

Table 3. Incipient Motion Results for Oscillatory Flow Over a Homogeneous Bed (Manohar's Data)

Material	d(mm)	Specific Gravity (s)	U_m(ft/sec)	C	
				$\Phi = 30^\circ$	$\Phi = 40^\circ$
Glass Beads	0.610	2.54	1.000	4.2	3.5
Sand	0.786	2.63	1.072	3.8	3.2
Sand	1.006	2.60	1.129	3.6	3.0
Sand	1.829	2.60	1.355	3.2	2.7
Sand	1.981	2.63	1.380	3.1	2.6

Table 4. Incipient-Motion for Jet Flow over a Homogeneous Bed (Laursen's Data)

d (mm)	X_L (in)	V (ft/sec)	C
0.240	7.4	0.27	1.3
	10.9	0.31	1.5
	14.7	0.30	1.4
	18.5	0.32	1.5
	20.3	0.34	1.6
	25.0	0.32	1.5
	32.9	0.32	1.5
	41.4	0.32	1.5
0.690	4.8	0.39	1.1
	6.0	0.43	1.2
	6.9	0.44	1.2
	8.5	0.42	1.2
	11.4	0.53	1.5
	13.1	0.49	1.4
	14.7	0.53	1.5
	16.5	0.48	1.3
	22.3	0.50	1.4
	25.0	0.59	1.6
	28.5	0.61	1.7
	31.8	0.50	1.4
	36.1	0.62	1.7
	39.5	0.61	1.7
1.600	6.0	0.72	1.3
	10.7	0.75	1.4
	14.1	0.81	1.4
	15.0	0.84	1.5
	18.1	0.89	1.6
	21.8	0.84	1.5
	25.0	0.77	1.4
	26.8	0.91	1.7
	32.9	0.78	1.4
	37.0	0.87	1.6
	39.6	0.90	1.6

REFERENCES

1. Rouse, H., "Criteria for Similarity in the Transportation of Sediment," Proceedings, 1st Hydraulics Conference, University of Iowa Studies in Engineering, Bulletin 20, 1940, pp 33-49.

2. Laursen, E. M., "Observations on the Nature of Scour," Proceedings, 5th Hydraulics Conference, State University of Iowa, Bulletin 34, 1952, pp 179-197.

3. Ahmad, Mushtaq, "Experiments on the Design and Behavior of Spur Dikes," Proceedings, Minnesota International Hydraulics Convention, University of Minnesota, Minneapolis, August, 1953, pp 145-159.

4. Laursen, Emmett M., "An Analysis of Bridge Scour," Journal of Hydraulics Division, Proc., American Society of Civil Engineers, Vol. 89, No. HY3, May, 1963, p 116.

5. White, C. M., "The Equilibrium of Grains on the Bed of a Stream," Proceedings, Royal Society of London, Vol. 174A, 1940, pp 322-334.

6. Ippen, A. T. and R. P. Verma, "Motion of Particles on Bed of a Turbulent Stream," Transactions, American Society of Civil Engineers, Vol. 120, 1955, pp 921-938.

7. Eagleson, P. S. and R. G. Dean, "Wave-Induced Motion of Bottom Sediment Particles," Transactions, American Society of Civil Engineers, Vol. 126, 1961, pp 1162-1189.

8. Manohar, M., "Mechanics of Bottom Sediment Movement due to Wave Action," U. S. Dept. of Army, Beach Erosion Board Tech. Memo. No. 75, 1955, 121 pp.

9. Albertson, M. L., et al, "Diffusion of Submerged Jets," Transactions, American Society of Civil Engineers, Vol. 115, 1950, pp 639.697.

10. Chabert, J., and Endeldinger, "Etude des Affouillements Autor des Piles de Pont," Laboratoire National D'Hydraulique, Chatou, France, October, 1956.

11. Lamb, H., Hydrodynamics, Dover Publications, 6th Ed., New York, p 369.

APPENDIX B

A THEORETICAL AND EXPERIMENTAL INVESTIGATION OF FLOW UNDER A PARTIALLY-IMBEDDED CYLINDER

C. S. Martin

Flow of a fluid under a circular cylinder which is half-imbedded in sand is amenable to theoretical analysis as long as the critical gradient at the bed is not attained. The theoretical solution for a partially-imbedded cylinder is untenable in that singular points occur at points of imposed nonorthogonality of flow lines and potential lines. In the following, an experimental study shows the behavior of the bed in the vicinity of the singular points. The effect of flow out of or into a sand bed on the angle at which the bed makes with the horizontal is discussed. Experimental results are given on vertical piezometric-head gradients required to cause boiling and, finally, piping.

Theoretical Solution

In Figure 1 is shown a circular cylinder partially imbedded in sand. Water flows through the sand from right to left under the cylinder by virtue of the water level h_2 being larger than h_1. The problem is to determine the variation of the piezometric head, h, within the sand. Flow through homogeneous porous media can be represented by Darcy's Law; namely,

$$V_x = - \kappa \frac{\partial h}{\partial x} \quad ; \quad V_y = - \kappa \frac{\partial h}{\partial y}$$

in which V_x and V_y are the x- and y-components of macroscopic velocity in the bed, and κ is the coefficient of permeability.

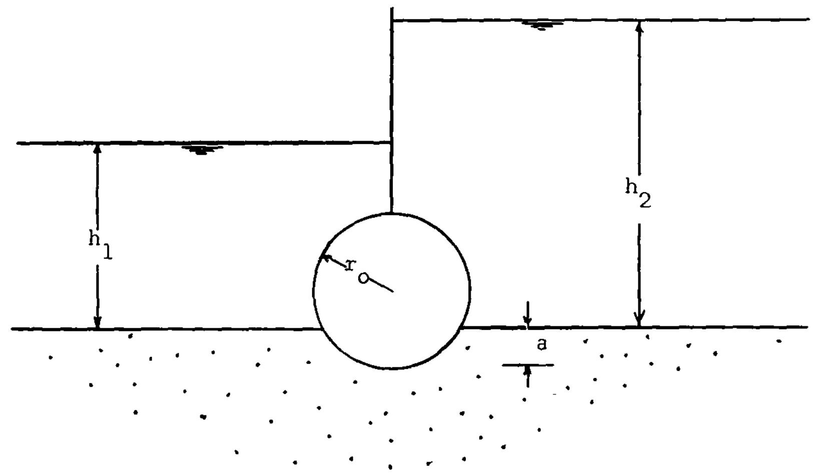

Figure 1. Sketch of Imbedded Cylinder

Satisfying the equation of continuity of fluid flow through the sand results in Laplace's equation

$$\frac{\partial^2 h}{\partial x^2} + \frac{\partial^2 h}{\partial y^2} = 0 \tag{1}$$

or, if $\Phi = -\kappa h$,

$$\frac{\partial^2 \Phi}{\partial x^2} + \frac{\partial^2 \Phi}{\partial y^2} = 0 \tag{2}$$

The two constant piezometric heads, h_1 and h_2, make the sand-water interfaces on each side of the cylinder potential lines. These are boundary conditions. The imbedded portion of the cylinder is regarded as a streamline. The solution to this boundary-value problem is approached by the technique of conformal mapping. The physical plane is the z-plane in which

$$z = x + i\ y$$

The complex function

$$w = \Phi + i\ \psi$$

in which ψ is the stream function, represents what is known as the w-plane. The problem is to map the w-plane into the z-plane, a procedure which requires two intermediate planes, the z'-plane and the t-plane. These four planes, and the corresponding points, are shown in Figure 2. In Table 1 are listed the complex values of each point for the four planes.

Table 1. List of Complex Values of the Four Planes

Point	z-plane	z'-plane	t-plane	w-plane
A	$-\infty$	0	∞	$\Phi_1 + i\ \psi_A$
B	$-\sqrt{a(2r_o - a)}$	$\infty + i(-\theta/2 \text{ to } 0)$	1	$\Phi_1 + i\ \psi_1$
C	$-ia$	$-i\theta/2$	0	$\Phi_c + i\ \psi_1$
D	$\sqrt{a(2r_o - a)}$	$\infty + i(-\theta/2 \text{ to } 0)$	-1	$\Phi_2 + i\ \psi_1$
E	∞	0	$-\infty$	$\Phi_2 + i\ \psi_E$

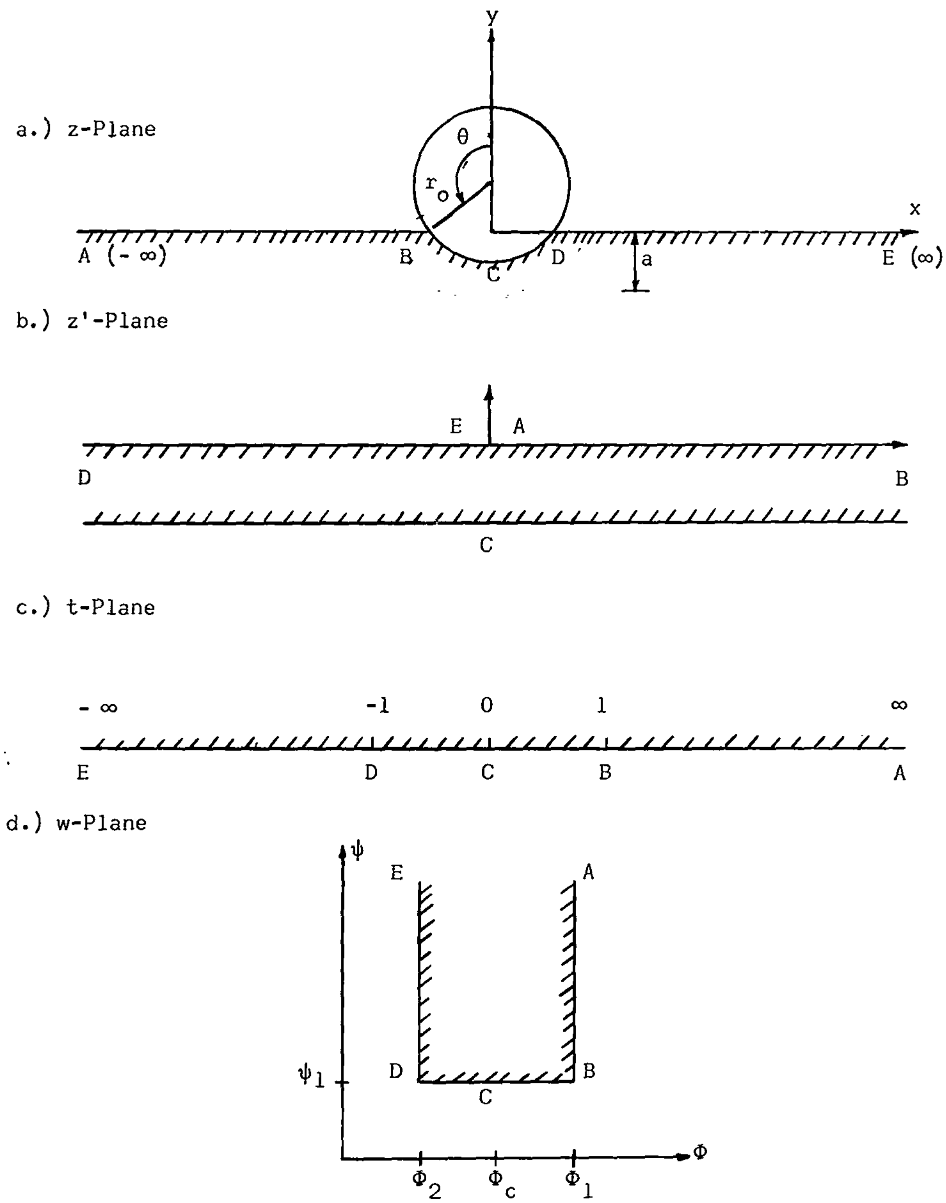

Figure 2. Complex Planes Used in Transformations

The transformation from the z-plane to the z'-plane, as listed by Kober (1), is

$$z' = \frac{1}{2} \ln \left[\frac{z - \sqrt{a(2r_o - a)}}{z + \sqrt{a(2r_o - a)}} \right] \tag{3}$$

The Schwarz-Christoffel transformation is used to go from the z'-plane to the t-plane. The integral

$$z' = A \int \frac{dt}{(-1 - t)(1 - t)} + B$$

appears, in which $A = -\theta/2\pi$ and $B = 0$ upon satisfying all conditions. Hence,

$$z' = -\frac{\theta}{2\pi} \ln\left[\frac{t - 1}{t + 1}\right],$$

and

$$t = \frac{(z - c)^{\pi/\theta} + (z + c)^{\pi/\theta}}{(z - c)^{\pi/\theta} - (z + c)^{\pi/\theta}} \quad , 0 < \theta < \pi$$

in which $c = \sqrt{a(2r_o - a)}$.

The remaining transformation is also obtained by employment of the Schwarz-Christoffel technique

$$w = A' \int \frac{dt}{\sqrt{-1 - t}\sqrt{1 - t}} + B'$$

or

$$w = \frac{i}{\pi}(\Phi_1 - \Phi_2)\cosh^{-1} t + \Phi_1 + i\psi_1$$

upon joining the w-plane and the t-plane. The solution connecting the z-plane to the w-plane is

$$w = \frac{i}{\pi}(\Phi_1 - \Phi_2)\cosh^{-1}\left[\frac{(z-c)^{\pi/\theta} + (z+c)^{\pi/\theta}}{(z-c)^{\pi/\theta} - (z+c)^{\pi/\theta}}\right] + \Phi_1 + i\psi_1 \qquad (4)$$

The vertical piezometric-head gradient, $\partial h/\partial y$, is determined by differentiating the real part of equation (4). The vertical piezometric-head gradient on the bed

$$\left.\frac{\partial h}{\partial y}\right|_{y=0} = \left[\frac{2(h_1 - h_2)}{r_o \theta \sin\theta}\right]$$

$$\left[\frac{(x/c-1)^{\pi/\theta}(x/c+1)^{\pi/\theta-1} - (x/c-1)^{\pi/\theta-1}(x/c+1)}{\left[(x/c-1)^{\pi/\theta} - (x/c+1)^{\pi/\theta}\right]^2}\right]$$

$$\cdot \left[1\Big/\sqrt{\left[\frac{(x/c-1)^{\pi/\theta} + (x/c+1)^{\pi/\theta}}{(x/c-1)^{\pi/\theta} - (x/c+1)^{\pi/\theta}}\right]^2 - 1}\right] \qquad (5)$$

It is of interest to know the magnitude of $\partial h/\partial y$ at point B, since the sand might tend to become "quick" there. Unfortunately, however, the value of $\partial h/\partial y$ is mathematically indeterminate at B and at D.

Except for the case in which the cylinder is half-imbedded, potential lines AB and DE are not orthogonal with streamline BCD at intersections B and D. Points B and D are called singular points. Whenever orthogonality is not satisfied, the piezometric-head gradient will have either of two values, as discussed by Casagrande (2). He states that at points where boundary flow lines (streamlines) intersect potential lines (lines of constant piezometric head) at a predetermined angle, the piezometric-head gradient is either zero or theoretically infinite. If, as shown in Figure 3, the angle β defines the angle of intersection of boundary flowline and potential line, criteria from Casagrande may be stated as follows

If	$\beta < 90°$,	the piezometric-head gradient is zero.
If	$\beta = 90°$,	the piezometric-head gradient is finite, not necessarily zero.
If	$\beta > 90°$,	the piezometric-head gradient is theoretically infinite.

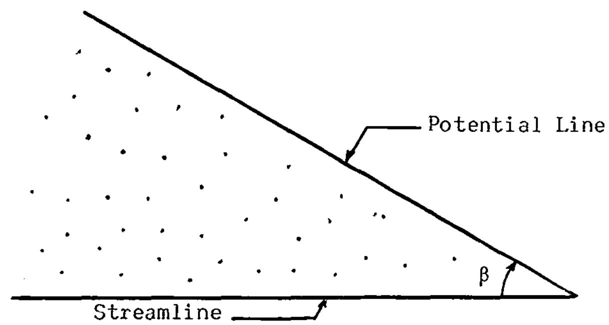

Figure 3. Boundary Angle between Streamline and Potential Line

Casagrande further points out that the condition of infinite gradient (or infinite velocity) is the cause of erosion in dams at points for which $\beta > 90°$. Furthermore, large velocities will render Darcy's law invalid since velocity-head changes cannot be neglected.

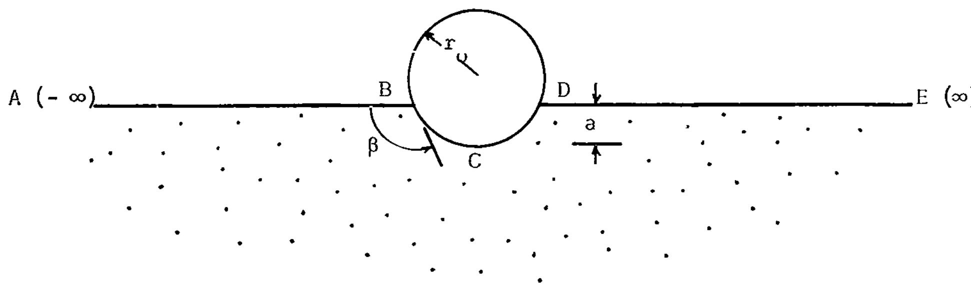

Figure 4. Sketch of Angle of Intersection of Streamline and Potential Line for Cylinder

Casagrande's criteria will be used with reference to Figure 4. If $a/r_o > 1$, $\beta < 90°$; and if $a/r_o < 1$, $\beta > 90°$. At point B the piezometric-head gradient is zero for $a/r_o > 1$, finite for $a/r_o = 1$, and infinite for $a/r_o < 1$. For the half-imbedded case, that is, $a/r_o = 1$, the vertical piezometric-head gradient at the bed is given by

$$\frac{\partial h}{\partial y}\bigg|_{y=0} = \frac{h_2 - h_1}{\pi\, x} \tag{6}$$

At point B,

$$\frac{\partial h}{\partial y}\bigg|_{B} = \frac{h_2 - h_1}{\pi\, r_o}$$

If the mathematical limit is indeed a physical limit, then movement of the bed material at point B could be expected whenever the cylinder is less than one-half buried regardless of the magnitude of $h_2 - h_1$. From the physical standpoint this conclusion seems preposterous. Only by experiment can this dilemma be resolved.

Experimental Setup

A photograph of the experimental apparatus used is shown in Figure 5. The walls and bottom are made of 1/2-in plexiglas and are glued and screwed together. The flow passage is 4 in wide. The black circular disc in the center is the end of cylinder which is 4-in in diameter. The lower flow boundary is a plastic strip which is bent in the shape of a 12-in circular arc. The bed material is placed between the cylinder and the arc up to any desired level on the cylinder. Water enters through an orifice in the right-hand wall and flows through the sand bed under the cylinder. A constant piezometric head, h_1, is maintained on the left-hand side by means of a sharp-crested weir. For a given rate of flow through the sand the piezometric head, h_2, reaches a level of equilibrium, provided that $h_2 - h_1$ is below that value at which piping occurs.

Permeability Tests

Tests were conducted to determine the coefficient of permeability, κ, of each bed material. The physical characteristics of the two bed materials used are listed below

Material	d (mm)	Geometric Standard Deviation (σ_g)	Specific Gravity (s)	Angle of Repose (Φ)
Glass Beads	0.220	1.08	2.49	22°
Ottawa Sand	0.585	1.16	2.62	32.5°

Only for $a/r_o = 1$ does an analytical solution exist for relating rate of flow to the coefficient of permeability and $h_2 - h_1$. The variation of the vertical velocity component, V_y, along the bed is, from equation (6)

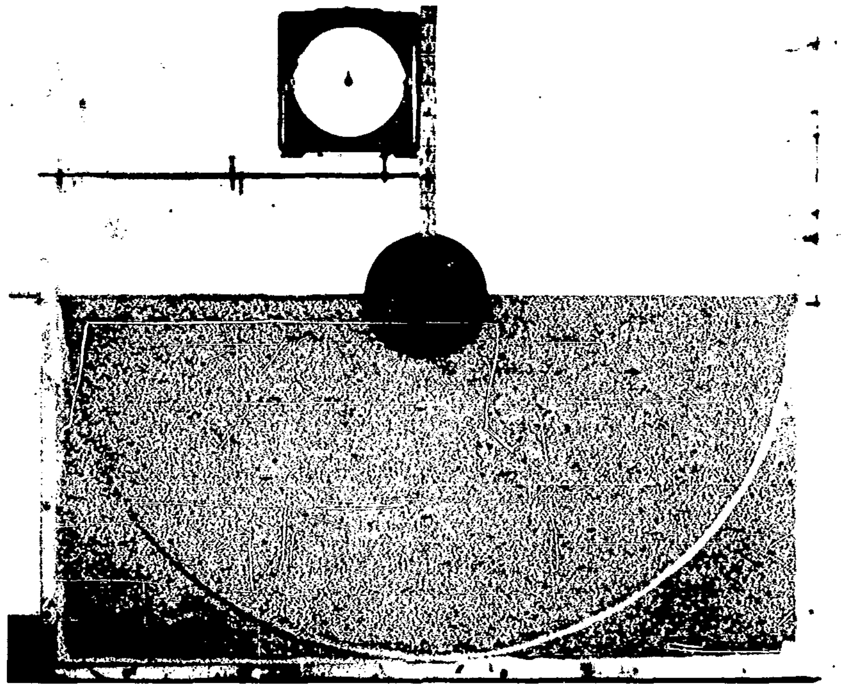

Figure 5. Photograph of Experimental Set-up with $a/r_o = 1$.

$$V_y\Big|_{y=0} = \kappa \frac{\Delta h}{\pi x} \qquad (7)$$

in which $\Delta h = h_2 - h_1$. The total flow rate, Q is obtained by integrating equation (7) over the area of the interface

$$Q = \kappa \int_A \left[V_y\right]_{y=0} dA = \kappa \frac{b\Delta h}{\pi} \int_{r_o}^{6r_o} \frac{dx}{x}$$

in which b is the width of flow passage. Upon integrating and reducing

$$Q = 0.512\, b\kappa\, \Delta h \qquad (8)$$

The test procedure consisted of setting the flow rate Q, waiting until a state of equilibrium was reached, and then measuring all pertinent quantities. The discharge Q was measured gravimetrically, the change in piezometric head Δh was read off the scale in Figure 5 and the coefficient of permeability was computed from equation (8). At 60°F the coefficient of permeability, κ, is 0.00103 ft/sec and 0.00465 ft/sec for the glass beads and Ottawa sand, respectively.

Boiling and Heaving

Tests were conducted in order to study boiling and heaving near point B on the cylinder. Of particular interest is the behavior of the flow near singular point B for the case in which the cylinder is partially-imbedded.

Cylinder Half-Imbedded

With the cylinder half-imbedded in the bed material the sequence of events from initial boiling to piping were observed. The glass beads and the Ottawa sand were used as bed materials. The bed was screeded and made plane as shown in Figure 5. The test procedure consisted of increasing the piezometric head h_2 slowly until boiling and, finally, piping occurred. As the water level h_2 was raised the first sand movement at B was localized boiling for the glass beads and slow heaving for the Ottawa sand. For the glass beads, the boiling was localized at first but then nearly uniformly distributed over the bed adjacent to the cylinder at B. As the piezometric head h_2 was slowly increased the boiling became violent to the extent that the glass beads began to move in mass, forming a mound adjacent to the cylinder. For the Ottawa sand the mound grew from initial heaving rather than boiling but the shape of the mound is similar to that for the glass beads. A photograph of the mound at B and the depression at D for the glass beads is shown in Figure 6a. The mound for the Ottawa sand is shown in Figure 6b. Each mound grows in size but is similar in shape until a pipe forms.

As stated above, piping does not immediately follow boiling. There is definitely a self-correcting mechanism present, up to a limit, during the heaving process. For several mound sizes no piping will occur provided Δh is maintained constant. The limiting case occurs when a pipe develops. Hence there is a factor of safety (S.F.) in designing for a critical gradient. This factor varies from 1.16 to 1.36, as shown in the table below.

The angle that the sloping portion of the mound makes with the horizontal can be explained qualitatively. This angle is always less than the natural angle of repose of the particular bed material because of the water flowing out of the bed. The value of this angle before piping

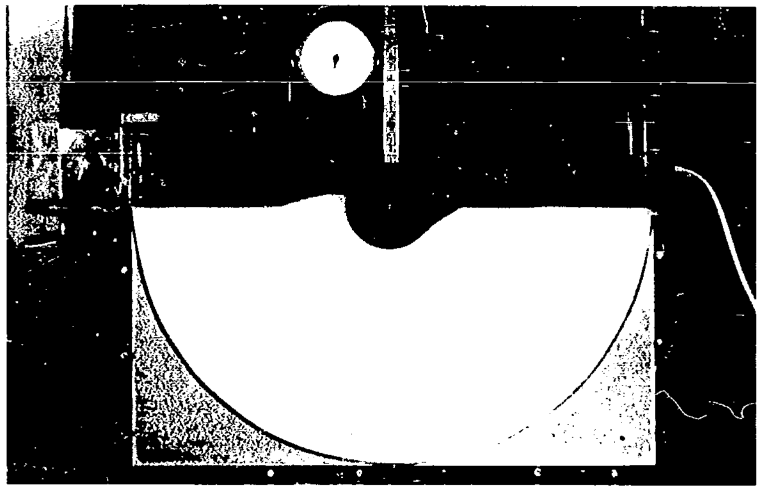

a. Glass Beads as Bed Material

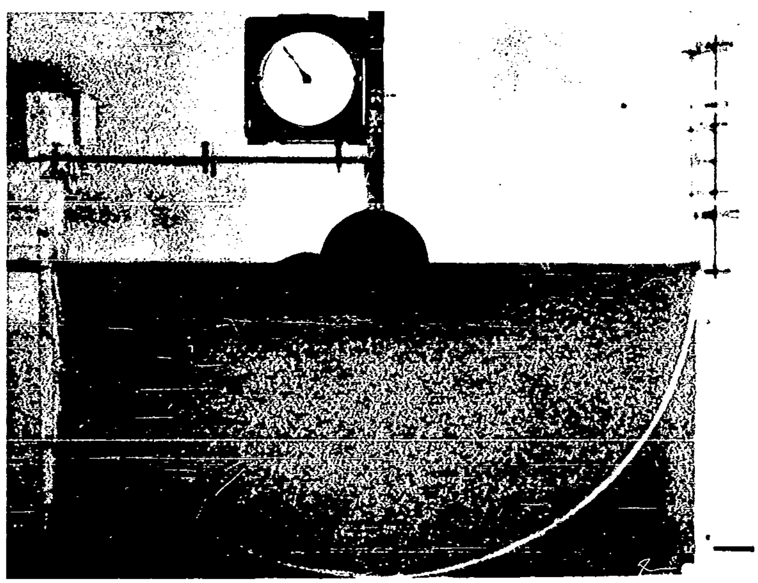

b. Ottawa Sand as Bed Material

Figure 6. Profile of Mound for $a/r_o = 1$.

occurs is 15° for the glass beads and 20° for the Ottawa sand. As discussed by Haefeli (3), a bed is rendered less stable with flow out of the bed and more stable with the flow into the bed. Such an effect causes the bed slope to be less than the natural angle of repose when flow is out of the bed and more than the natural angle of repose when flow is into the bed. Both of these cases are borne out by the mild slope on the mound and the steep slope on the depression near D. The angle that the depression makes with the horizontal is nearly 34° for the glass beads and 42° for the Ottawa sand.

Cylinder Partially-Imbedded

The main objective for the tests with the cylinder partially-imbedded was to observe the behavior of the bed in the vicinity of singular point B. Tests were run with a/r_o = 0.25, 0.50, and 0.75. Tests with a/r_o = 0.25 and 0.50 were unsatisfactory as piping occurred before a mound formed completely across the channel. All data presented are for a/r_o = 0.75. Both the glass beads and the Ottawa sand were used as bed materials. The bed was screeded plane at a level 1/2 in below the centerline level of the cylinder, Figure 7. The bed adjacent to singular point B was observed as the piezometric head h_2 was increased slowly.

Boiling was not observed immediately as one might expect from the theoretical solution. In fact, for the Ottawa sand, initial movement was by heaving, as with a/r_o = 1. Boiling or heaving do occur, of course, at a value of Δh less than that required for the half-imbedded cylinder. As the water level h_2 increased the boiling for the glass beads became more violent until a mound was formed. The interesting feature is that

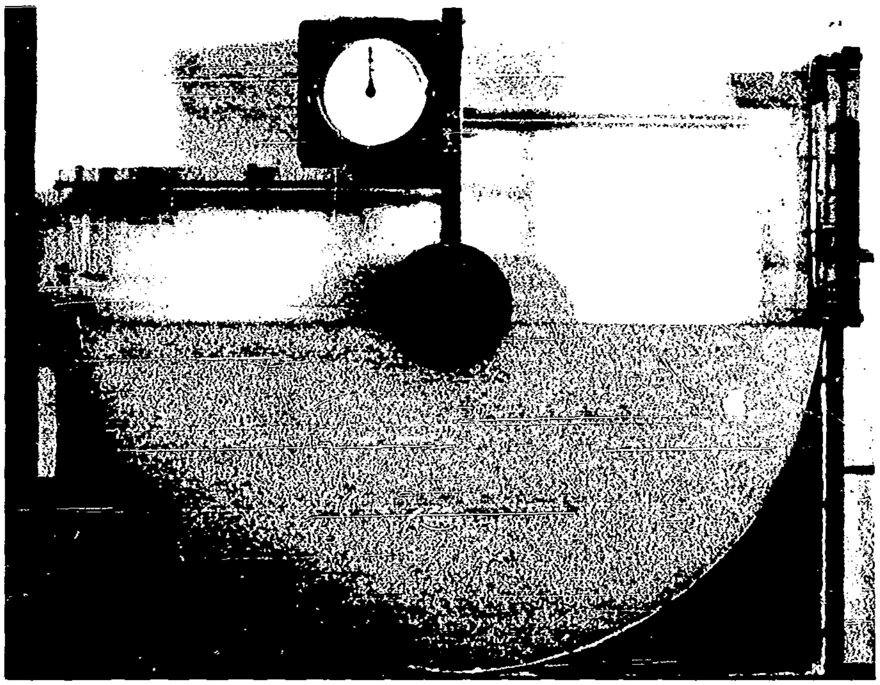

Figure 7. Photograph of Experimental Set-up with $a/r_o = 0.75$.

the mound is curved, unlike the rectilinear features of the mound for the half-imbedded cylinder. In Figure 8 are shown photographs of a typical mound for the glass beads and for the Ottawa sand. Upon close scrutiny it is noticed that the mounds intersect the cylinder at essentially right angles. Nature apparently corrects for the anomaly of non-orthogonality at such singular points as B. With a further increase in Δh, piping finally occurs. Values of Δh for the initial boiling and piping and values of S.F. are given in the table below.

The self-correcting mechanism is also present for $a/r_o < 1$. The initial formation of a mound takes place fairly rapidly once boiling commences but, if h_2 is held constant the heaving of the mound ceases. Only if h_2 is increased further does any movement occur. Hence the mound is stable, up to a limit, for a constant h_2. The heaving process for $a/r_o < 1$ is similar to that for $a/r_o = 1$.

Piping and Scour

As the piezometric head, h_2, is further increased the mound and depression grow in size until a pipe is formed. Once a pipe develops under the cylinder an unstable condition exists such that scour is imminent. The piping and scour for the partially-imbedded cylinder is so similar to that for the half-imbedded one that no distinction between the two is necessary.

Motion pictures were taken of the entire piping and scour sequence. Once piping appeared imminent to the observers a stop-clock was started and the inlet flow was stopped. The motion-picture camera was started and the entire sequence photographed. The sequence will be described

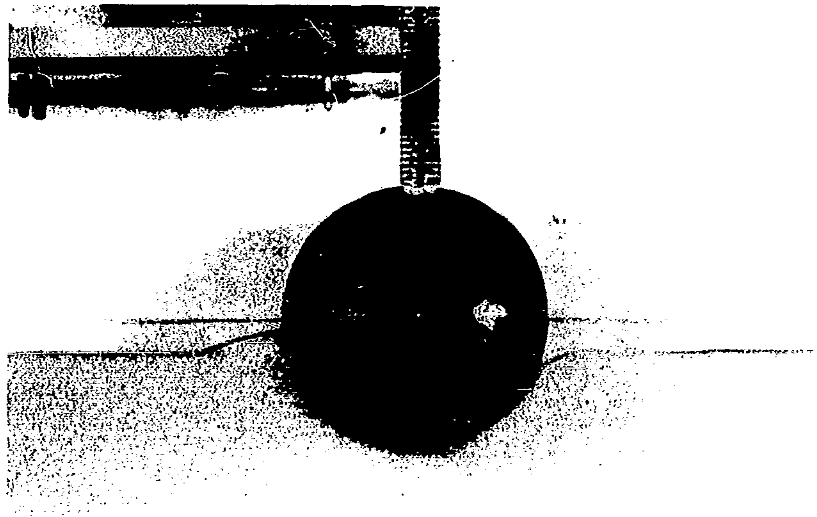

a. Glass Beads as Bed Material

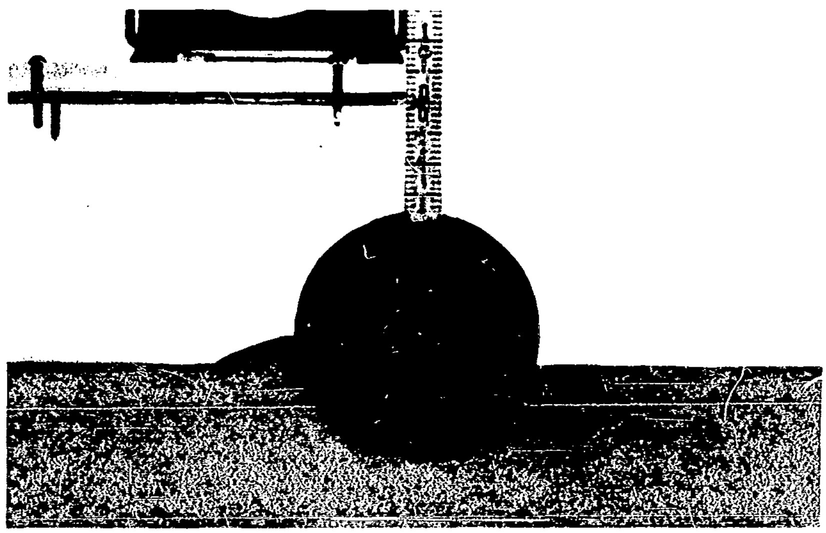

b. Ottawa Sand as Bed Material

Figure 8. Profile of Mound for $a/r_o = 0.75$.

with reference to Figures 9 a, b, c, and d. In Figures 6 and 8 the mound and depression are in a stable state. In Figure 9a a pipe is seen adjacent to the cylinder at the near wall. At this instance scour is inevitable as a channel is forming under the cylinder. In Figures 9b and c is shown the development of the scour channel beneath the cylinder. Since the flow into the apparatus is stopped just before piping, and the piezometric head h_2 falls rapidly, the velocity out of the channel decreases to a value below which scour will occur. At this condition the bed material can no longer be carried out of the hole and sloughing back into the channel occurs. The sloughing continues until, finally, with $h_1 = h_2$, the slopes of the bed on the left- and right-hand sides reach the natural angle of repose of the bed material. This final state is shown in Figure 9d.

Conclusions

Singular points which occur at imposed conditions of nonorthogonality of flow lines and potential lines are not as critical as mathematical analysis indicates. Boiling does not occur immediately but, when it does, the bed takes on a shape such that orthogonality is satisfied at these singular points. A safety factor defined by the ratio of the piezometric-head gradient required to cause piping to that required to cause boiling varies from 1.16 to 1.57 for all tests involving a cylinder being either partially- or half-imbedded.

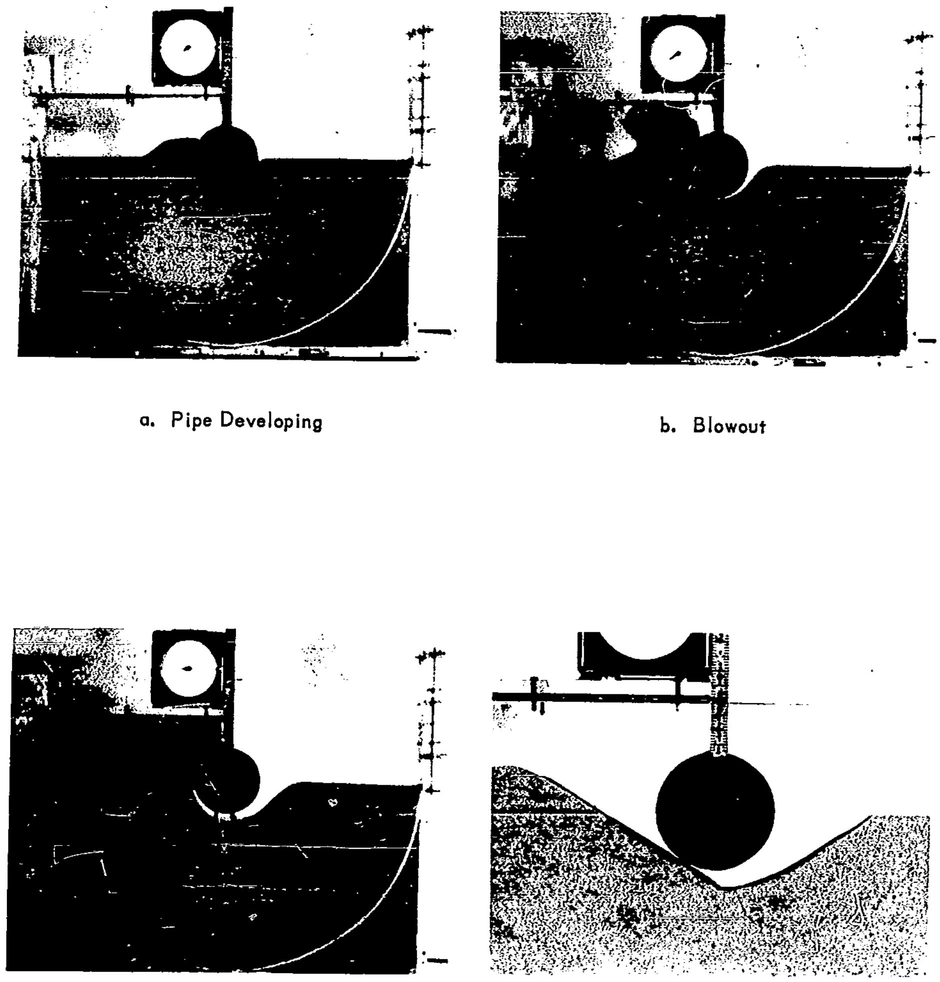

a. Pipe Developing

b. Blowout

c. Scour Channel

d. Final State

Figure 9. Piping and Scour Sequence.

Table. Results for Initial Boiling and Piping

a/r_o	Bed Material	Δh (in) Initial Boiling	Initial Piping	S.F.
1.00	Glass Beads	6.34	7.34	1.16
1.00	Glass Beads	5.72	7.59	1.32
1.00	Glass Beads	6.50	7.70	1.18
1.00	Glass Beads	5.90	7.49	1.27
1.00	Glass Beads	5.82	7.35	1.26
1.00	Ottawa Sand	8.52	10.27	1.21
1.00	Ottawa Sand	7.53	10.25	1.36
0.75	Glass Beads	3.75	5.78	1.54
0.75	Glass Beads	3.84	6.02	1.57
0.75	Ottawa Sand	6.53	8.03	1.23

REFERENCES

1. Kober, H., Dictionary of Conformal Representations, Dover Publications, 2nd Ed., New York, 1957, p. 89.

2. Casagrande, A., "Seepage through Dams," Journal of the New England Water Works Association, Vol. 51, No. 2, June 1937, pp. 165-166.

3. Haefeli, R., "The Stability of Slopes Acted upon by Parallel Seepage," Proc. Second Int. Conf. on Soil Mechanics and Foundation Engineering, Vol. I, Rotterdam, June 1948, pp. 57-62.

DEPARTMENT OF THE NAVY
OFFICE OF NAVAL RESEARCH
800 NORTH QUINCY STREET
ARLINGTON, VA 22217-5660

Rec'd 1/24/2001

IN REPLY REFER TO
5510/1
Ser 43/020
12 Jan 01

From: Chief of Naval Research
To: Commanding Officer, Naval Research Laboratory (Code 7030.1)

Subj: CLASSIFICATION CHANGE

Ref: (a) Your memo 5500 Ser 7030.1/115 of 26 Sep 00

Encl: (1) Copy of Georgia Institute of Technology Report A-628 "Settlement of Cylindrical Mines Into the Sea Bed Under Gravity Waves" dtd November 1963 **(AD 350 001)**

1. In response to reference (a), enclosure (1) has been downgraded to UNCLASSIFIED by authority of the Chief of Naval Research and marked "Distribution Statement A: Approved for Public Release; Distribution is Unlimited."

2. Questions may be directed to me on (703) 696-4619, DSN 426-4619.

Peggy Lambert

PEGGY LAMBERT
By direction

Copy to:
DTIC (Bill Bush, DTIC-OCQ)